MAX-PLANCK-INSTITUT FÜR PLASMAPHYSIK

GARCHING BEI MÜNCHEN

INTOR rescaling for non-indented plasma shape applying preliminary scalings for energy confinement and density limit

A. F. Knobloch

IPP 4/224 November 1986

Die nachstehende Arbeit wurde im Rahmen des Vertrages zwischen dem Max-Planck-Institut für Plasmaphysik und der Europäischen Atomgemeinschaft über die Zusammenarbeit auf dem Gebiete der Plasmaphysik durchgeführt.

IPP 4/224

INTOR rescaling for non-indented plasma shape applying preliminary scalings for energy confinement and density limit.

November 1986

A. F. Knobloch

Abstract

On the basis of a simplified rescaling procedure with INTOR, as of Phase IIA Part 1, serving as reference case, alternative design points are discussed that take into account more recent findings on ß-limits, density limits and possible extrapolations with respect to plasma elongation. Two tentative scalings for the energy confinement time as derived from ASDEX results and by Goldston are applied to find minimum size INTOR alternatives, which, of course, could be quite different for the two scalings. Large plasma elongation is needed for getting close to the original outlay for INTOR. The density limit according to some possible scalings requires some adjustment of the plasma temperature to above 10 keV. The neutron wall load, being the important parameter with respect to the INTOR test programme, can be practically kept at the reference level. For ASDEX confinement scaling this requires that an ignition margin of about 2 be adhered to. A sensitivity study on the impact of individual modifications in input assumptions of the order of 10% shows that only a limited range of such alternatives remains acceptable.

Table of contents

1. Introduction

In an earlier report /1/ simplified rescaling relations were derived that could serve for sensitivity studies investigating the impact of input assumptions on tokamak reactor designs, specifically on possible INTOR alternatives. Such studies are readily done in a relative representation of all quantities, with a consistent reactor design point serving as reference case. For the INTOR- oriented studies the INTOR version as of Phase IIA part 1 /2/ is used as this reference.
This report extends the work in /1/ by including preliminary results on energy confinement and density limits and establishing a picture of INTOR alternatives that could be selected on the basis of existing knowledge. It is written as a contribution to the present INTOR Phase IIA part 3 workshop activities (see /3/).

2. Rescaling procedure

Rescaling from a consistent reactor design point saves manifold detailed repetition of design oriented evaluations and can help towards an easier understanding of the impact of modifications in the physics and engineering input assumptions. INTOR as of Phase IIA part 1 is a consistent tokamak test reactor design point based on a documented mission definition. Its operation data and scenario are well defined on the basis of the actual or - if necessary - somewhat extrapolated state of the art in plasma physics and technology. As time goes on, that state of the art develops and consequently has to be continually incorporated. The consequences are clearly seen in comparison with the reference case. All quantities therefore are shown in relative terms, i.e. in relation to their value in the reference case (INTOR Phase IIA part 1).

Figure 1 shows a simple picture of the radial build of a tokamak reactor, as will be used for the rescaling calculations. E, F, G and H are geometry factors that describe the most essential constituents of the radial build and their engineering and nuclear design in relation to the reference. For any alternative design these constituents can be rescaled.

According to Figure 1 one gets for the major plasma radius (composed of the central solenoid radius, the toroidal field coil thickness, the inner blanket/shield thickness and the inner vessel minor radius)

$$\frac{R}{R_o} = \rho = \frac{R_{OH}}{R_o}\left(\frac{I}{I_o}\rho\right)^{1/2} + \frac{T_{TFo}}{R_o}\,\frac{R_{OH}\,(I/I_o)^{1/2} + T_{TF}}{R_{OH} + T_{TF}} + \frac{T_{BS}}{R_o} + \frac{R_V}{R_o}\,\frac{a}{a_o}$$

$$\rho = E \cdot \left(\frac{I}{I_o}\rho\right)^{1/2} + F + G\,\frac{a}{a_o} \qquad (1)$$

using the abbreviations

$$E = E_1 + E_2 \quad \text{with} \quad E_1 = E + H\left\{1 - \left(\frac{E}{H} + 1\right)^{1/2}\right\}$$

and

$$F = H + \frac{T_{BS}}{R_o} = \frac{T_{TF}^2}{R_o(R_{OH} + T_{TF})} + \frac{T_{BS}}{R_o}$$

This formulation represents the radial build in an approximate manner on the assumption of an appropriate adjustment of the flux density swing $\Delta B/\Delta B_o$ in the central solenoid for full inductive current drive. The blanket/shield thickness is kept constant for each set of geometry factors, which is justified in a narrow range around a certain wall loading.

The two geometry conditions (2) and (3) to be fulfilled are mainly related to the engineering design of the magnets and their structure and to the design of the inner shield/blanket portion, the inner plasma-wall distance being contained in G:

$$\frac{A}{A_o} = E\left(\frac{I}{I_o}\rho\right)^{1/2}\frac{A/A_o}{\rho} + F\,\frac{A/A_o}{\rho} + G \qquad (2)$$

$$\frac{B}{B_o} = \frac{E(I/I_o.\rho)^{1/2} + H}{(E_o + H_o)\rho} \cdot \frac{B_{max}}{B_{maxo}} \qquad (3)$$

with E_o, H_o as defined for the reference case.

For the plasma current one has the equation

$$\frac{I}{I_o} = \frac{B}{B_o}\,\rho\,\left(\frac{A_o}{A}\right)^2 \frac{g}{g_o}\,M \qquad (4)$$

$$\text{with} \quad M = \frac{g_o\, q_o}{g\, q} \cdot \frac{1 + k^2}{1 + k_o^2} \qquad (4a)$$

$$\text{From} \quad \frac{\beta}{\beta_o} = \frac{g}{g_o}\,\frac{I/I_o}{B/B_o}\,\frac{a_o}{a} = \left(\frac{g}{g_o}\right)^2 M\,\frac{A_o}{A} = \frac{n}{n_o}\,\vartheta\left(\frac{B_o}{B}\right)^2 \text{ (Troyon ß-scaling)} \qquad (5)$$

and a Murakami-Hugill definition of the density limit (units: 10^{20} m^{-3}, T, MA, m) (where it is assumed that the relative boundary-q is equal to the relative current-q),

$$n_e = \frac{B}{R} \cdot \frac{1}{q} M_n \left(\frac{M_n}{q} = 1.5\right), \qquad \text{hence} \quad \frac{n_e}{n_{eo}} = \frac{n}{n_o} = m\,\frac{B}{B_o}\,\frac{1}{\rho}\,\frac{q_o}{q} \qquad (6)$$

it is possible to derive a relation for the plasma current to be used in eqs. (2) and (3):

$$\frac{I}{I_o} = m\vartheta\,\frac{g_o\, q_o}{g\, q}\,\frac{A_o}{A} \qquad (7)$$

Instead of the Murakami density limit other density limit definitions have been proposed which, however, in their relation to B/B_o, ρ and q/q_o are still Murakami-like. These can be introduced by replacing m correspondingly for a given n/n_o:

For $$n_e = \frac{k\ I}{\pi\ a^2 k} M_n' \quad (M_n' = 1), \quad \text{hence} \quad \frac{n}{n_o} = m' \frac{B}{B_o} \frac{1}{\rho} \frac{g}{g_o} M \qquad (8)$$

one gets $$m' = m \frac{g_o\ q_o}{g\ q} \frac{1}{M} \qquad (8a)$$

For $$n_e = \frac{1.3.I}{\pi\ a^2 k} M_n'' \quad (M_n'' = 1), \quad \text{hence} \quad \frac{n}{n_o} = m'' \frac{B}{B_o} \frac{1}{\rho} \frac{g}{g_o} M \frac{k_o}{k} \qquad (9)$$

one gets $$m'' = m \frac{g_o\ q_o}{g\ q} \frac{1}{M} \frac{k}{k_o} \qquad (9a)$$

Using the relation (5) one has

$$m\vartheta = \rho \frac{B}{B_o} \frac{\beta}{\beta_o} \frac{q}{q_o} \qquad (10a)$$

$$m'\vartheta = \rho \frac{B}{B_o} \frac{\beta}{\beta_o} \frac{g_o}{g} \frac{1}{M} \qquad (10b)$$

$$m''\vartheta = \rho \frac{B}{B_o} \frac{\beta}{\beta_o} \frac{g_o}{g} \frac{1}{M} \frac{k}{k_o} \qquad (10c)$$

In order to meet the density limit, m, m', m" will have to take the values m*, m'*, m"* respectively based on the data of the reference design.

For the poloidal beta one has

$$\frac{\beta_{pol}}{\beta_{polo}} = \frac{g\ q\ A}{g_o\ q_o\ A_o} \qquad (11)$$

For evaluating the power-related quantities one has to distinguish between the useful density n_{DT}/n_{DTo} and the total density n/n_o. This is done by defining

$$C = \frac{\beta_{DT}}{\beta_{DTo}} \frac{\beta_o}{\beta} \qquad (12)$$

C depends somewhat on the plasma temperature. For the relative fusion power one gets

$$n = C_f \left(C \frac{n}{n_o} \vartheta \right)^2 \frac{V}{V_o} = C_f \left(C \frac{n}{n_o} \vartheta \right)^2 \rho^3 \left(\frac{A_o}{A}\right)^2 \frac{k}{k_o} \qquad (13)$$

C_f accounts for profile dependent deviations from the reference fusion power density. In this study $C_f = 1$ is used.

Using eqs. (4), (5), (7), (8) and (9), one gets

$$n\rho = \left(\frac{I\ A}{I_o\ A_o} \right)^4 \left(\frac{C}{M} \right)^2 \frac{k}{k_o} = \left(m\vartheta \frac{q_o}{q}\right)^4 \left(C \frac{\beta_o}{\beta} \frac{A_o}{A} \right)^2 \frac{k}{k_o} \qquad (14)$$

$$= \left(m\vartheta \frac{g_o\ q_o}{g\ q}\right)^4 \left(\frac{C}{M} \right)^2 \frac{k}{k_o} = (m'\vartheta)^4\ (MC)^2 \frac{k}{k_o} = (m''\vartheta)^4\ (MC)^2 \left(\frac{k_o}{k} \right)^3$$

For the relative average neutron wall loading one obtains

$$\delta \simeq \frac{\eta}{\rho^2} \frac{A}{A_o} \left(\frac{1+k_o^2}{1+k^2} \right)^{1/2} \qquad (15)$$

Eq. (14) indicates the relative outlay of a tokamak reactor (power times major radius) to be entirely dependent on the plasma-related quantities $m\vartheta$, C, q/q_o, g/g_o and k/k_o. These determine the parameters I/I_o, ρ, B/B_o and A/A_o of the so-called electromagnetic configuration and the power related quantities η and δ. This configuration can be evaluated by an iterative calculation from eqs. (2), (3), (4) and (7). So far all relations are independent of the energy confinement scaling.

To determine an INTOR-like reactor design point, a further condition is necessary, namely that the performance parameter γ^ϑ have a certain level.

$$\gamma\vartheta = C \frac{n}{n_o} \frac{\tau_E}{\tau_{Eo}} \vartheta \qquad (16)$$

That level is prescribed by the necessity of achieving a certain ignition margin. Putting that ignition margin in a simplified form yields with eq. (13)

$$m_i = \frac{P_\alpha}{P_{\alpha o}} \frac{\tau_E/\tau_{Eo}}{n/n_o . \vartheta} \frac{V_o}{V} = \eta \frac{n_o}{n} \frac{1}{\vartheta} \frac{\tau_E}{\tau_{Eo}} \frac{V_o}{V} = C^2 \frac{n}{n_o} \frac{\tau_E}{\tau_{Eo}} \vartheta = C\gamma\vartheta \qquad (17)$$

Because of eqs. (16) and (6) - or (8) or (9) - the required γ^ϑ has an impact on the choice of $m\vartheta$ (within the boundaries set by the density limit).

At this point the scaling of the energy confinement time is important. Many attempts have been made in the past to derive the dependence of the energy confinement time on the characteristics of the respective plasmas in different experimental devices. Up to now there has been no well-established

general form for such a scaling. There is even a question whether the concept of an energy confinement time would have to be modified by conditions on the plasma profiles which are not tackled in this study at all (assuming similarity of the profiles with the ones in the reference case).

One can, however, show that most τ_E-scalings known so far can be reduced to the relative form (see Appendix I)

$$\frac{\tau_E}{\tau_{Eo}} = F_\tau\left(\frac{g}{g_o}, \frac{q}{q_o}, \frac{k}{k_o}, C, M, \vartheta, \ldots\right).\left(\frac{I}{I_o}\right)^{\lambda}.\rho^{\mu}.\left(\frac{A}{A_o}\right)^{\nu} \qquad (18)$$

when applying eqs. (4), (5), (7), (12) and (17).

For example one has

for the ASDEX H-mode scaling $\quad F_\tau = 1; \quad \lambda = 1; \quad \mu = 1; \quad \nu = 0,$

for the Goldston scaling /4/ $\quad F_\tau = M; \quad \lambda = 0; \quad \mu = 1.76; \quad \nu = -0.26,$

where for the latter a continuous degradation of τ_E with the heating power $P^{-0.5}$ and $P/P_{OH} \gg 1$ is assumed. These two scalings will be applied as examples in this study in order to show the possible impact of different scalings for τ_E. The Goldston scaling as used here applies a larger numerical factor for absolute τ_E values, in agreement with /5/, and the ASDEX H-mode scaling here does not contain an isotope effect.

Eq. (18) can now be used to complete the conditions for an iterative evaluation of a consistent electromagnetic tokamak reactor configuration (characterized by I/I_o, B/B_o, ρ and A/A_o on the basis of given g/g_o, q/q_o, k/k_o, C) mentioned above. Together with eqs. (4), (5), (7) and (16) one obtains

$$\rho = m\vartheta\frac{g_o}{g}\frac{q_o}{q}\left(\frac{1}{\gamma\vartheta}\frac{C}{M}\frac{A}{A_o}\frac{\tau_E}{\tau_{Eo}}\right)^{1/2} \qquad (19)$$

which together with eqs. (2), (3), (4), (7) and (18) allows one to find, for example, for a given minimum γ^{ϑ} as required for ignition a consistent minimum-size configuration under the input conditions selected. Eq. (19) can be rewritten to include the impact of a specific τ_E-scaling:

$$\rho = \left(\frac{F_\tau}{\gamma^{\vartheta}} \frac{C}{M} \right)^{1/(2-\mu)} \cdot \left(m^{\vartheta} \frac{g_o}{g} \frac{q_o}{q} \right)^{(2+\lambda)/(2-\mu)} \cdot \left(\frac{A}{A_o} \right)^{(1+\nu-\lambda)/(2-\mu)} \qquad (20)$$

For the numerical execution of the iteration to find the configuration it is expedient to use the following form of eq. (20) for faster convergence:

$$\rho = \left(\frac{F_\tau}{\gamma^{\vartheta}} \frac{C}{M} \right)^{1/(1+\lambda-\mu-\nu)} \cdot \left(\frac{B}{B_o} M \, m^{\vartheta} \frac{q_o}{q} \right)^{(1+\nu-\lambda)/(1+\lambda-\mu-\nu)} \cdot \left(m^{\vartheta} \frac{g_o}{g} \frac{q_o}{q} \right)^{(3\lambda-2\nu)/(1+\lambda-\mu-\nu)} \qquad (20a)$$

The dependence of the reactor size on the ignition margin for a given τ_E-scaling is evident, but only after the configuration iteration.

It must be mentioned that, in order to calculate correctly the relative quantities of any INTOR alternative, the reference confinement time τ_{Eo} has to be evaluated for each τ_E-scaling. If the result is a confinement time less than that specified for the reference case, γ^{ϑ} will accordingly have to be increased above 1 for the rescaling to lead to the same ignition margin as specified in the reference, and vice versa.

The scaling relations shown here are simplified ones. They were derived on the assumption of a temperature-independent D-T fusion reaction rate $\sim <\sigma v>/(kT)^2$ which is approximately true in a temperature range $1 \leq \vartheta \leq 2$ with 10 keV as the reference temperature. Hence any of the density limits as described in eqs. (6), (8) or (9) can be accommodated - if necessary - by a temperature increase within the range mentioned. Since C is somewhat dependent on ϑ (C decreases if ϑ increases), such an increase in temperature will decrease the power density in a given configuration to some extent. As can be seen, eq. (9) constitutes the most stringent density limit and hence would require the largest temperature increase. $C = 0.11\,(2-\vartheta)+0.89$ is used here.

Once a certain electromagnetic configuration has been determined by using certain input data, the question can be asked what the impact of input data variations would be when that configuration is retained. This situation would exist in reality for any device built on certain assumptions and scalings that have hitherto been only approximately verified. The scalings mentioned for β/β_0, m, m', m" and τ_E/τ_{E0} are all described in terms of the characteristics of the electromagnetic configuration. Eq. (20) contains two quantities

$$\frac{F_\tau}{\gamma\vartheta}\frac{C}{M} \tag{20b}$$

$$m\vartheta \cdot g_0 q_0/(g \cdot q) \tag{20c}$$

consisting of input data that could be modified. If they are kept constant while their constituents are varied in an appropriate way ρ remains constant, and so also does A/A_0 when the confinement scaling is maintained. Note that the performance parameter and the ignition margin - see eqs. (16) and (17) - may change! In order to prove that the plasma current and the toroidal field also remain the same the eqs. (4), (7), (16) and (18) are combined. One finds - equivalent to eq. (20) -

$$\frac{I}{I_0} = \left(\frac{\gamma\vartheta}{F_\tau}\frac{M}{C}\right)^{1/(2+\lambda)} \cdot \rho^{(2-\mu)/(2+\lambda)} \cdot \left(\frac{A_0}{A}\right)^{(3+\nu)/(2+\lambda)} \tag{21}$$

and with eq. (4)

$$\frac{B}{B_0} = \left(\frac{\gamma\vartheta}{F_\tau}\frac{M}{C}\right)^{1/(2+\lambda)} \cdot \rho^{(1-\lambda-\mu)/(2+\lambda)} \cdot \left(\frac{A_0}{A}\right)^{(1-2\lambda+\nu)/(2+\lambda)} \cdot \frac{g_0}{g}\frac{1}{M} \tag{22}$$

Hence the electromagnetic configuration in fact remains the same, if also

$$M\frac{g}{g_0} = \frac{q_0}{q}\,\frac{1+k^2}{1+k_0^2} = \text{const.} \tag{23}$$

This expression constitutes a further quantity which - if kept constant - will leave the configuration essentially unchanged. It means for example that an increase in the value of the current-q can be compensated by a certain increase in elongation (provided that the plasma vessel provides enough space, and that the increased power for position control is available) and vice versa.

For the two confinement scalings considered here the conditions for keeping the electromagnetic configuration constant (in addition to keeping E, F, G and H constant) are

	ASDEX H-mode scaling	Goldston scaling
$\frac{F_\tau}{\gamma\vartheta}\frac{C}{M}$:	$\frac{C(\vartheta)}{M\gamma\vartheta}$! = const.	$\frac{C(\vartheta)}{\gamma\vartheta}$! = const.
$m\vartheta\frac{g_o\ q_o}{g\ q}$:	---------- $m\vartheta\frac{g_o\ q_o}{g\ q}$! = const.	----------
$M\frac{g}{g_o}$:	------- $\frac{q_o}{q}\ \frac{1+k^2}{1+k_o^2}$! = const.	----------

A difference due to the different functions F_τ is, for example, that with Goldston scaling a change in g/g_o corresponds to a change in density at constant temperature with the performance parameter remaining constant, while with ASDEX scaling the performance parameter increases if g/g_o increases. Independently of the confinement scaling, a change in g/g_o implies a change in margin compared with the density limit. If the design point always has to correspond to the respective density limit, a change in g/g_o implies different electromagnetic configurations, where an increase in g/g_o leads to somewhat larger size.

On the basis of the relations described above the rescaling procedure is as follows:

- Select the input data: g/g_o, q/q_o, k/k_o, $C(\vartheta)$, ϑ, E, F, G, H, B_{max}/B_{maxo}

- According to the confinement scaling evaluate τ_{Eo} and select γ^{ϑ} to achieve, for example, the same ignition margin as in the reference.

- Iteration: calculate ρ from eq. (20a) with $B/B_o = 1$, $\vartheta = 1$ and m from eqs. (6), (8) or (9) as starting data using eqs. (2), (3) and (7). Iterate by varying m^{ϑ} until the results of eqs. (3) and (4) coincide. Note that for cases where $1 + \nu - \lambda \neq 0$, a double iteration is necessary, as can be understood from eq. (20a); results are A/A_o, m^{ϑ}, B/B_o, ρ, γ^{ϑ}, m_i; calculate I/I_o from eq. (7), η and δ from eqs. (14) and (15), β/β_o from eq. (5), β_{pol}/β_{polo} from eq.(11), the alternative parameters for the density limit according to the definitions of eq. (8a) and (9a). Finally an adjustment of the plasma temperature can follow in order to accommodate the respective density limit m*, m'* or m"* . If according to the density limit scaling selected the reference density turns out to be too large, ϑ has to be increased accordingly. Since $C(\vartheta)$ decreases with increasing some power reduction will occur with the electromagnetic configuration remaining constant. For m_i = const. the configuration will change somewhat with ϑ.

- If the electromagnetic configuration including k/k_o and the selected confinement scaling is kept the operating range of any configuration can generally be evaluated by changing g/g_o, C, γ^{ϑ} so that the quantities (20b) and (20c) remain constant for a certain range of parameter variation. For example, g/g_o could improve by cross section shaping, C by impurity reduction and control, and γ^{ϑ} by profile control; the ignition margin will also change and limit the operating range.

- In a similar way the condition (23) shows a possibility of adjustment within generally the same configuration; in practice, however, it may just serve for compensation of a variation in q/q_o by some variation in elongation.

The results can also be used for evaluating the overall outlay, e.g. by means of relative estimated direct capital cost /6/ assuming similar design configurations for all data sets considered.

3. Limitations with impact on accessible parameter range

Rescaling of INTOR - and of possible later steps in a similar way - must aim at a minimum outlay/size device for a desired performance. Limitations to reducing the device size are imposed by (reference: INTOR Phase IIA Part I)

- a maximum g/g_0 of 0.6-0.7 (some increase may be achieved by shaping)
- a minimum q/q_0 of 1 (may change somewhat in either direction)
- a maximum k/k_0 of 1.25 (an increase to $k/k_0 = 1.375$ may be tolerable)
- a maximum C of 1 (some increase may be achievable)
- a maximum m of $0.86 \cdot q/q_0$
- a maximum m' of 0.78
- a maximum m" of 0.63
- a maximum ϑ of 2 (for keeping the scaling approximately valid)
- a minimum γ^{ϑ} of 0.95 for ASDEX H-mode scaling and C = 1 ($\gamma^{\vartheta}C=m_i=$const.) corresponding to $n_i \tau_E = 1.5 \cdot 1.96 \cdot 10^{20}$ m^{-3} s at 10 keV (ignition margin 1.5)
- a minimum γ^{ϑ} of 2.26 for Goldston scaling and C = 1 ($\gamma^{\vartheta}C=m_i=$const.) corresponding to $n_i \tau_E = 1.96 \cdot 10^{20}$ m^{-3} s at 10 keV (ignition margin 1)
- a minimum E of 0.40)
- a minimum F of 0.25) This is the standard set of geometry factors
- a minimum G of 0.26) used in this study.
- a minimum H of 0.07)

  All geometry factors may be changed somewhat.
  Geometry factors for existing INTOR designs are, for example,
  Phase IIA Part 1: $E_0/F_0/G_0/H_0 = 0.45/0.27/0.28/0.08$
  Phase IIA Part 2: E /F /G /H = 0.40/0.24/0.26/0.06
- a maximum B_{max}/B_{max0} of 1 (may be changed somewhat)
- a minimum δ of 0.77 (there is also an upper limit at $\delta \simeq 1$ for wall lifetime with present technology)
- a maximum $\Delta B/\Delta B_0$ of 1 (may be increased)

No distinction is made in this study between a possible limiter or divertor version of INTOR.

4. Results

The results of iterative evaluations for INTOR alternatives with INTOR as of Phase IIA Part One as reference case are mainly described in their dependence on the major radius as the quantity that characterizes the device size and outlay. The resulting figures are to be compared with the limitations listed in Section 3.

4.1 Overview

Looking at a somewhat wider parameter range than finally turns out to be relevant for INTOR alternatives Figs. 2 and 3 give the achievable neutron wall load as a function of ρ with the density limit definitions m, m' and m" and the plasma current $I/I_0 = 1.563$ (corresponding to 10 MA) indicated as limitations and for orientation, respectively. It was found practical to select discrete values for elongation and to plot $\delta(\rho)$ for a certain range of γ^{ϑ} (above an ignition margin of 1 for Goldston scaling in Fig. 2 and above an ignition margin of 1.5 for ASDEX H-mode scaling in Fig. 3). In order to prevent the plots from appearing congested the temperature range was restricted to $1 = \vartheta = 1.5$, which, however, is sufficient for showing the impact of the different density limit definitions. The results, of course, refer only to the set of input parameters indicated. The impact of varying the input assumptions will be shown in section 4.3.

In both Figs. 1 and 2 sections of the same curves $\delta(\rho)$ appear, but with different scales for the performance parameter γ^{ϑ} and the ignition margin. They show the typical size reduction with increasing elongation. The dependence of the wall loading on elongation/major radius at a fixed performance parameter or for a given ignition margin is, however, completely different. While Goldston scaling tends to result in a roughly constant wall load vs. major radius in the range considered for a certain ignition margin, ASDEX H-mode scaling leads to strongly decreasing wall load with increased

major radius for any fixed ignition margin (see Fig. 4). For Goldston scaling the ignition margin has to be close to 1 for getting close to the reference INTOR parameters, while for ASDEX H-mode scaling the ignition margin would be around 2. That margin might cover the possible degradation of confinement - if present - which is not contained in that scaling.

It is interesting to identify a design point with a major radius as of Phase IIA Part Two (ρ = 0.943). Figs. 2 and 3 indicate for an elongation of 2.2 the same design point at the m" density limit for ϑ = 1.2 and δ = 0.99. The respective Goldston and ASDEX H-mode ignition margins are 1.07 and 2.12. The plasma current is somewhat above 9 MA. Depending on which density limit definiton would be valid and which confinement scaling applies, the possibilities to use a notably smaller elongation appear very much restricted for an INTOR-size device, given the present input assumptions. Already for an elongation of 2 the size for the same wall load of δ = 0.99 increases to ρ = 1.05 and the plasma current exceeds 10 MA (always at the m" density limit).

In general, m" is the most restrictive density limit definition, whereas m allows some more margin. For elongations above 2 the limit m' practically does not impose any restriction. Besides the fact that for elongations below 2 INTOR-like configurations comparable in outlay cannot be found any more, in that range m" may require to go beyond ϑ = 1.5 and m' becomes more restrictive than the density limitation by m. The situation of the design points with respect to the fixed density limits m*, m'* and m"* is shown in Figs. AII.1 through AII.6 of Appendix II, from which the parametric representation of the density limits in Figs. 2 and 3 was taken.

4.2 High-elongation design points

Figures 2 and 3 suggest looking in a more detailed manner into the alternatives for elongations beyond 2 and up to 2.2. For that purpose Figs. 5 and 6 plot the wall load, the plasma current and the density characteristics vs. ρ, for elongations of 2.1 and 2.2 respectively. The design points are all meant for an ignition margin of 1 for Goldston scaling, since that scaling provides the more pessimistic confinement times. The pertaining ignition margin for ASDEX H-mode scaling is also shown.

Figure 5 indicates that for the major radius as of Phase IIA Part Two no design point can be found, not even for the less restrictive Murakami density limit. This holds for an elongation of 2.1. The influence of raising g/g_o for the same configuration is seen in an increased wall load and a further shift of the density limitations towards larger major radii. For an elongation of 2.2 as assumed for Fig. 6 the situation appears more relaxed concerning the density limitations. For the Phase IIA Part Two major radius device there is now even some margin in density.

4.3 Principal impact of varying the input data

Table 1 lists 20 cases, including the basic cases 1 and 2 which can serve for comparison since they are close to INTOR as of Phase IIA Part Two. In order to show the influence of a temperature variation in the range $1 \leqq \vartheta \leqq 2$, pairs of data sets are given for each variation referring to those extreme temperature values. It can be shown that the restriction due to the density limitation m"* is always found between those extreme values for the pairs mentioned (with the exception of case 17 through 18). The main tendencies are illustrated by plotting the wall loading, the plasma current, the fusion power and the estimated relative direct capital cost figures versus the major radius (Figs. 7 through 10). All the design points have an ignition margin of one based on Goldston scaling. Table 1 also gives the ignition margins based on ASDEX H-mode scaling, which turn out to be between 1.58 and 2.52, hence far more optimistic than for Goldston scaling. (One has to take into account, however, that the ASDEX H-mode scaling does not contain any confinement degradation from heating, which might translate into lower ignition margins.)

The modifications introduced are as follows:

- Cases 3 and 4 show the same configurations as 1 and 2 but are for $g/g_o = 0.7$, which corresponds to a g-factor of about 4.
- Cases 5, 6 and 7, 8 are for a 10% decrease and a 10% increase in maximum toroidal field where the current density in the magnets decreases and increases roughly with the field variation.
- Cases 9, 10 and 11, 12 are for a 10% decrease and a 10% increase of all radial component dimensions, which means a corresponding increase and

decrease, respectively, in current density of the magnets and in their radiation dose.

- Cases 13, 14 are for roughly constant magnet current density with an increased radiation dose, whereas cases 15, 16 refer to an again roughly constant magnet current density at a larger field level and a lower radiation dose.
- Cases 17, 18 show the impact of lowering the current-q when keeping the elongation at $k/k_0 = 1.375$ as for all cases so far, while cases 19, 20 imply that the reduction of q is used to decrease the elongation to such a value that the configurations (except for the elongation) of cases 1, 2 are reproduced.

The main findings from this kind of representation are:

- Cases 9/10 and 13/14 as well as cases 11/12 and 15/16 deviate most from the basic cases 1/2. They are therefore not further considered here.
- All the other cases cluster around the basic cases, although in a considerable range. The general tendencies seen are the following: The neutron wall load is somewhat lower than the reference value, the plasma current can be kept below the 10 MA level, the power can be about the reference value and the cost might be about 10% larger than in Phase IIA Part 1.
- The temperature level has a strong impact on some parameters such as plasma current, power and cost. Hence the introduction of the specific density limit scaling that will determine the temperature level is essential. This is done in section 4.4.

4.4 Accessible INTOR design points at the density limit with fixed ignition margin

4.4.1 GOLDSTON scaling

For a more systematic overview and orientation within the interesting parameter space a further series of plots is shown where the same ignition margin as in the reference case (Goldston ignition margin 1) and a density corresponding to the density limit m"* are valid throughout. The latter

condition, which is the most stringent one among the three scalings mentioned previously, is attained by appropriately increasing the plasma temperature. All quantities are again plotted versus the major radius. On the basis of the standard set of geometry factors 0.4/0.25/0.26/0.07, which is very close to INTOR Phase IIA Part 2 conditions, the influence of varying the geometry by an overall variation of this set of factors is shown together with a variation in maximum toroidal field for two values of elongation, namely 2.1 and 2.2. These values of elongation were selected according to the findings of section 4.1. The effect of increasing possibly g/g_0 to 0.7 was also looked for. The variation of geometry and maximum toroidal field in a plot of a/a_0 versus ρ provides a "window" of reasonably attainable design points on which to project parametric curves for the other design parameters of interest such as the plasma currrent, beta, the neutron wall load, the fusion power and the cost.

Comparing Figs. 11 and 12 for k = 2.1 and 2.2, one sees that within the range of interest for the neutron wall load between 1 and 1.3 MW/m^2 and above a beta of 4.9% (which is the Phase IIA Part 2 value) the lower elongation would give the possibility of maintaining major and minor plasma radii at about the reference values with near Phase IIA Part 2 geometry factors and a slightly reduced maximum toroidal field. The plasma current remains below 10 MA and the cost would be about 20% larger than for the reference case. At a 10% larger minor radius the previous beta of 5.6% could be reached. In that case some additional reduction in geometry and in field would be required. The plasma current would increase beyond 10 MA as would the relative cost beyond 1.2. If the elongation were increased to 2.2, the Phase IIA Part 2 large plasma radius could be reached at a minor radius reduced by 10%, again for the Phase IIA Part 2 geometry factors and a slightly reduced maximum toroidal field with an even lower plasma current (about 9 MA) and lower fusion power than in the first case. Consequently the cost is also lower, namely about 5% larger than in the reference case. If within the "window" of reasonably attainable design points the case for $a/a_0 = 1$ is looked at, one finds a plasma current larger than 10 MA and a reduced major radius, a beta value beyond 5.6%, an increased fusion power and cost increased by about 15%.

Comparing the two figures with respect to the electromagnetic configuration (dimensions, plasma current) one finds that the impact of increasing elongation is similar to increasing the maximum toroidal field, and that the level of plasma current in a/a_0-ρ-space is practically fixed for fixed g/g_0. The cost level is mainly determined by a/a_0 and decreases somewhat with increasing elongation. Note that all design points shown are of minimum size in the sense that they all have the same ignition margin as INTOR Phase IIA Part 1 but expressed in terms of the Goldston scaling with continuous confinement degradation according to alpha power.

Essential findings are the following:

- With the INTOR Phase IIA Part 2 like set of geometry factors the elongation can be chosen approximately at 2.1 in order to restrict the outlay to about 1.2 times the reference cost.
- Within that range the neutron wall load can be kept between 1 and 1.3 MW/m^2, the plasma current can be lower than 10 MA and beta can remain above 4.9%, the major radius at about 5.3 m.
- A more challenging possibility is to increase the elongation to 2.2 which shifts the major radius to typically 5 m. The plasma current can be close to 9 MA. An increase in current and minor radius, which implies a reduction in geometry factors - hence advanced engineering compared with Phase IIA Part 2 - would allow one to attain the original beta of 5.6%. The associated increase in neutron wall load, however, would be small.
- These results are based on assuming a density limit $\sim 1.3 \times j$. If Murakami scaling is taken the results are slightly more favourable (Fig. 13).
- The alternative of increasing the maximum toroidal field and the geometry factors in general leads to very low beta, which makes such alternatives irrelevant despite their low current and outlay.

With constant Goldston ignition margin

- the achievable neutron wall load decreases with increasing major radius,
- the level of estimated cost increases essentially with increasing minor plasma radius.

Further Figs. 14 through 27 show the pertaining dependences of the individual quantities on ρ, generally for two values of g/g_0.

Figs. 11a and 12a indicate that the "window" remains almost the same when changing g/g_0 to 0.7, but keeping the elongation. The plasma current increases somewhat, but the fusion power and hence the neutron wall loading rise strongly.

For INTOR an increase in g/g_0 above 0.6 if achievable, might thus be considered as safety margin rather than be fully exploited. A similar argument can be made for the density limit in case the threshold m"* could be made somewhat larger than assumed.

4.4.2 ASDEX-H-mode scaling

A similar overview can be provided in comparison for ASDEX H-mode scaling. The pertaining results with $g/g_0 = 0.6$ are shown in Figs. 28 through 35. For that scaling the "window" has been defined such that the respective design points for the two elongations for standard geometry and $B_{max}/(B_{maxo}) = 1$ are the same for the two confinement scalings. This definition leads to the values of the ignition margins for ASDEX H-mode scaling: 2.131 for $k/k_0 = 1.3125$ and 1.931 for $k/k_0 = 1.375$. For ASDEX H-mode scaling the appearance of the a/a_0 vs. ρ plots (Figs. 28 and 29) is notably changed compared with that for Goldston scaling.

The window of accessible design points compared with the case of Goldston scaling is stretched in the ρ-direction and somewhat squeezed in the a/a_0-direction, the lines for B_{max}/B_{maxo} = const. being rotated. The lines of constant β/β_0 are very nearly the same for the same elongation, whereas the lines of constant I/I_0 are in a similar position, but somewhat rotated.

The same design points as discussed in section 4.4.1 can of course be found in the ASDEX H-mode based diagrams.

The essential findings are thus the same, but with the difference, that with constant ASDEX H-mode ignition margin

- the achievable neutron wall load decreases with both increasing major and increasing minor radius,

- the level of estimated cost increases mainly with increasing major plasma radius,
- the fusion power is a function of the major radius only. Hence parametric curves in the a/a_0 vs. ρ diagram for η do not exist. This can be proved by combining eqs. (45) and (20).

Furthermore Figs. 30 through 35 show the pertaining dependences of the individual quantities for $g/g_0 = 0.6$.

5. Conclusions

On the basis of a standard geometry close to that of INTOR Phase IIA Part 2 and by means of a simplified rescaling procedure it could be shown that for the input assumptions as used here and based on /3/

- an elongation in the range of 2.1 to 2.2 is needed in order to attain attractive parameter sets not too far in outlay from the INTOR reference case, when applying Goldston scaling with an ignition margin of 1 or ASDEX H-mode scaling with an ignition margin of about 2 (not taking into account an isotope effect), and keeping the m" density limit by temperature adjustment;
- the plasma current can be kept below 10 MA under such conditions;
- a minor plasma radius reduction allows one to keep the major radius as in INTOR Phase IIA Part 2, a corresponding data set with $k = 2.2$ being shown in Table 2 as an example; alternative data sets with $k = 2.1$ retain the reference major radius;
- using the two confinement scalings for finding a common range of accessible data sets for each elongation, respectively, leads to rather narrow domains in a/a_0 vs. ρ. Figures 36 and 37 show those domains. If the standard geometry is taken, it is obvious that lowering the elongation would mean further increase in cost and decrease of β/β_0 below the Phase IIA Part 2 level. For the design points indicated see also Table 3;
- the necessary temperature increase for keeping the density limit is smaller if the elongation is larger.

6. Acknowledgements

The author extends special appreciation to Mrs. Claudia Alberter for doing much of the numerical evaluation and for the layout of the report including the tables and figures.
He had the opportunity of discussing results presented in this report in the European INTOR/NET steering committee and with colleagues at IPP.

7. References

/1/ A.F. Knobloch, Report IPP 4/220, Max-Planck-Institut für Plasmaphysik, Garching, March 1985

/2/ INTOR Phase Two A Part 1 report STI/PUB/638 IAEA Vienna, December 1983

/3/ INTOR Phase Two A Third Part, Conclusions from the 13th workshop meeting, EURFUBRU/XII-52/86/EDV14, Brussels, March 1986

/4/ R.J. Goldston, Plasma Physics and Contr. Fusion, Vol. 26, No. 1A, p. 93, Pergamon 1984

/5/ P.R. Thomas, Europhysics Abstracts, Vol. 10C, Part 1, p. 37, EPS 1986

/6/ A.F. Knobloch, Report IPP 4/185, Max-Planck-Institut für Plasmaphysik, Garching, January 1980

/7/ INTOR Phase Two A, Part 2, report STI/PUB 714, IAEA Vienna, January 1986, p. 494.

Table 1: Compilation of INTOR alternative design points demonstrating impact of modifications in input data (k/k_o = 1.375)
GOLDSTON scaling: ignition margin 1

No.	ϑ	$\gamma\vartheta$	$\frac{\gamma\vartheta ASD.}{ign.m.}$	$\frac{m\vartheta}{m}$	A/A_o	I/I_o	δ	ρ	a/a_o	B/B_o	η	β/β_o	$\frac{\beta pol}{\beta polo}$	$\beta-\beta_{DT}$ (%)	$\frac{m'\vartheta}{m'}$	$\frac{m''\vartheta}{m''}$	$\frac{cost}{cost_o}$	$\frac{g}{g_o}$	$\frac{q}{q_o}$	dim.	$\frac{B max}{B max_o}$	Remarks
1	1	2.261	1.2097 / 1.9031	0.8632 / 0.8632	1.089	1.321	0.914	0.902	0.828	1.060	0.874	0.903	0.654	1.355	0.526 / 0.526	0.723 / 0.723	0.959	0.6	1.0	1.0	1.0	
2	2	2.540	1.4812 / 2.0771	0.9902 / 0.4951	1.061	1.555	0.929	0.988	0.931	1.081	1.094	0.928	0.637	1.810	0.604 / 0.302	0.830 / 0.415	1.175	0.6	1.0	1.0	1.0	
3	1	2.261	1.4090 / 2.2201	1.0071 / 1.0071	1.089	1.321	1.244	0.902	0.828	1.060	1.189	1.054	0.763	1.581	0.614 / 0.614	0.844 / 0.844	1.026	0.7	1.0	1.0	1.0	large wall load,
4	2	2.540	1.7284 / 2.4238	1.1553 / 0.5777	1.061	1.555	1.265	0.988	0.931	1.081	1.490	1.082	0.743	2.111	0.704 / 0.352	0.968 / 0.484	1.259	0.7	1.0	1.0	1.0	high β
5	1	2.261	1.2344 / 1.9450	0.8918 / 0.8918	1.023	1.453	0.778	0.973	0.951	0.952	0.923	0.962	0.614	1.444	0.544 / 0.544	0.747 / 0.747	1.073	0.6	1.0	1.0	0.9	large I/I_o, low
6	2	2.540	1.5076 / 2.1141	1.0227 / 0.5114	0.998	1.708	0.784	1.069	1.071	0.970	1.150	0.986	0.599	1.924	0.623 / 0.312	0.857 / 0.429	1.325	0.6	1.0	1.0	0.9	wall load
7	1	2.261	1.1808 / 1.8605	0.8380 / 0.8380	1.156	1.209	1.051	0.844	0.730	1.166	0.829	0.852	0.693	1.278	0.511 / 0.511	0.702 / 0.702	0.873	0.6	1.0	1.0	1.1	low I/I_o, small a/a_o,
8	2	2.540	1.4530 / 2.0376	0.9616 / 0.4808	1.123	1.427	1.075	0.922	0.821	1.190	1.042	0.876	0.674	1.709	0.586 / 0.293	0.806 / 0.403	1.062	0.6	1.0	1.0	1.1	low β
9	1	2.261	1.4439 / 2.2751	0.8905 / 0.8905	0.975	1.523	1.196	0.828	0.849	1.065	1.078	1.010	0.585	1.515	0.543 / 0.543	0.746 / 0.746	0.990	0.6	1.0	0.9	1.0	large I/I_o, large wall
10	2	2.540	1.7685 / 2.4800	1.0214 / 0.5107	0.950	1.792	1.212	0.908	0.956	1.085	1.348	1.036	0.570	2.022	0.623 / 0.312	0.856 / 0.428	1.225	0.6	1.0	0.9	1.0	load, small ρ
11	1	2.261	1.0280 / 1.6197	0.8393 / 0.8393	1.206	1.160	0.718	0.974	0.808	1.055	0.723	0.816	0.723	1.225	0.512 / 0.512	0.703 / 0.703	0.948	0.6	1.0	1.1	1.0	low I/I_o, low wall load,
12	2	2.540	1.2621 / 1.7699	0.9629 / 0.4815	1.173	1.368	0.731	1.066	0.909	1.077	0.907	0.839	0.704	1.636	0.587 / 0.294	0.807 / 0.404	1.152	0.6	1.0	1.1	1.0	low β
13	1	2.261	1.4738 / 2.3222	0.9199 / 0.9199	0.915	1.675	1.015	0.894	0.977	0.956	1.136	1.075	0.549	1.613	0.561 / 0.561	0.771 / 0.771	1.112	0.6	1.0	0.9	0.9	large I/I_o, high β
14	2	2.540	1.7986 / 2.5222	1.0548 / 0.5274	0.893	1.968	1.021	0.983	1.101	0.974	1.415	1.102	0.536	2.149	0.643 / 0.322	0.884 / 0.442	1.385	0.6	1.0	0.9	0.9	
15	1	2.261	1.0039 / 1.5818	0.8147 / 0.8147	1.279	1.062	0.823	0.912	0.713	1.161	0.686	0.770	0.767	1.154	0.497 / 0.497	0.683 / 0.683	0.866	0.6	1.0	1.1	1.1	low I/I_o, small a/a_o,
16	2	2.540	1.2366 / 1.7341	0.9350 / 0.4675	1.243	1.254	0.844	0.996	0.801	1.185	0.863	0.792	0.746	1.545	0.570 / 0.285	0.784 / 0.392	1.045	0.6	1.0	1.1	1.1	low β
17	1	2.261	1.0596 / 1.6695	0.7518 / 0.7518	1.162	1.198	0.862	0.838	0.721	1.060	0.668	0.941	0.628	1.411	0.458 / 0.458	0.630 / 0.630	0.816	0.6	0.9	1.0	1.0	low I/I_o, small a/a_o
18	2	2.540	1.3045 / 1.8293	0.8627 / 0.4314	1.130	1.414	0.883	0.916	0.811	1.082	0.840	0.968	0.610	1.888	0.526 / 0.263	0.723 / 0.362	0.991	0.6	0.9	1.0	1.0	
19	1	2.261	1.2078 / 1.9030	0.7769 / 0.7769	1.089	1.321	0.904	0.902	0.828	1.060	0.819	0.903	0.588	1.355	0.526 / 0.526	0.678 / 0.678	0.948	0.6	0.9	1.0	1.0	k/k_o = 1.289
20	2	2.540	1.4813 / 2.0772	0.8912 / 0.4556	1.061	1.556	0.918	0.988	0.931	1.081	1.026	0.928	0.573	1.810	0.604 / 0.302	0.778 / 0.389	1.161	0.6	0.9	1.0	1.0	k/k_o = 1.289

+

performance parameter ASDEX H-mode
ignition margin ASDEX H-mode

Table 2: Evolution of the INTOR design parameters

Phase	0	I	IIA-1	IIA-2	IIA-3		
year	1979	1980/81	1981/82	1984/85	1986/88		
					input	examples	
R (m)	5.2	5.3	5.3	5.0		5.00	5.3 - 5.3
a (m)	1.3	1.2	1.2	1.2		1.07	1.18 - 1.2
k	1.6	1.6	1.6	1.6	2.0	2.2	2.1 - 2.1
b (m)	2.08	1.92	1.92	1.92		2.36	2.49 - 2.51
A	4.00	4.42	4.42	4.17		4.67	4.48 - 4.43
ß (%)	5	5.6	5.6	4.9		5.2	5.0 - 5.1
$ß_{DT}$ (%)		4.1	4.1	4.1		3.7	3.6 - 3.7
g (ß-scal.)				4.0	3.5	3.5	3.5 3.5
$ß_{pol}$		2.6	2.6	1.5		1.65	1.58 - 1.57
$M_{Murakami}$	16	17.5	17.5	16.5	15	13.3	12.8 - 15
T_i (keV)	10	10	10	10	10-20	11.9	12.7 - 10.6
$n_{DT}(10^{20}m^{-3})$	1.3	1.4	1.4	1.4		1.12	1.02 - 1.19
τ_E (s)		1.4	1.4	1.4		1.51	1.56 - 1.57
B (T)	5.5	5.5	5.5	5.5		5.6	5.7 - 5.5
q_I		2.1	2.1	1.8	2.1	2.1	2.1 2.1
I (MA)	6.4	6.4	6.4	8.0	$\sim$ 10	9.0	9.7 - 9.6
P (MW)	620	620	620	585		576	675 - 654
p_w (MW/m^2)	1.3	1.3	1.3	1.3		1.1	1.2 - 1.1

Remarks: In the sequence of numbers for any parameter those data are underlined that are changed with respect to the previous ones. The examples given for possible alternative data sets refer to the m" density limit except for the last column which implies the m (Murakami) density limit.
$M_{Murakami}$ is given in the units 10^{19} m^{-2} T^{-1}

Table 3: Data sets as calculated using the rescaling procedure: INTOR and alternative design points

INTOR	geom.f.	$\frac{B_{max}}{B_{maxo}}$	ϑ	C	$\frac{k}{k_o}$	$\frac{g}{g_o}$	$\frac{q}{q_o}$	$\frac{ign.G}{ign.A}^{+}$	$\gamma\vartheta$	$\frac{m\vartheta}{m}$	$\frac{A}{A_o}$	$\frac{I}{I_o}$	δ	ρ	$\frac{a}{a_o}$	$\frac{b}{b_o}$	$\frac{B}{B_o}$	η	$\frac{\beta}{\beta_o}$	$\frac{\beta_{pol}}{\beta_{polo}}$	$\beta-\beta_{DT}$ (%)	$\frac{m'\vartheta}{m'}$	$\frac{m''\vartheta}{m''}$	$\frac{cost}{cost_o}$
I = IIA-1	0.447 0.270 0.283 0.083	1.000	1.000	1.000	1.000	1.000	1.000	$\frac{0.442}{1.576}$	1.000	$\frac{1.000}{1.000}$	1.000	1.000	1.000	1.000	1.000	1.000	1.000	1.000	1.000	1.000	1.500	$\frac{1.000}{1.000}$	$\frac{1.000}{1.000}$	1.000
IIA-2	0.402 0.243 0.264 0.064	1.000	1.000	1.143	1.000	0.700	0.850	$\frac{0.681}{2.121}$	1.540	$\frac{0.701}{0.701}$	0.943	1.249	1.000	0.944	1.000	1.000	1.001	0.944	0.873	0.561	0.798	$\frac{0.701}{0.701}$	$\frac{0.701}{0.701}$	1.008
IIA-3 examp.	0.400 0.250 0.260 0.070	0.959	1.185	0.980	1.375	0.600	1.000	$\frac{1.000}{1.951}$	2.308	$\frac{0.896}{0.756}$	1.057	1.413	0.860	0.944	0.893	1.228	1.019	0.929	0.931	0.634	1.474	$\frac{0.546}{0.461}$	$\frac{0.751}{0.634}$	1.038
IIA-3 examp.	0.400 0.250 0.260 0.070	0.967	1.266	0.971	1.375	0.600	1.000	$\frac{1.000}{2.147}$	2.329	$\frac{0.925}{0.731}$	1.014	1.521	0.896	1.000	0.986	1.294	1.028	1.089	0.900	0.608	1.457	$\frac{0.609}{0.481}$	$\frac{0.799}{0.631}$	1.174
IIA-3 examp.	0.400 0.250 0.260 0.070	0.943	1.062	0.993	1.375	0.600	1.000	$\frac{1.000}{2.121}$	2.277	$\frac{0.907}{0.854}$	1.003	1.507	0.858	1.000	0.997	1.309	0.998	1.055	0.909	0.602	1.389	$\frac{0.597}{0.562}$	$\frac{0.784}{0.738}$	1.159

+ $\frac{\text{ignition margin GOLDSTON}}{\text{ignition margin ASDEX H-mode}}$

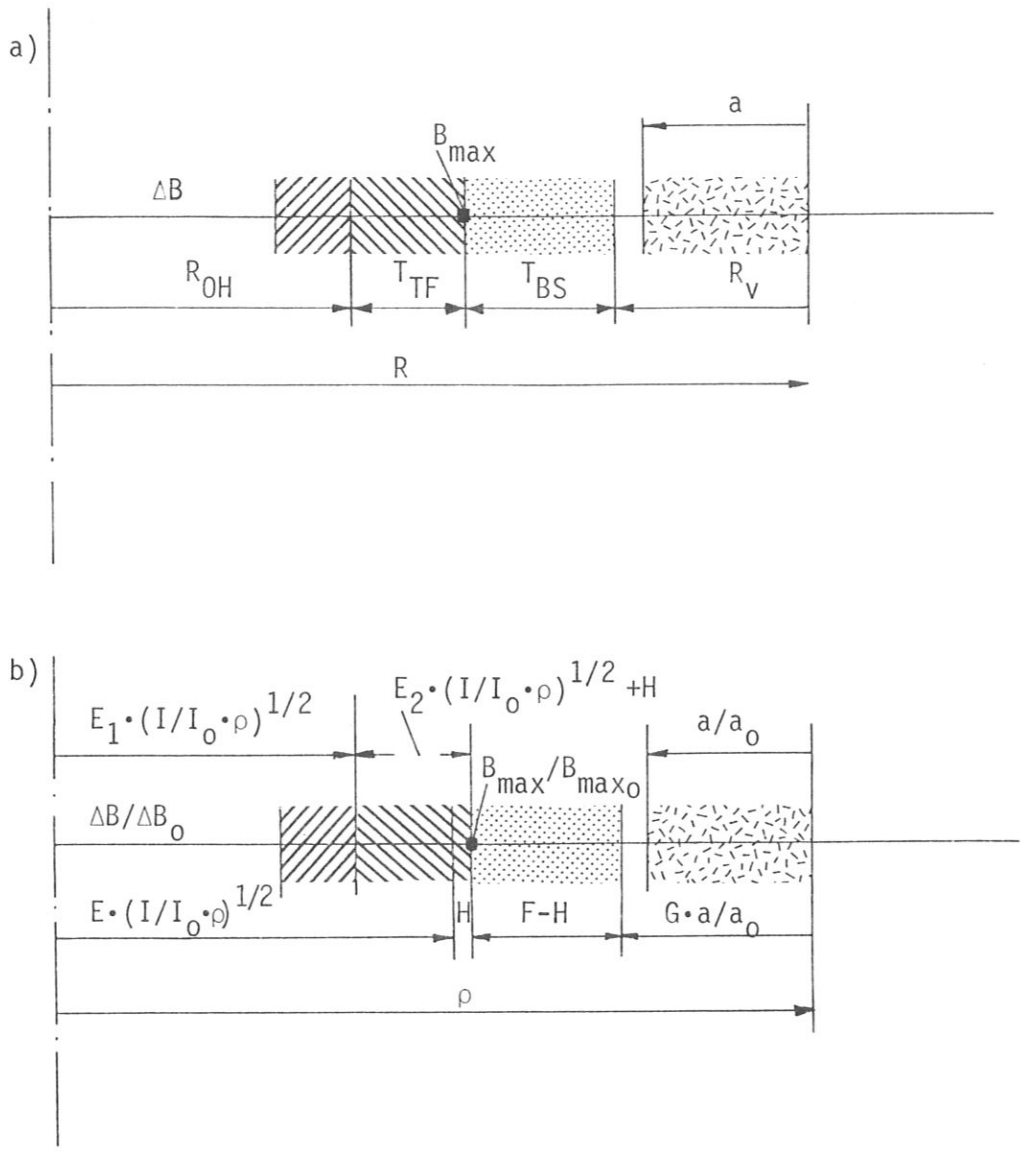

Fig. 1: Radial build of a tokamak reactor (schematic)
a) in absolute dimensions
b) in relative dimensions

GOLDSTON scaling

Ref.: INTOR Phase IIA Part One

$B_{max}/B_{maxo} = 1.0$

$q/q_o = 1.0$

$g/g_o = 0.6$

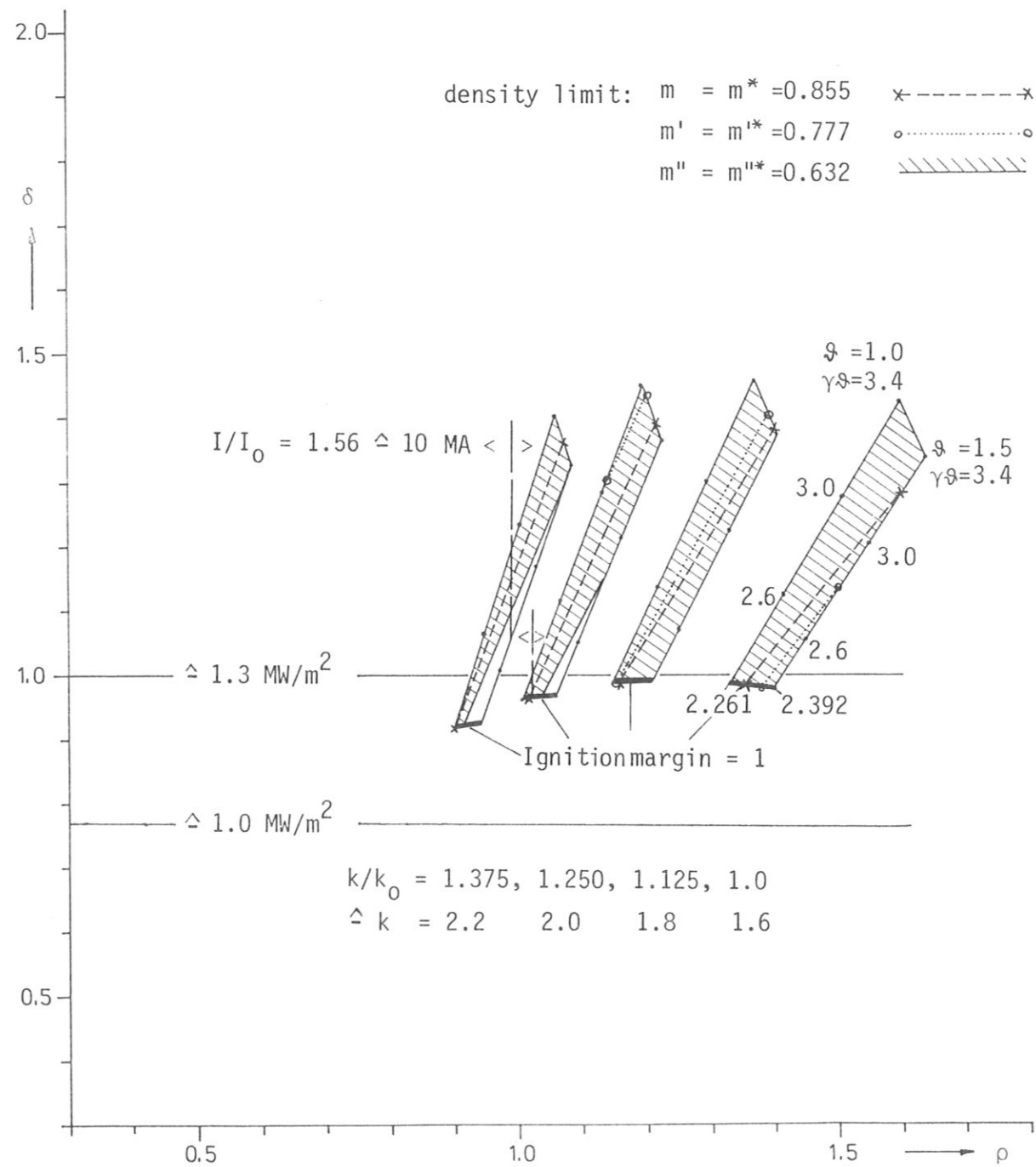

Fig. 2: Achievable neutron wall load vs. major radius (performance parameter $\gamma\vartheta$ for GOLDSTON scaling) for different elongations in a temperature range $1 < \vartheta < 1.5$. Hatched regions are forbidden according to density limit m"*.

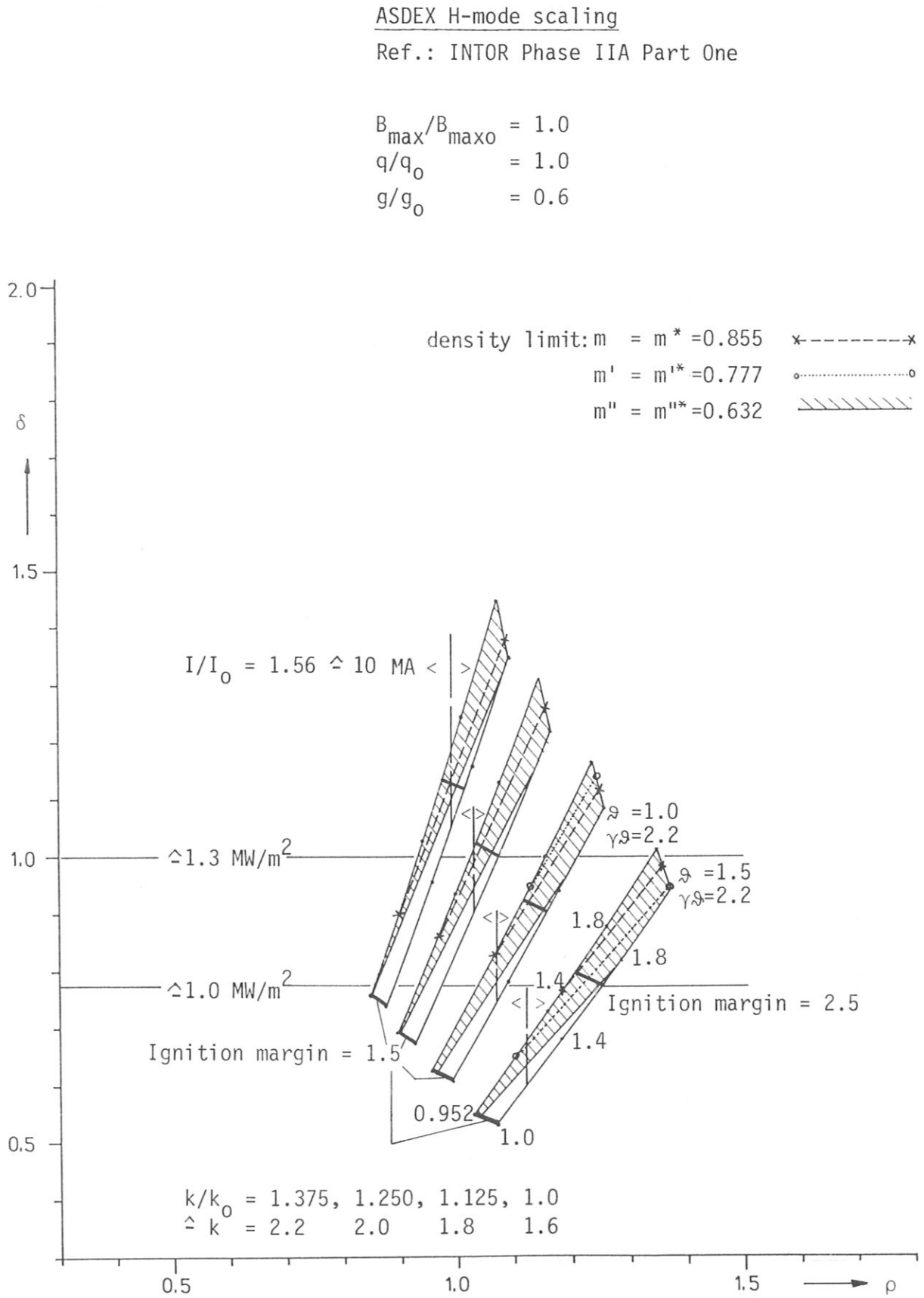

Fig. 3: Achievable neutron wall load vs. major radius (performance parameter $\gamma\vartheta$ for ASDEX H-mode scaling) for different elongations in a temperature range $1 < \vartheta < 1.5$. Hatched regions are forbidden according to density limit m"*.

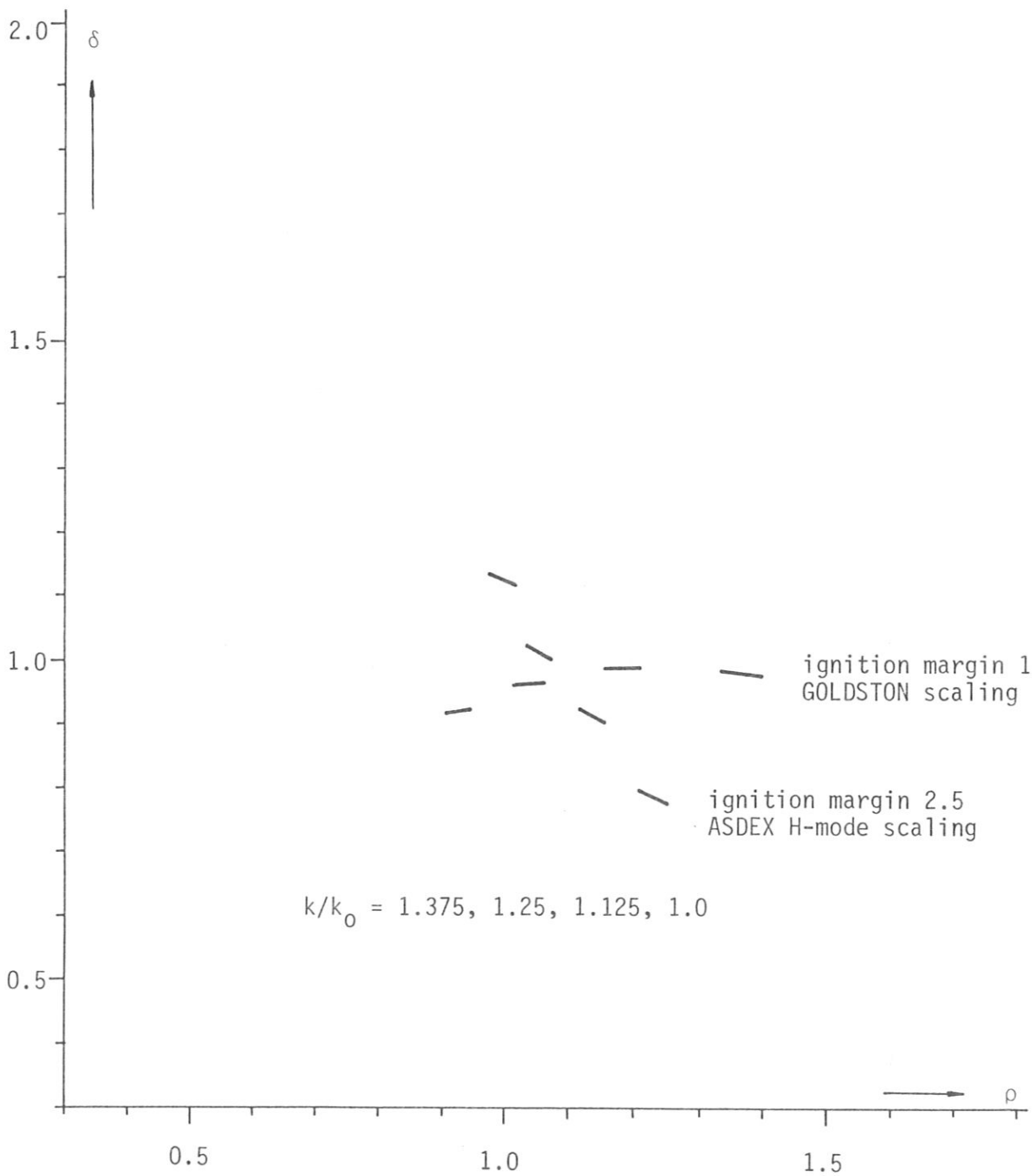

Fig. 4: Achievable neutron wall load vs. major radius for fixed ignition margins at different elongations assuming GOLDSTON and ASDEX H-mode scaling (see Figs. 2 and 3)

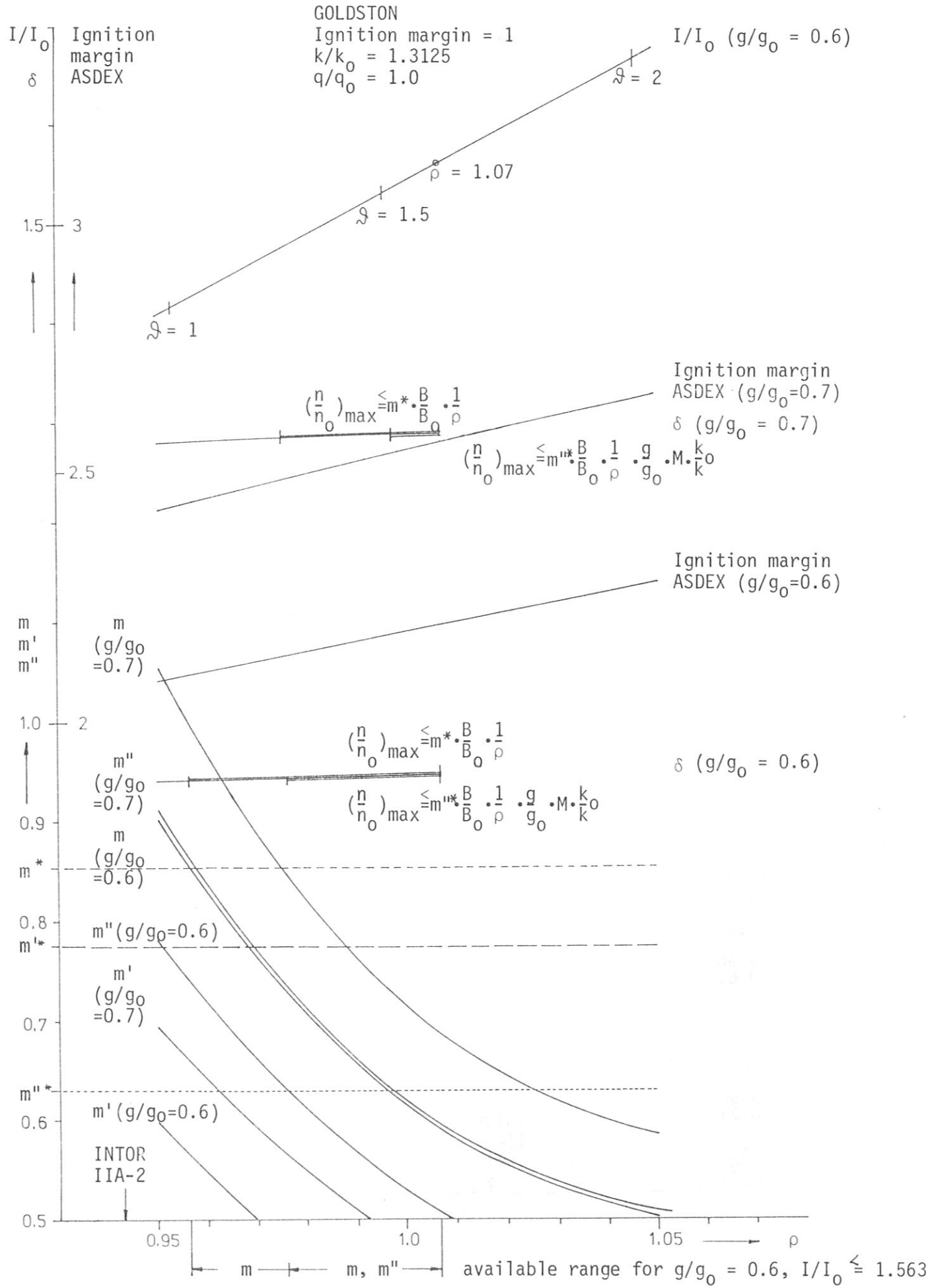

Fig. 5: Accessible parameter range between the density limits m* or m"* and I/I_o = 1.563 for an elongation of 2.1 and a GOLDSTON ignition margin of 1.

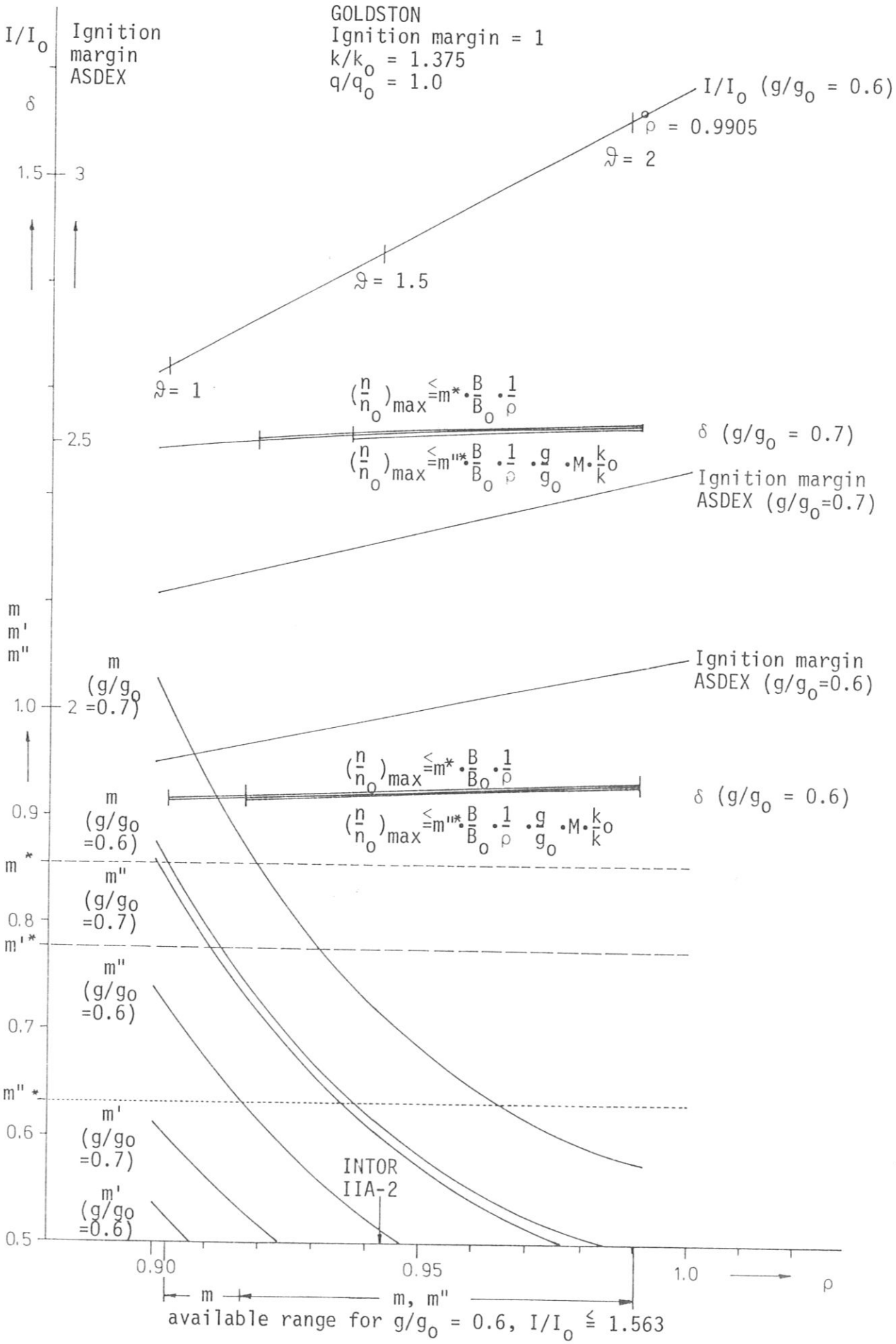

Fig. 6: Accessible parameter range between the density limits m* or m"* and I/I$_o$ = 1.563 for an elongation of 2.2 and a GOLDSTON ignition margin of 1.

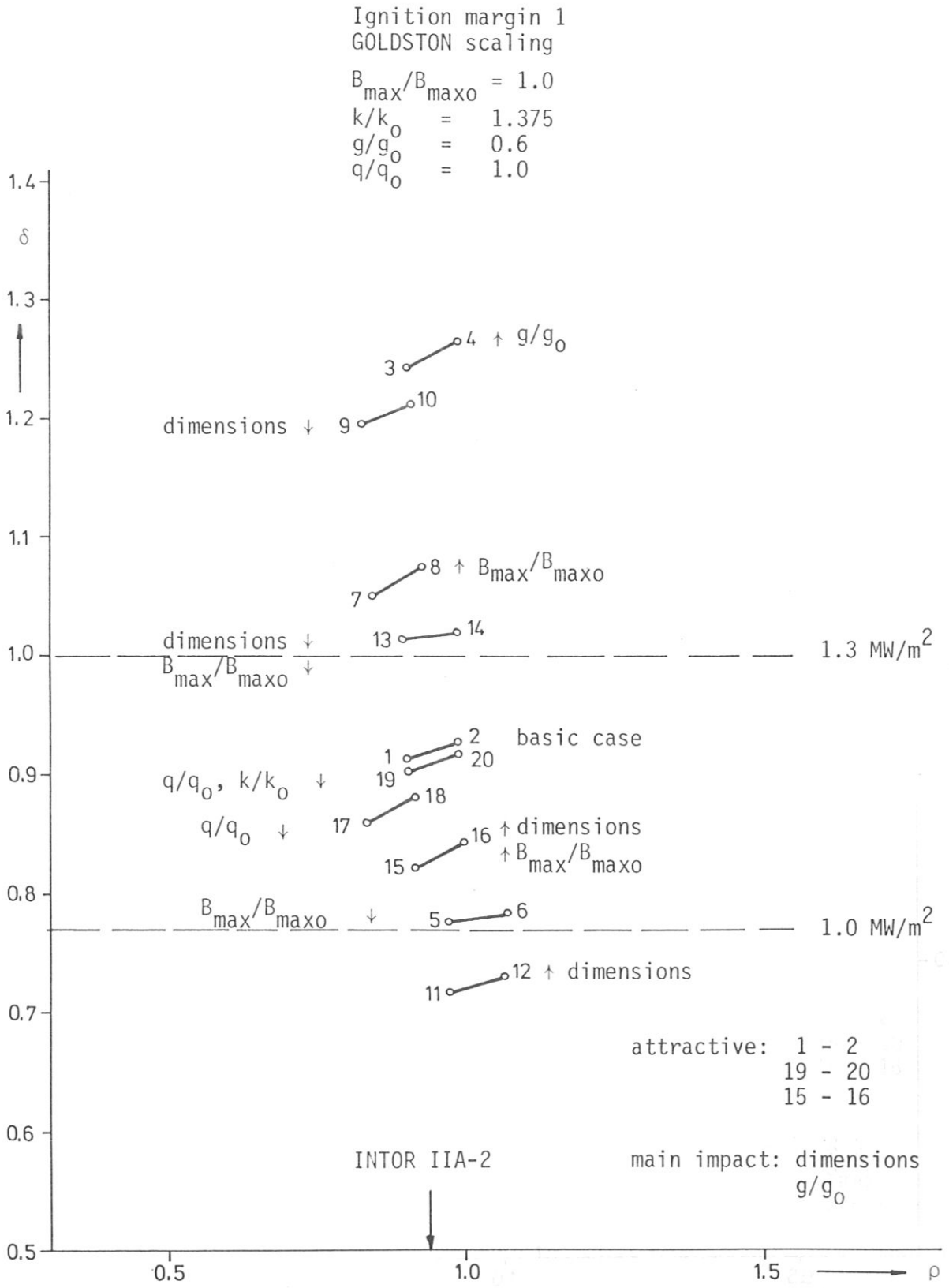

Fig. 7: Neutron wall load vs. major radius for GOLDSTON scaling at an ignition margin of 1 and an elongation of 2.2 in a plasma temperature range of 10 - 20 keV. For explanation of cases 1 - 20 see Table 1.

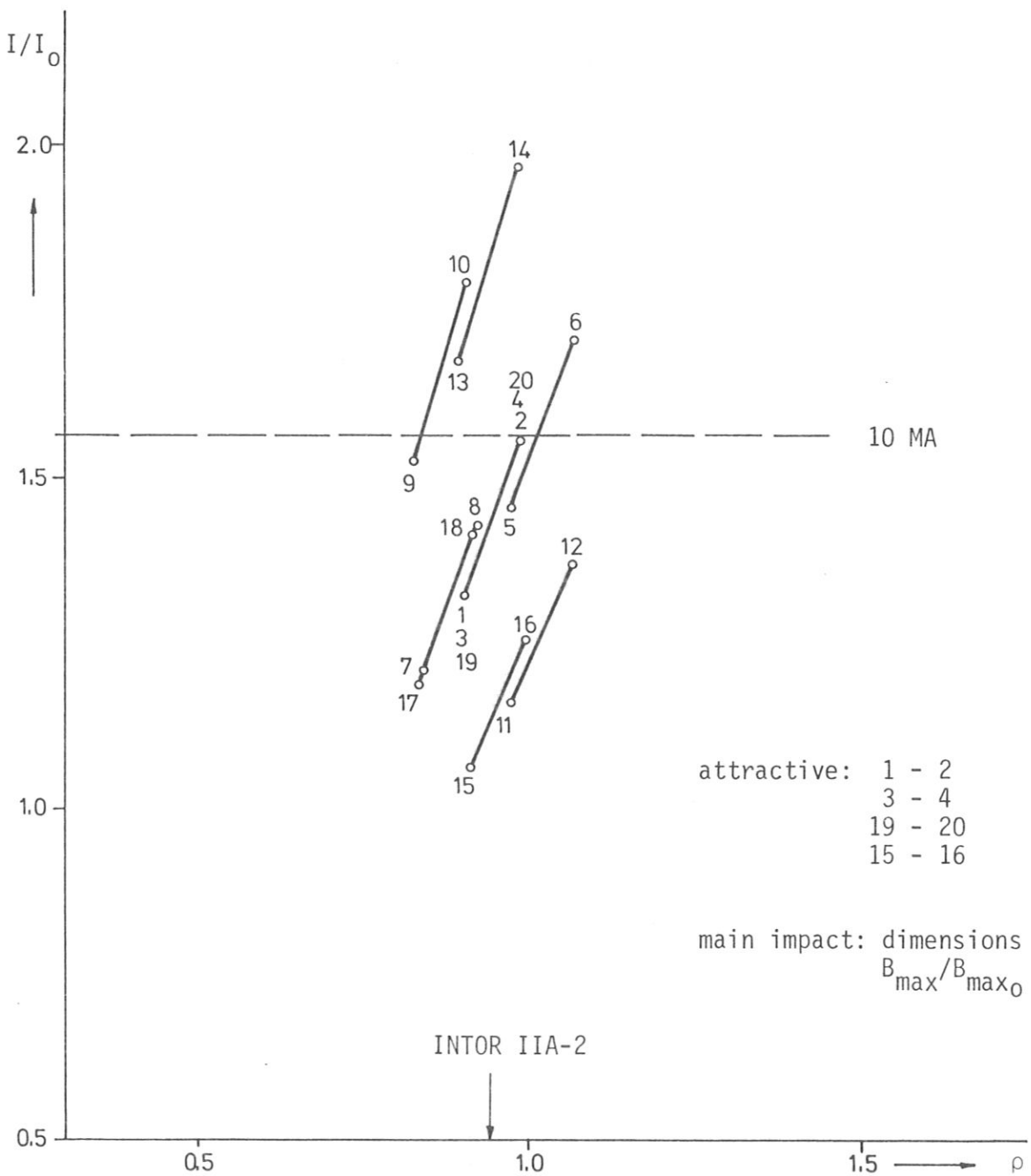

Fig. 8: Plasma current vs. major radius pertaining to cases of Fig. 7

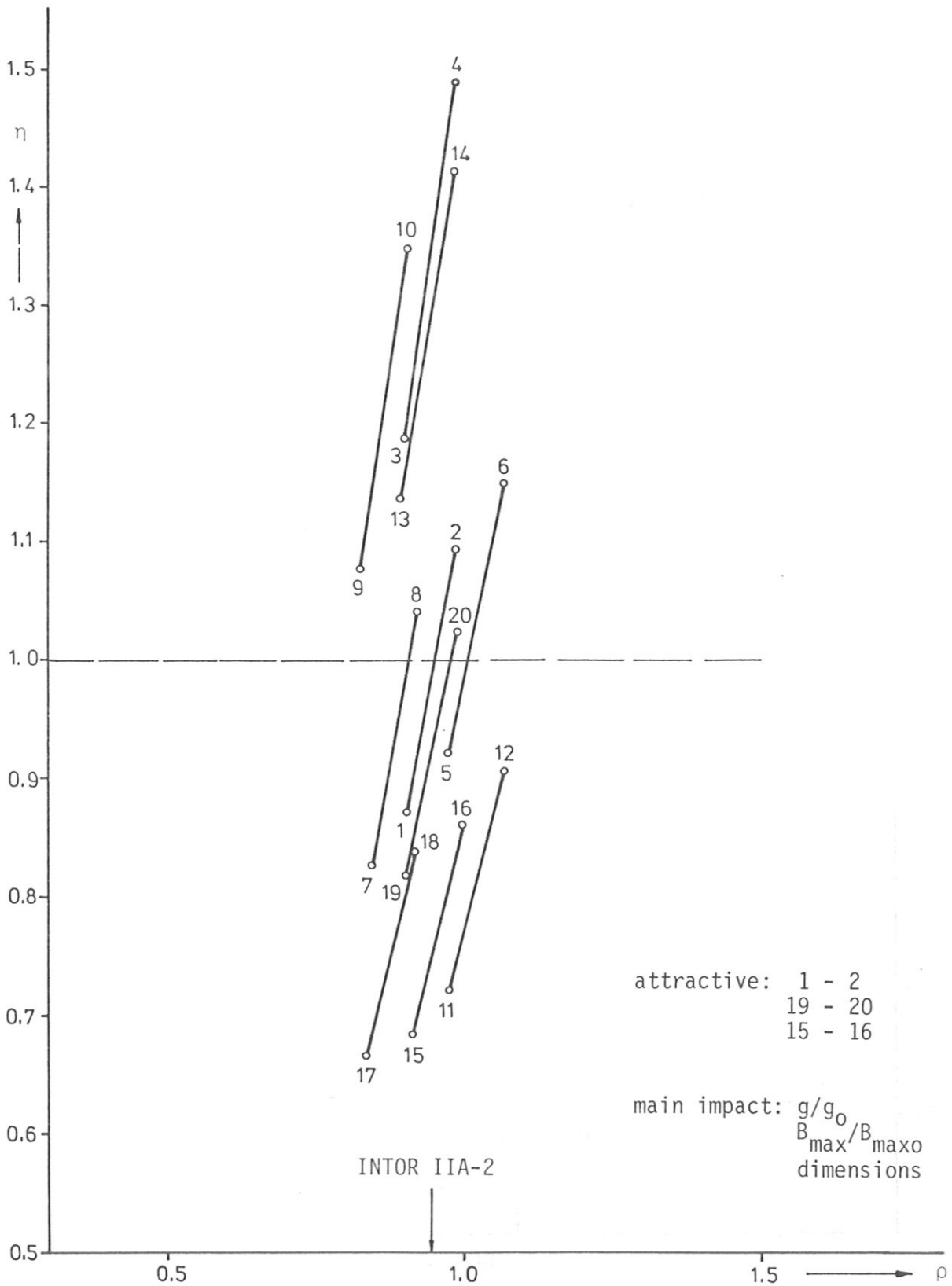

Fig. 9: Fusion power vs. major radius pertaining to cases of Fig. 7

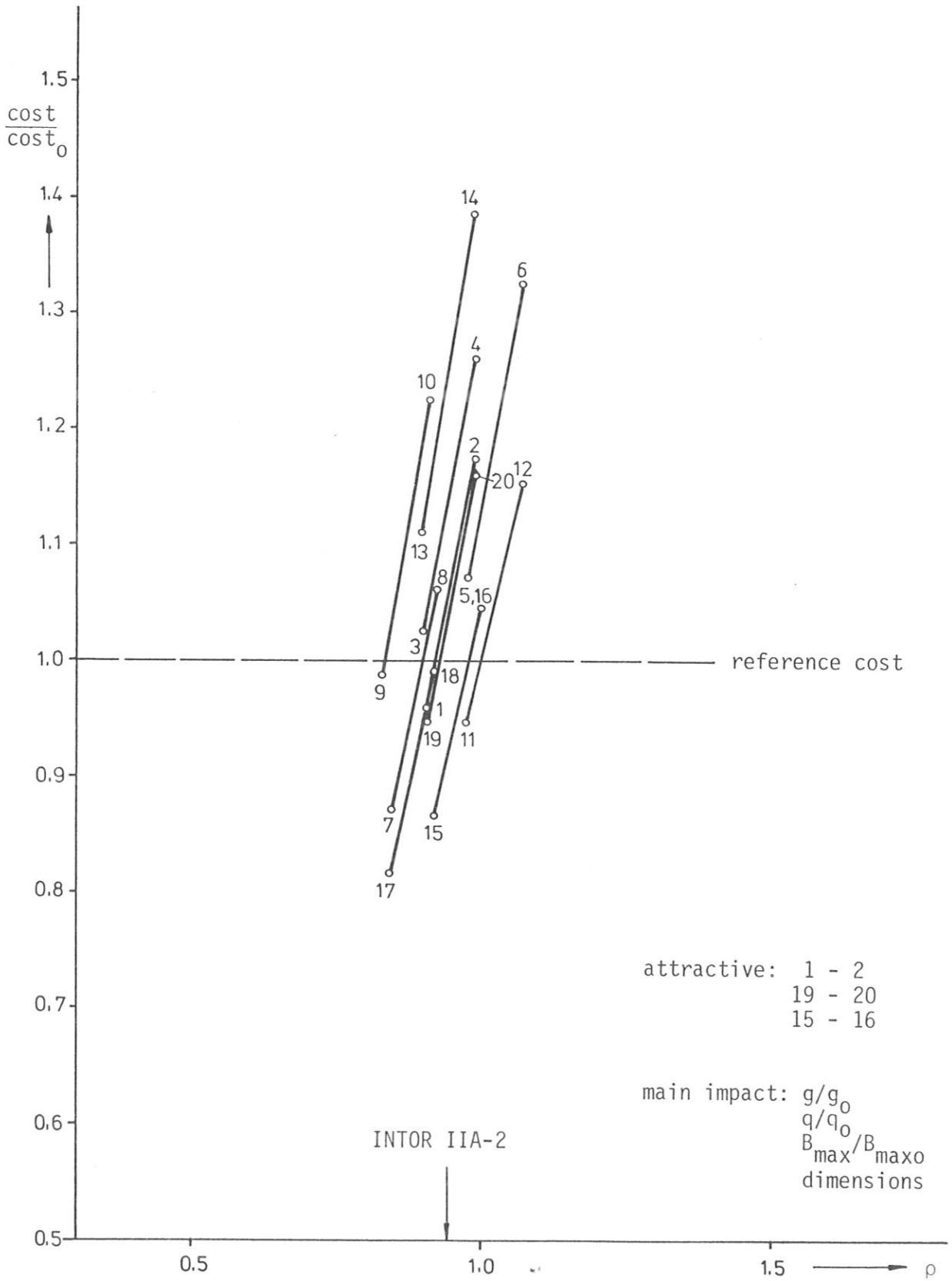

Fig. 10: Relative direct capital cost estimate vs. major radius pertaining to cases of Fig. 7

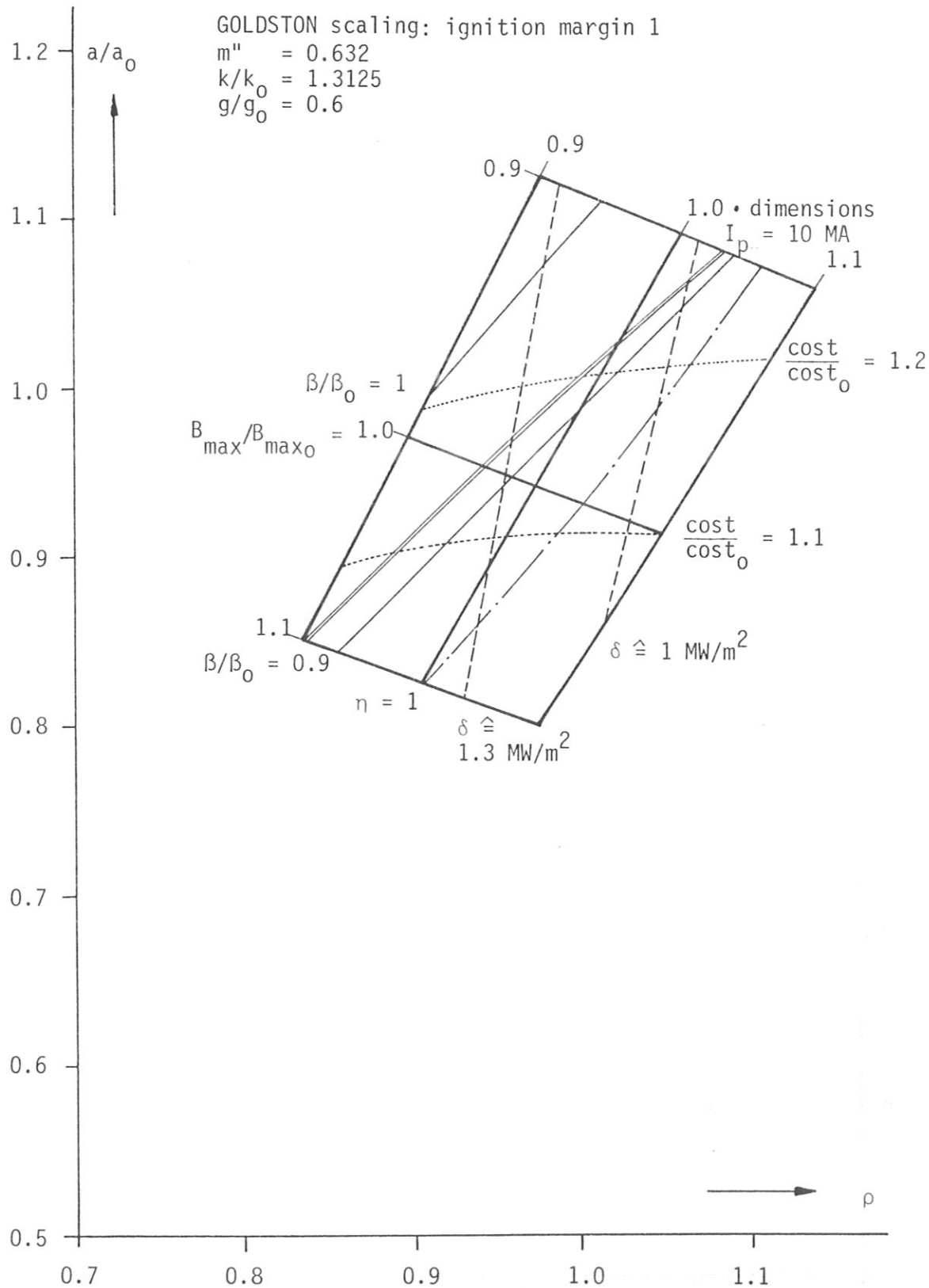

Fig. 11: Minor radius vs. major radius (density limit m"*) for an elongation of 2.1 and an ignition margin of 1 (GOLDSTON scaling) with a variation of ± 10% in maximum toroidal field and in geometry factors with parametric curves for constant neutron wall load, plasma current, total beta, fusion power and relative direct capital cost.

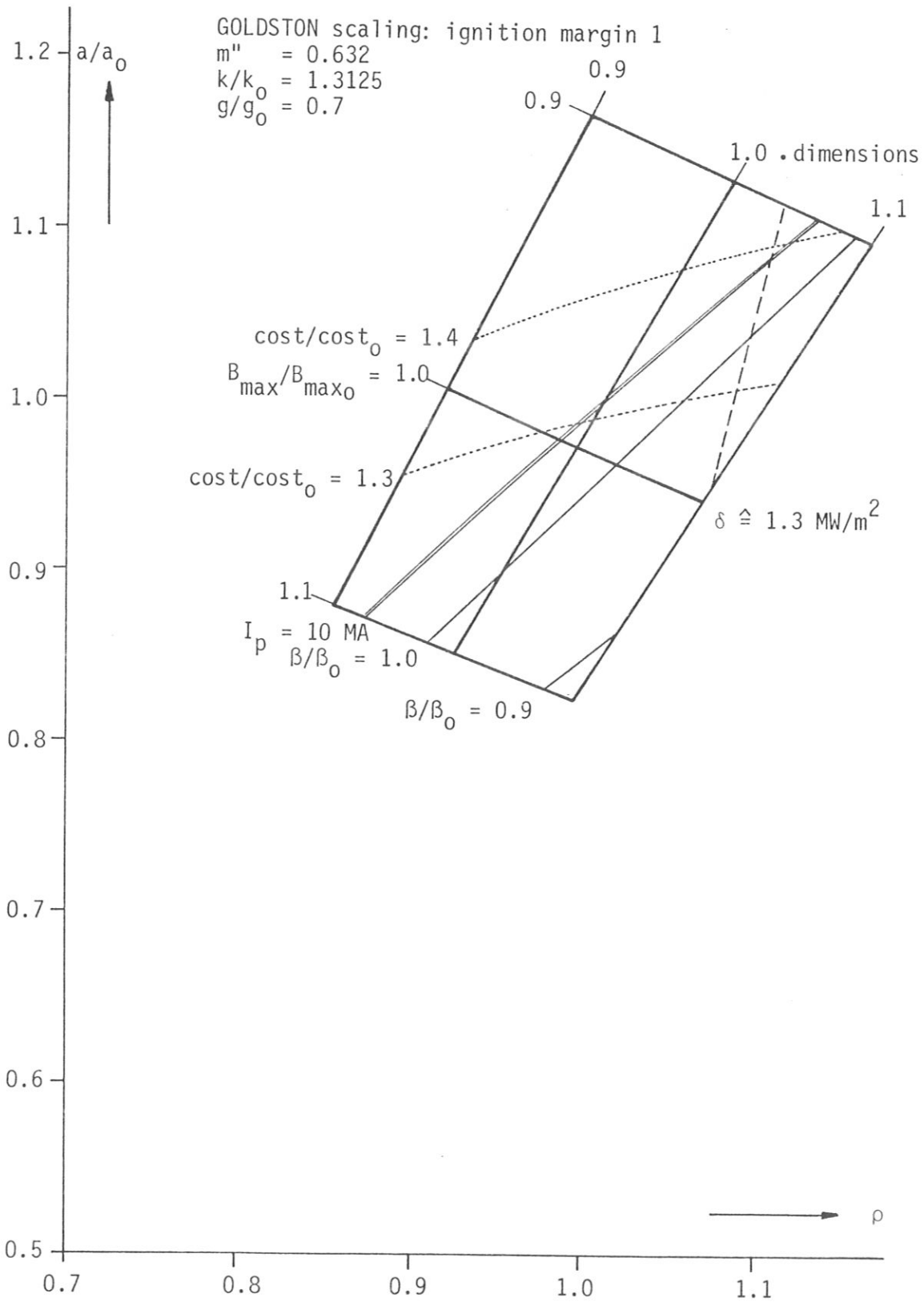

Fig. 11a: Minor radius vs. major radius (density limit m"*)
further figure caption see Fig. 11, but g/g$_o$ = 0.7

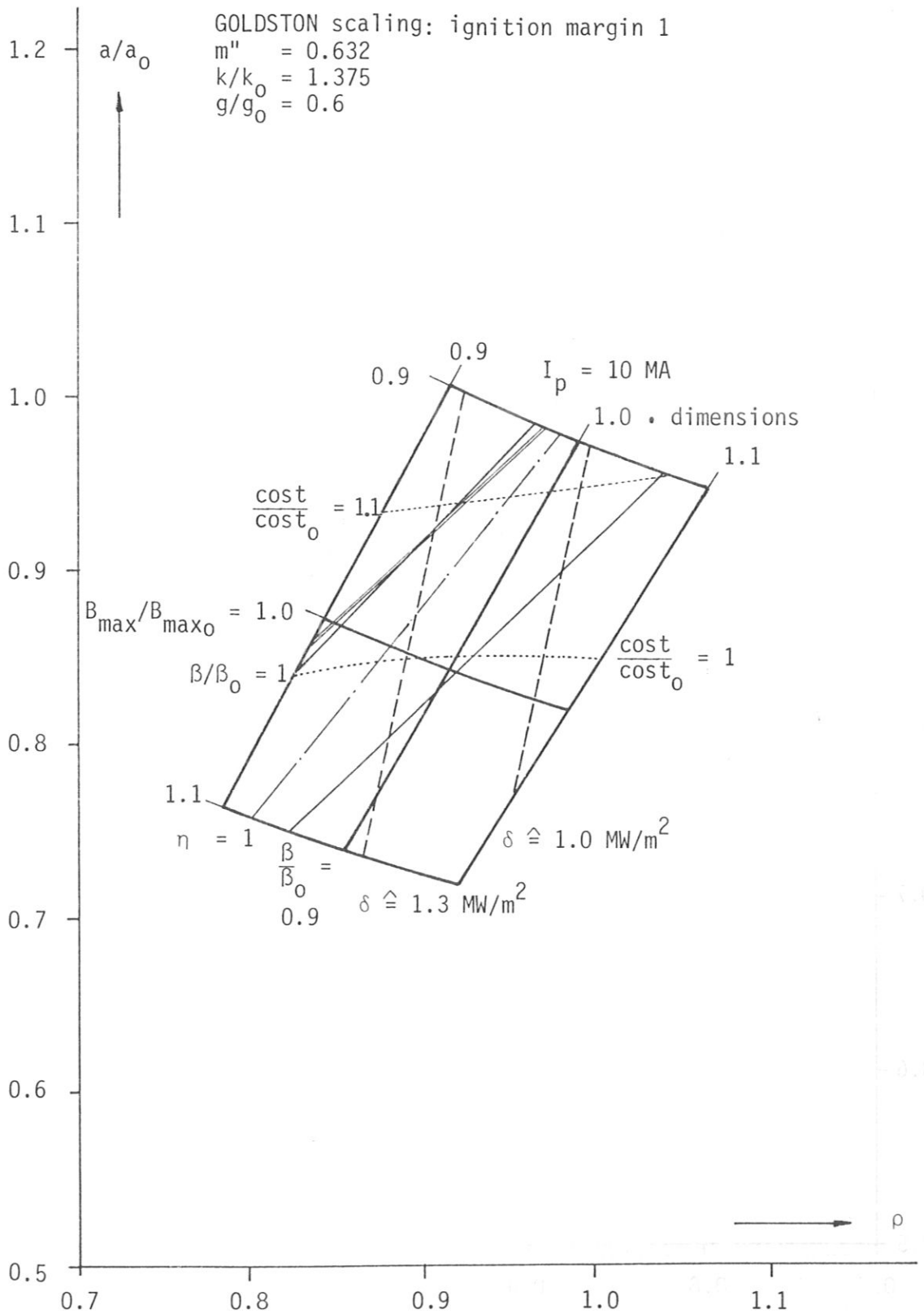

Fig. 12: Minor radius vs. major radius (density limit m"*) for an elongation of 2.2 and an ignition margin of 1 (GOLDSTON scaling) with a variation of ± 10% in maximum toroidal field and in geometry factors with parametric curves for constant neutron wall load, plasma current, toroidal beta, fusion power and relative direct capital cost

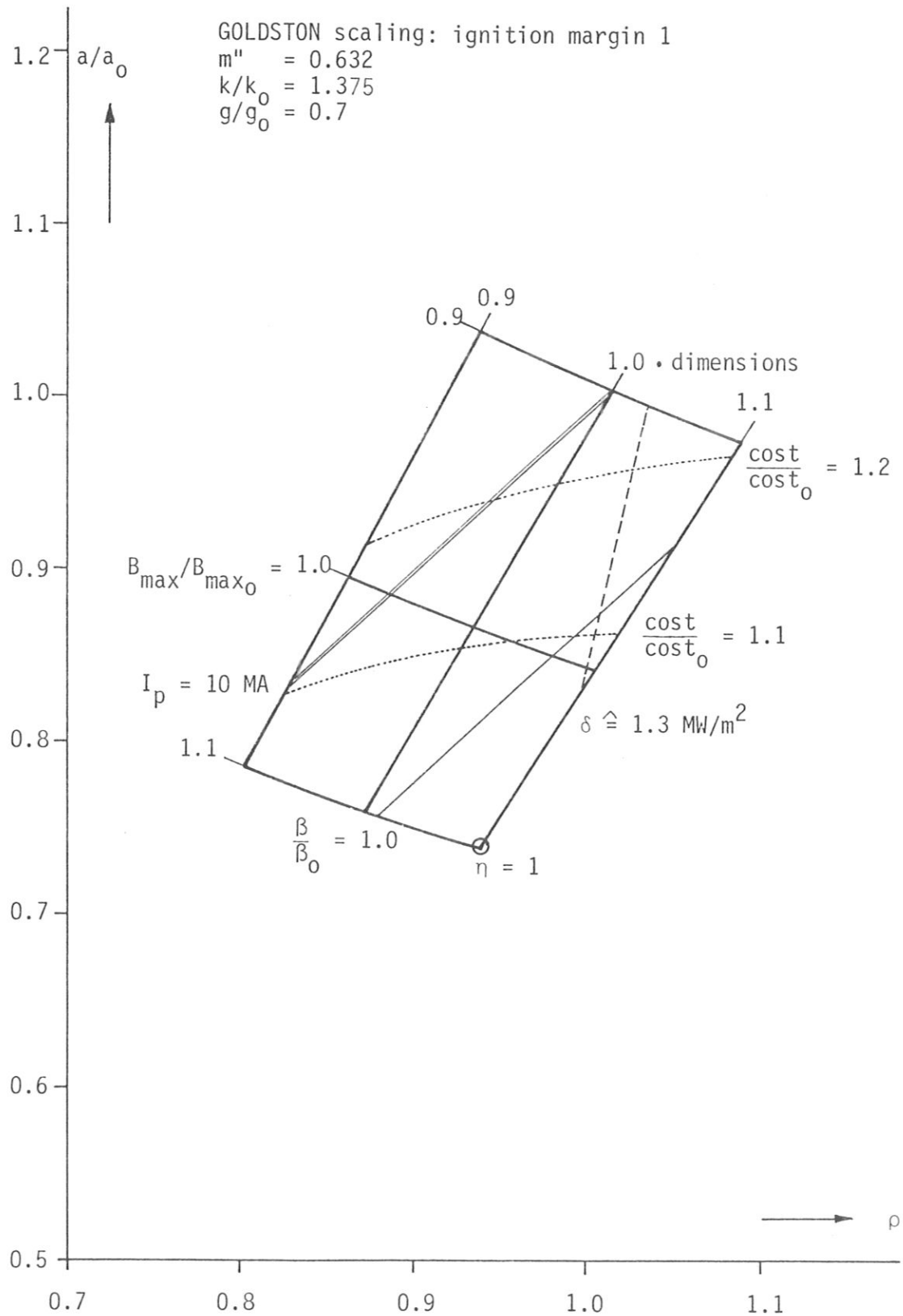

Fig. 12a: Minor radius vs. major radius (density limit m"*)
further figure caption see Fig. 12, but g/g$_o$ = 0.7

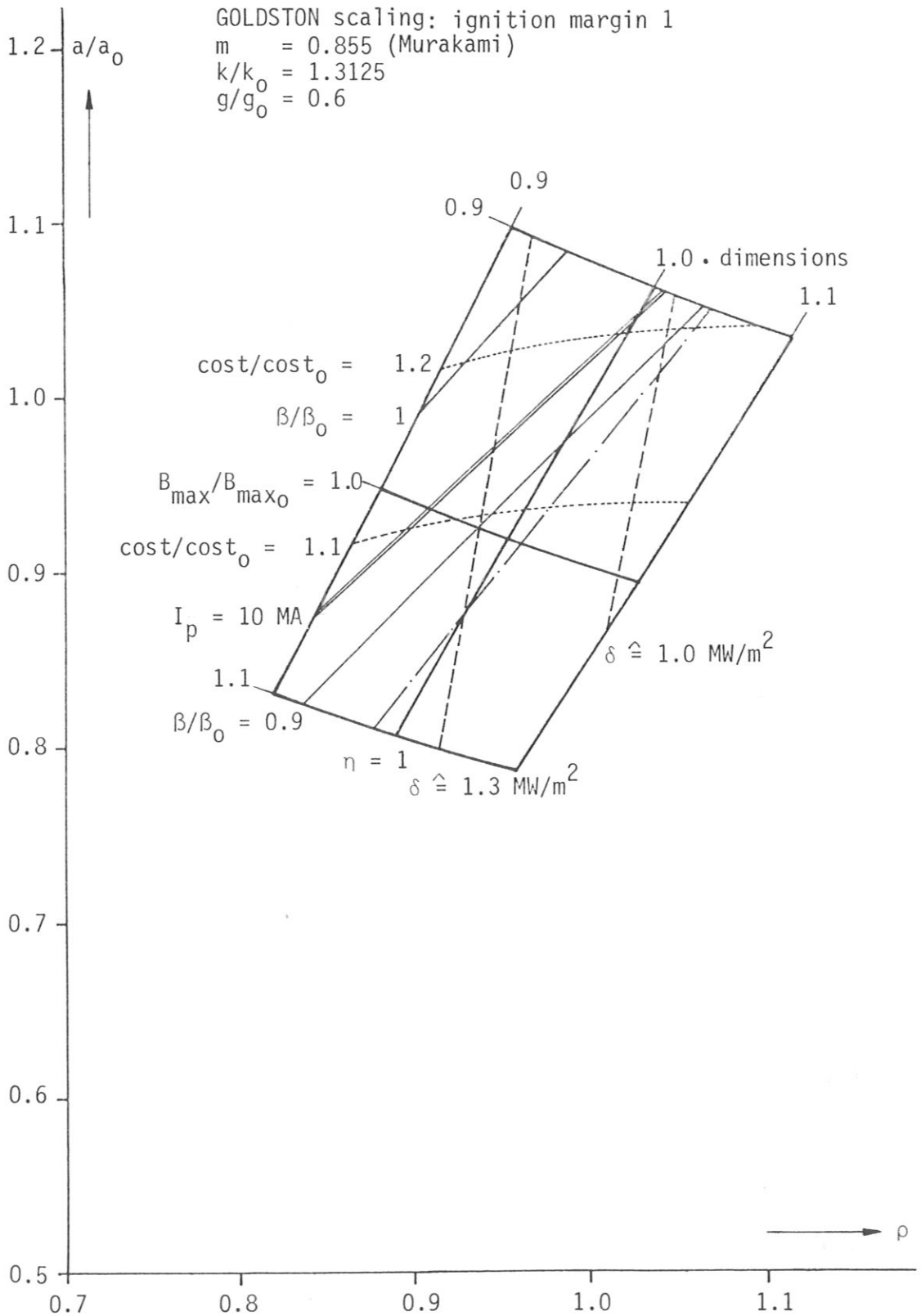

Fig. 13: Minor radius vs. major radius (density limit m*)
further figure caption see Fig. 11

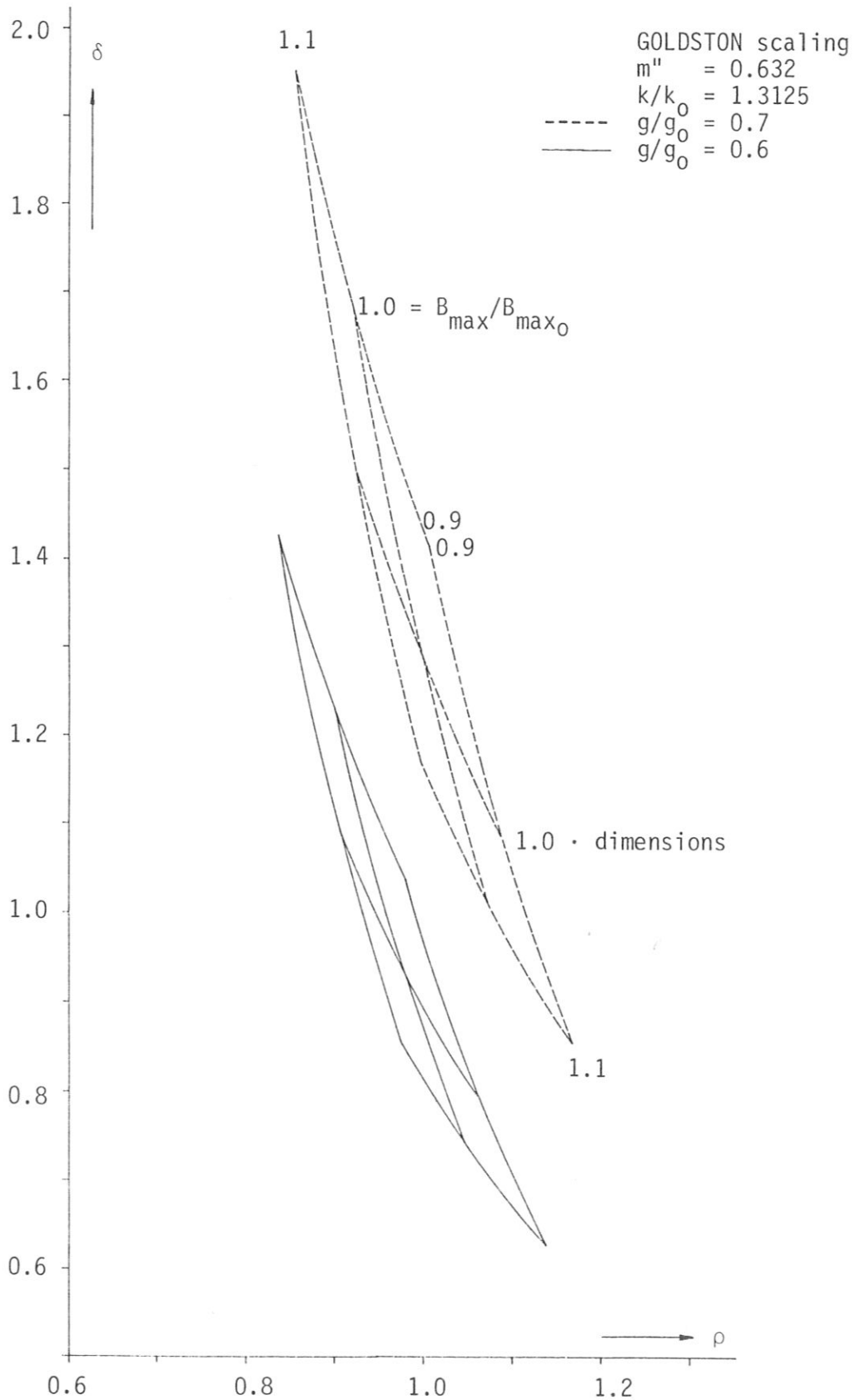

Fig. 14: Neutron wall load vs. major radius - see Figs. 11 and 11a

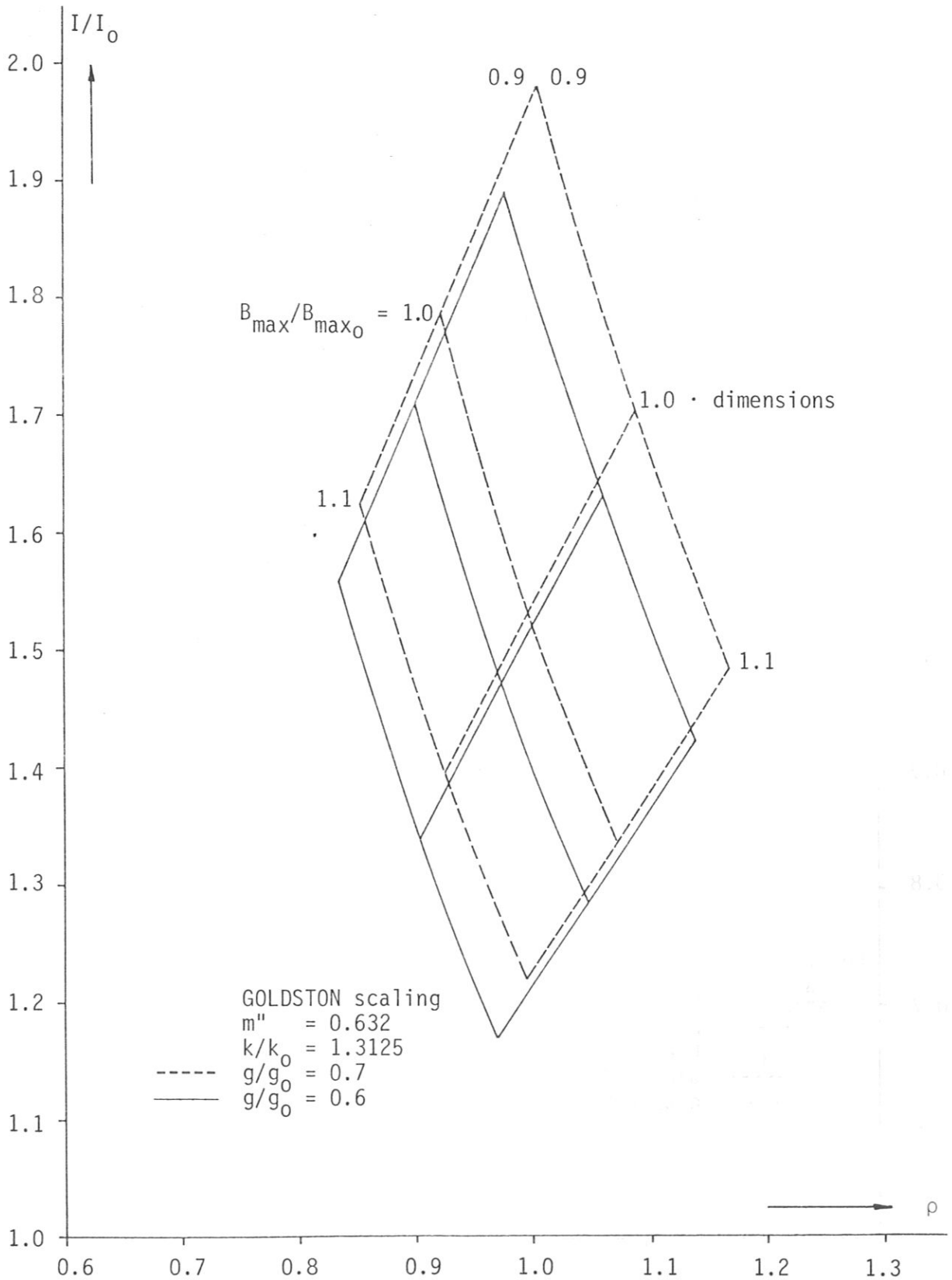

Fig. 15: Plasma current vs. major radius - see Figs. 11 and 11a

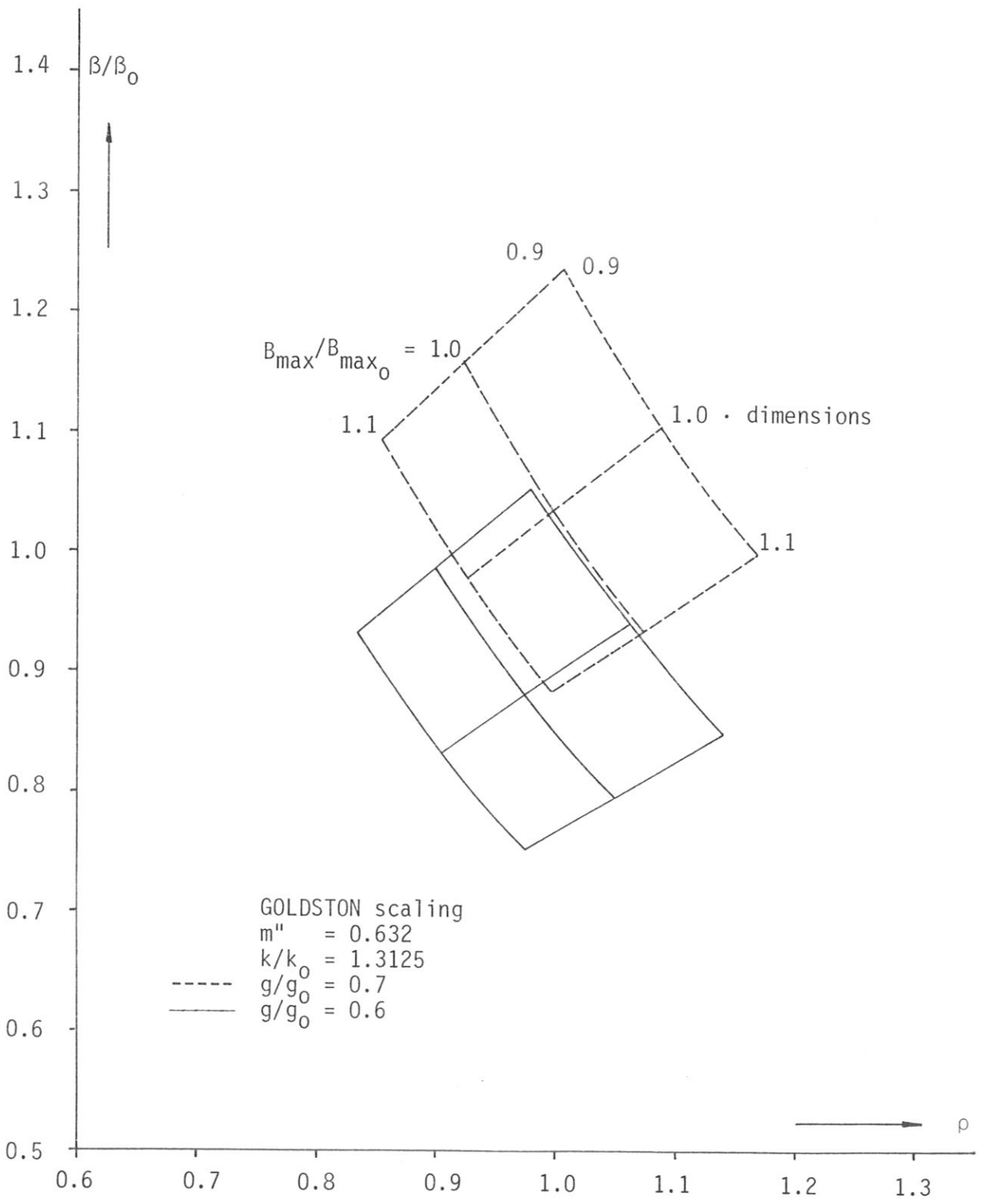

Fig. 16: Total beta vs. major radius - see Figs. 11 and 11a

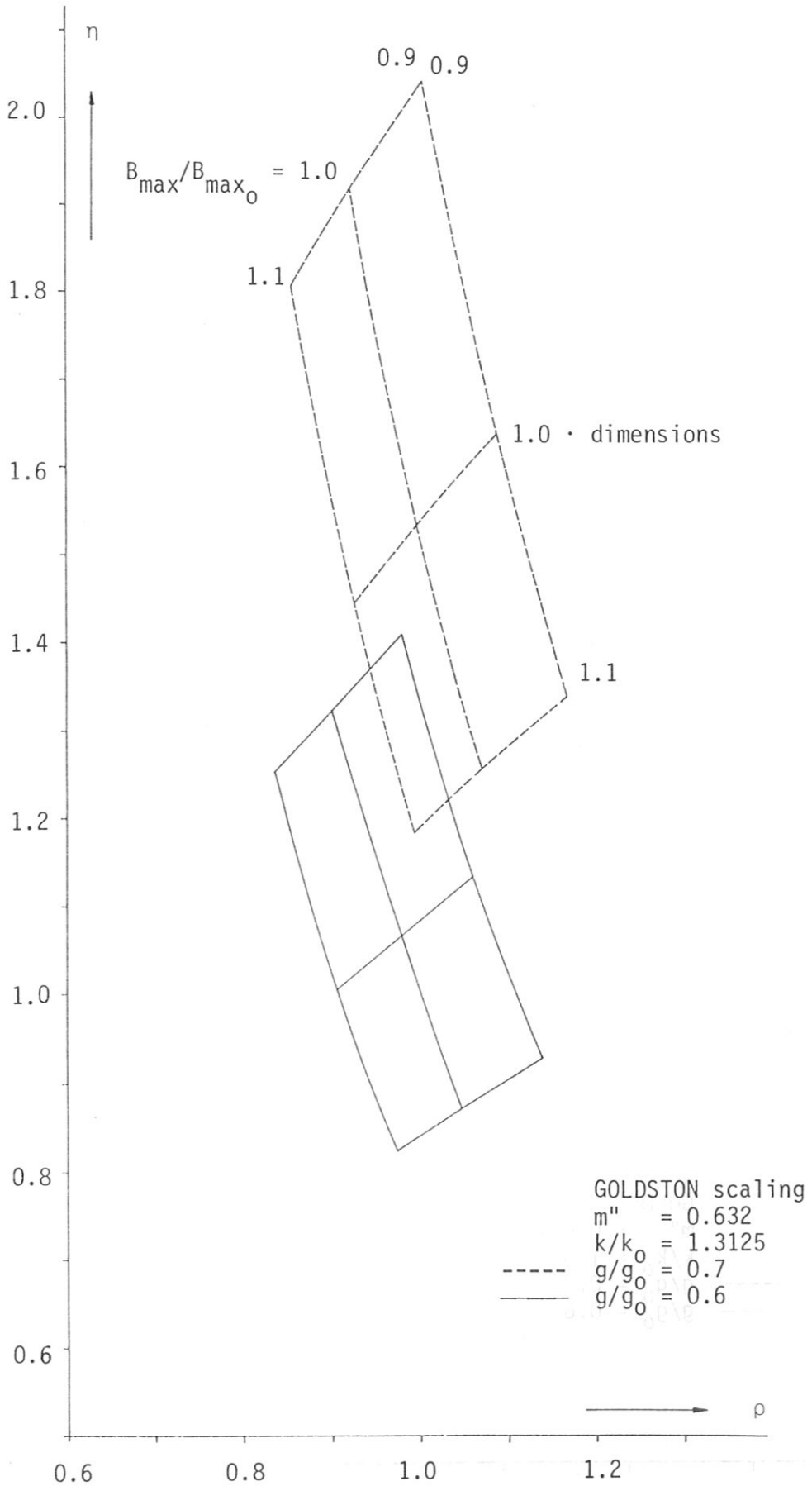

Fig. 17: Fusion power vs. major radius - see Figs. 11 and 11a

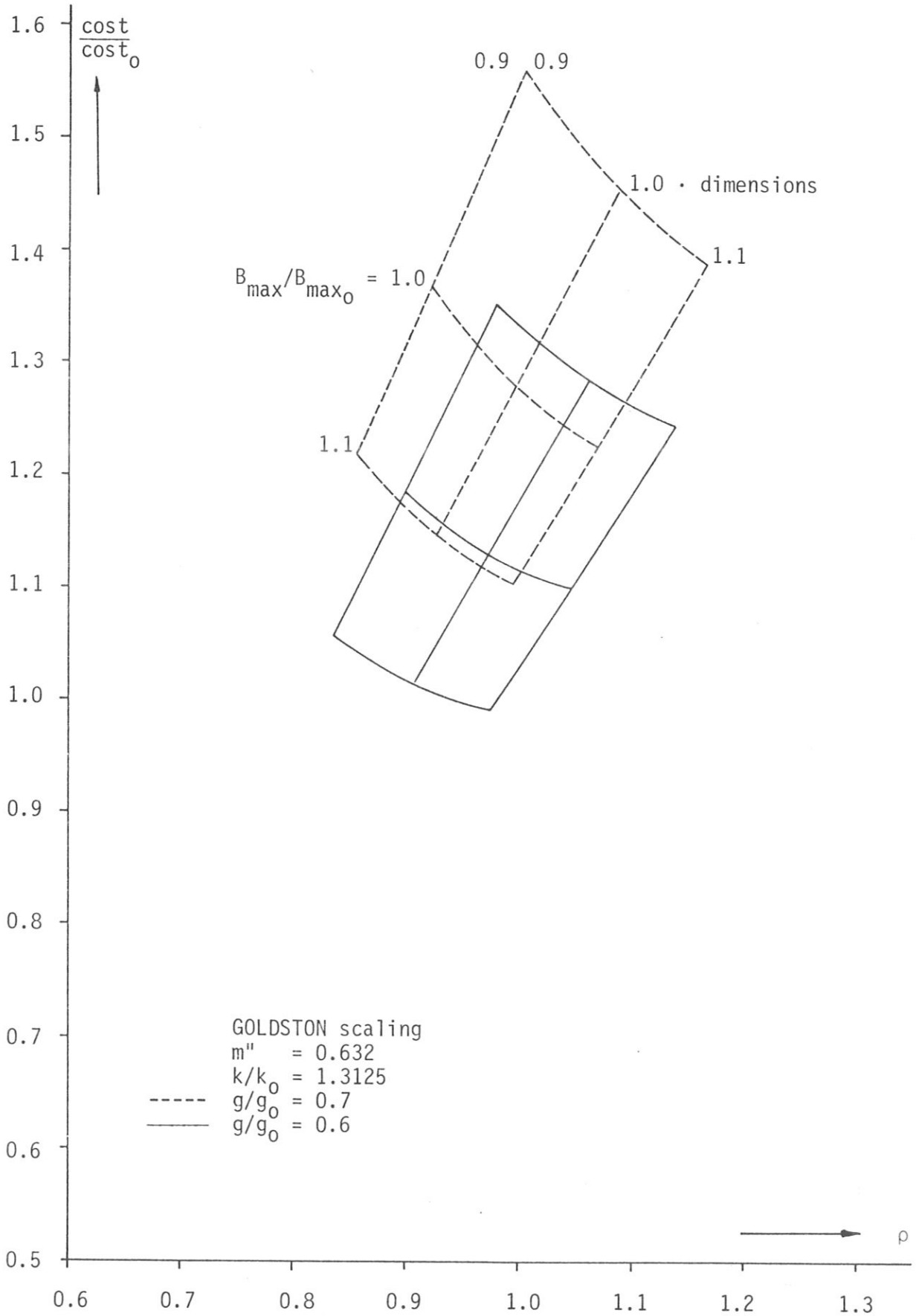

Fig. 18: Relative direct capital cost estimate vs. major radius - see Figs. 11/11a

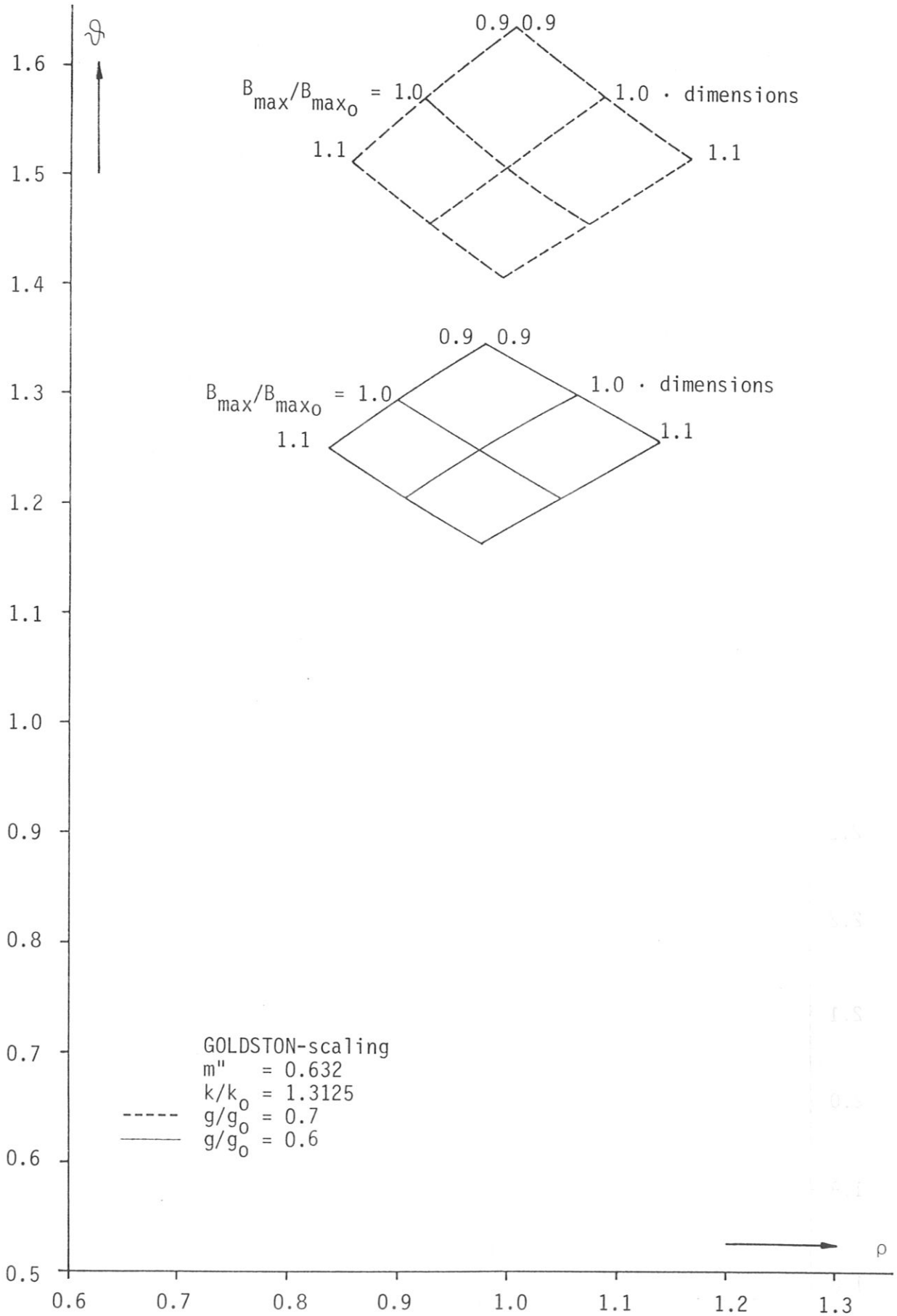

Fig. 19: Plasma temperature vs. major radius - see Figs. 11 and 11a

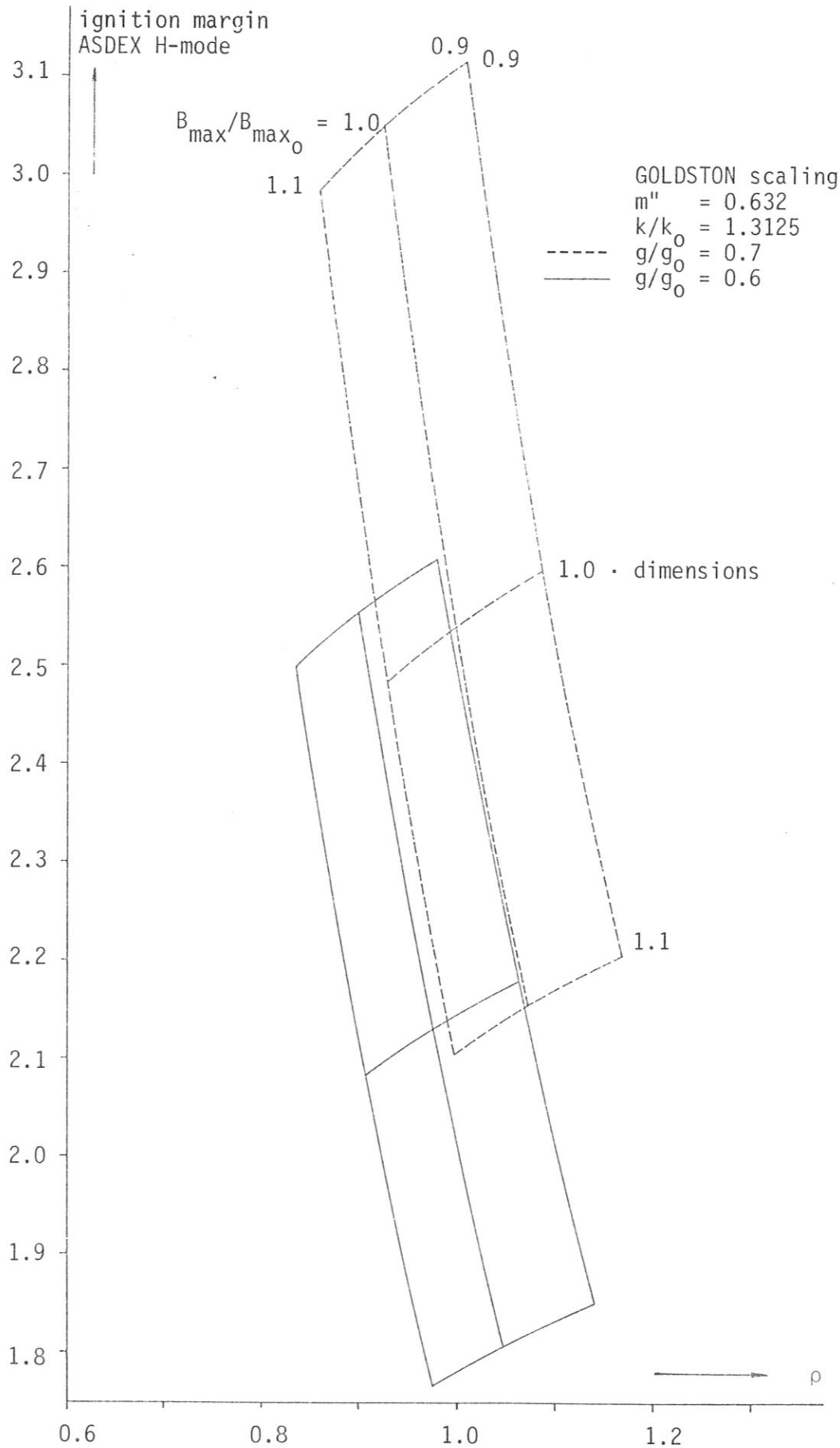

Fig. 20: ASDEX H-mode ignition margin vs. major radius - see Figs. 11/11a

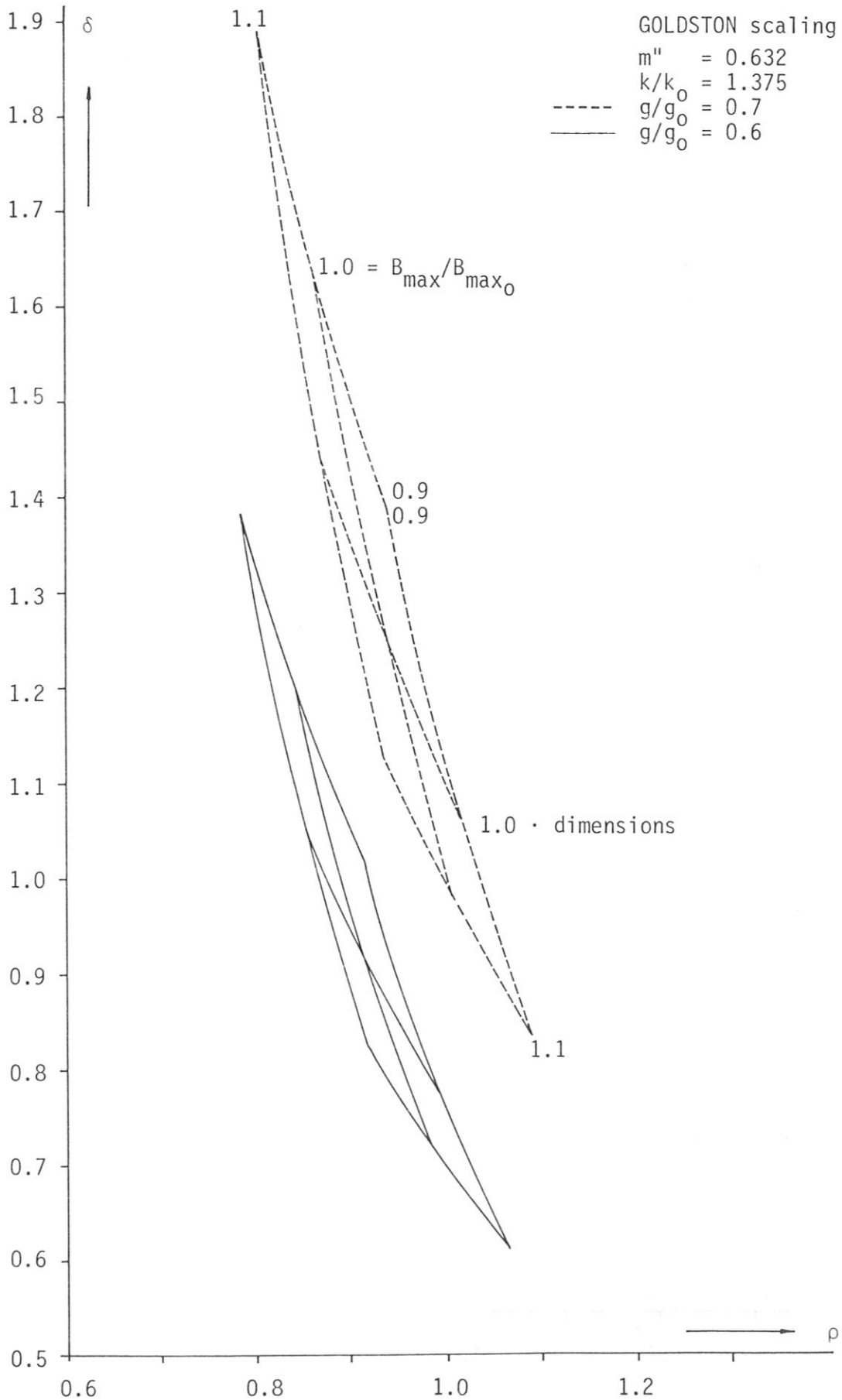

Fig. 21: Neutron wall load vs. major radius - see Figs. 12/12a

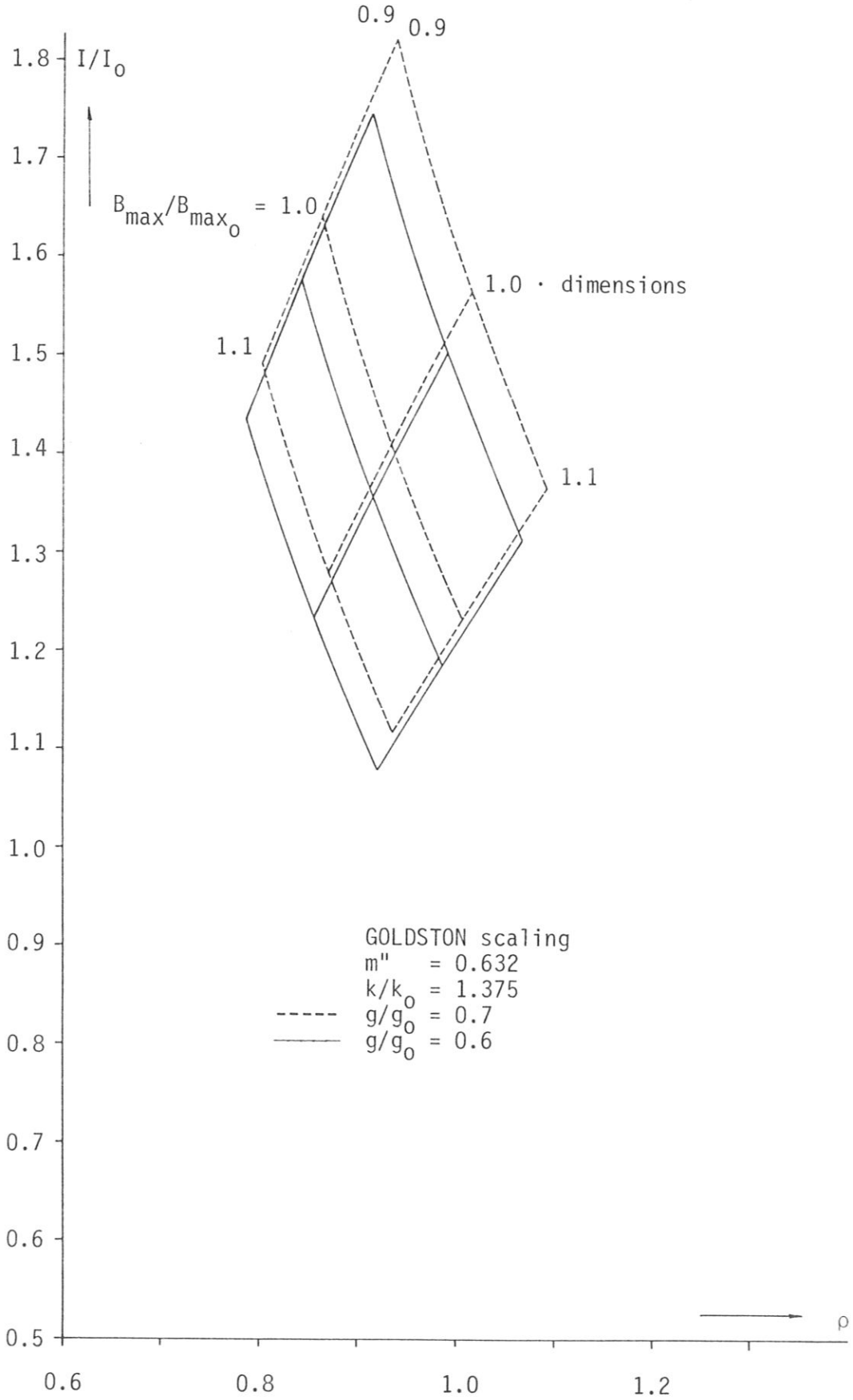

Fig. 22: Plasma current vs. major radius - see Figs. 12/12a

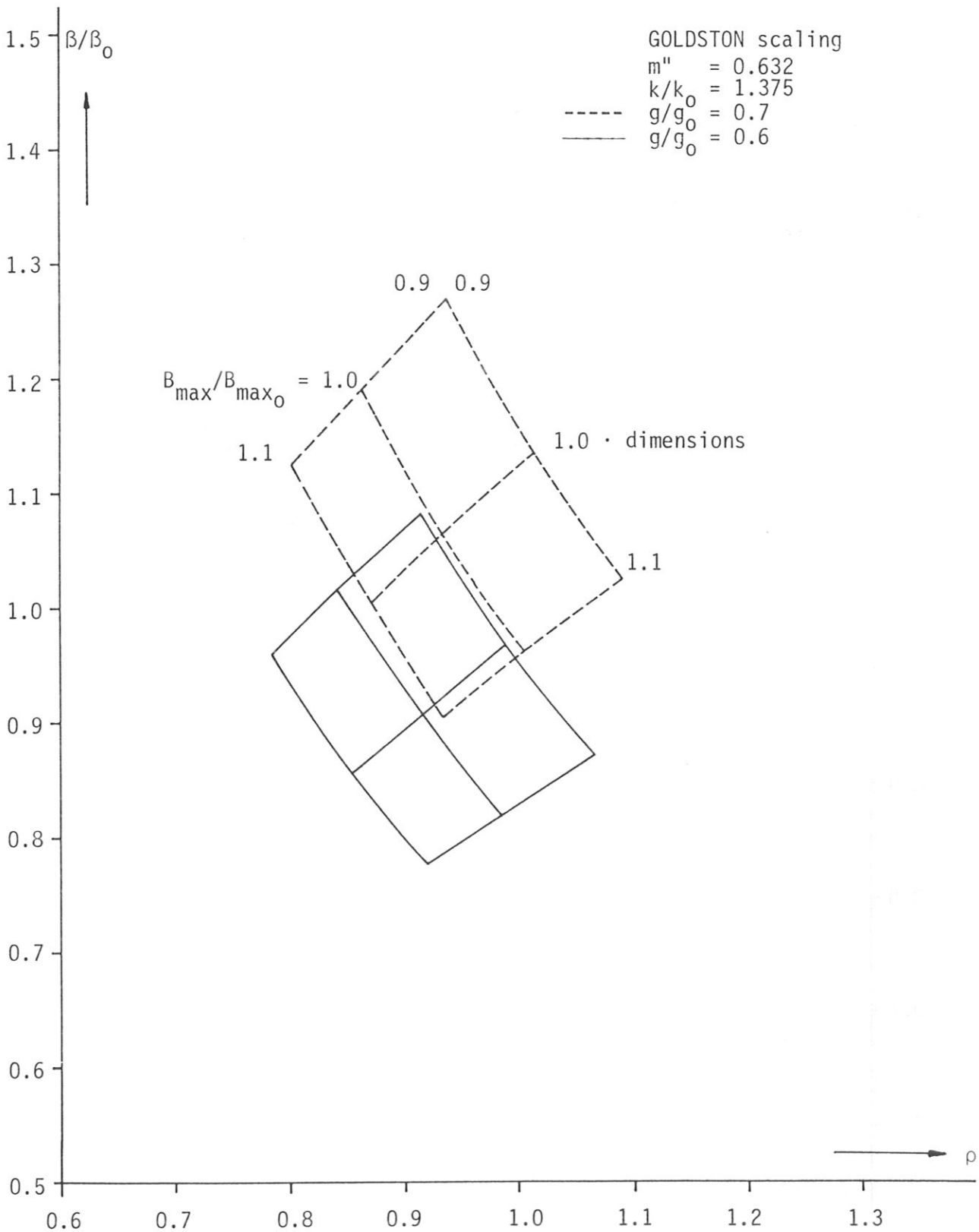

Fig. 23: Total beta vs. major radius - see Figs. 12 and 12a

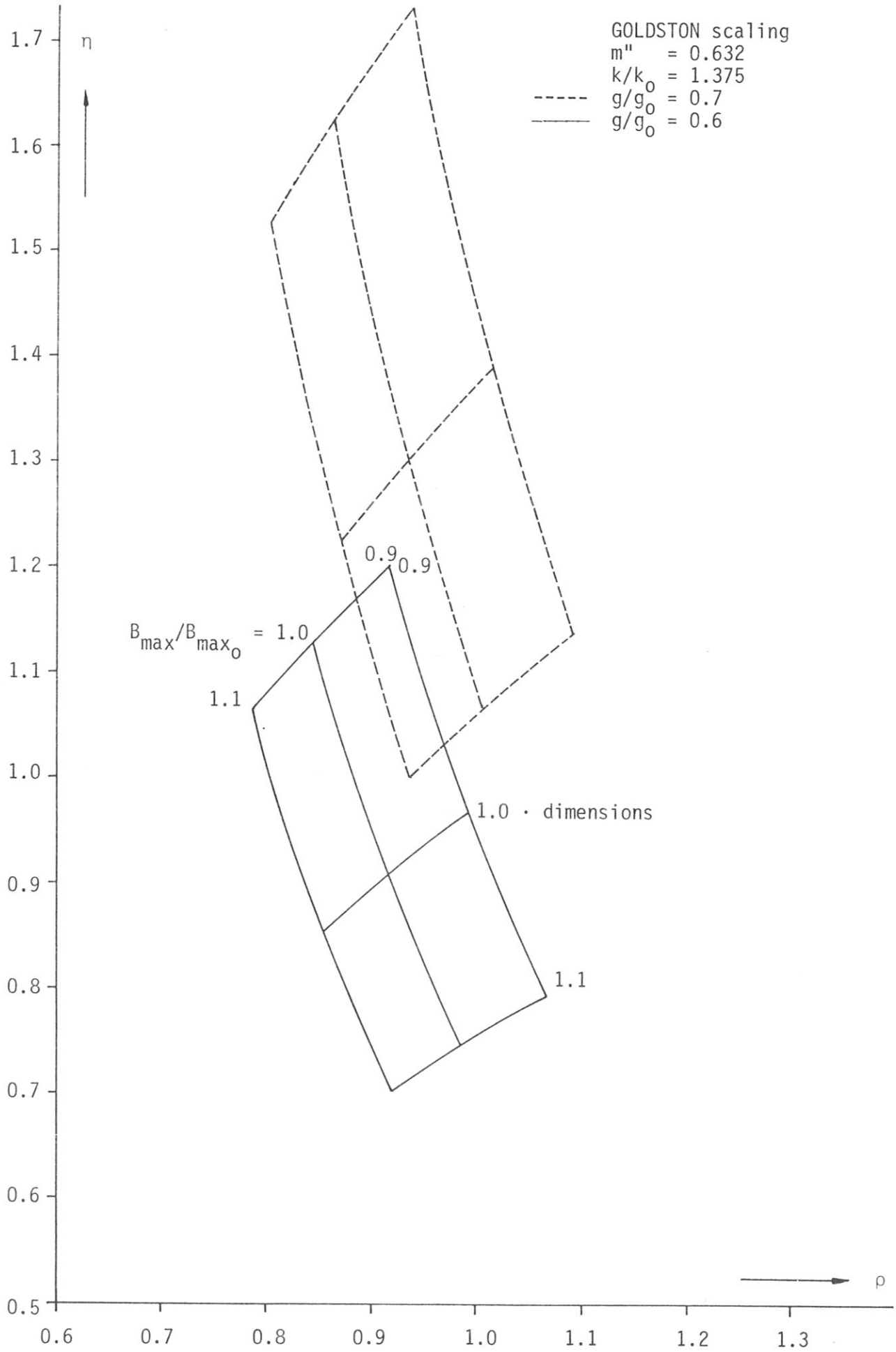

Fig. 24: Fusion power vs. major radius - see Figs. 12 and 12a

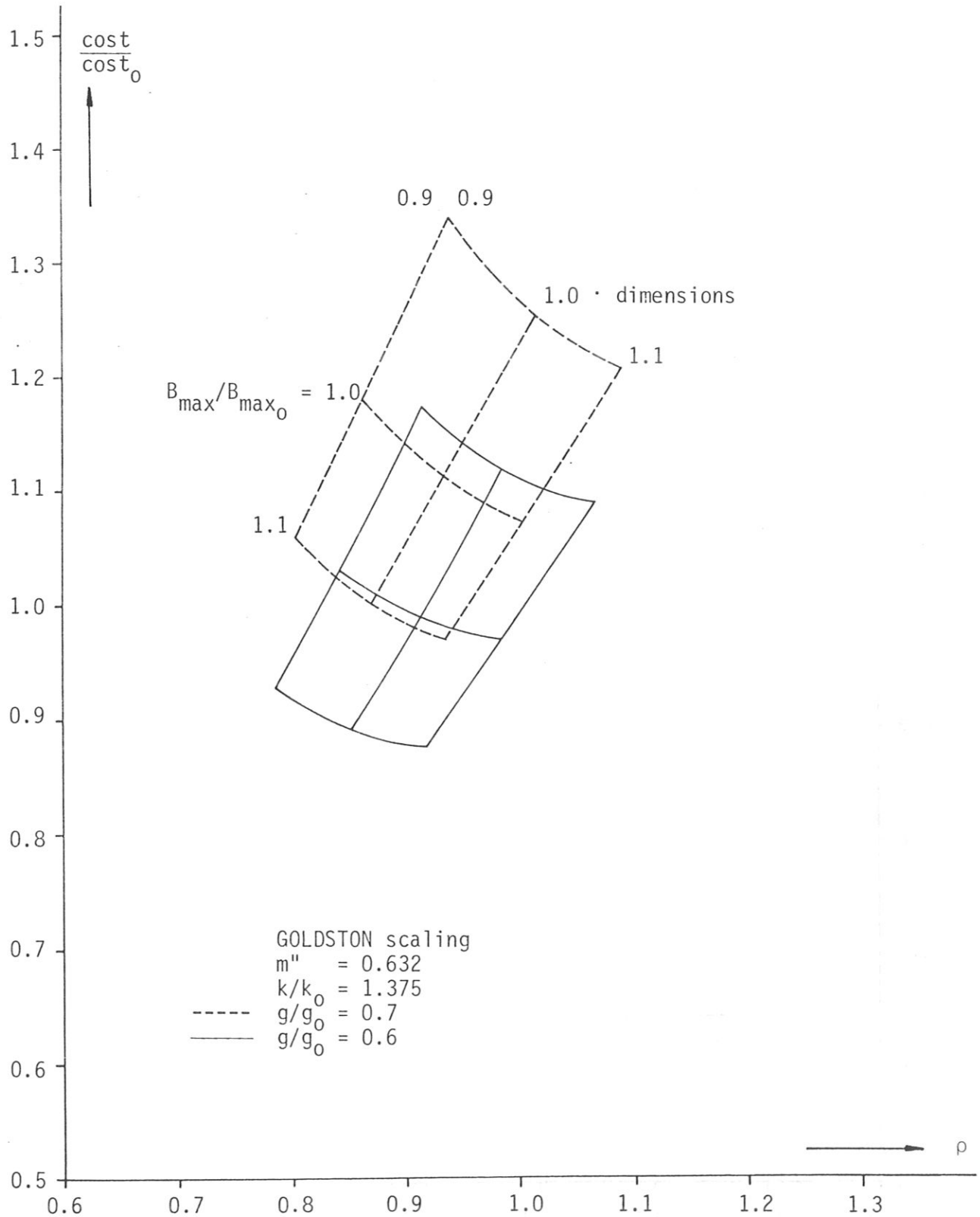

Fig. 25: Relative direct capital cost estimate vs. major radius - see Figs. 12/12a

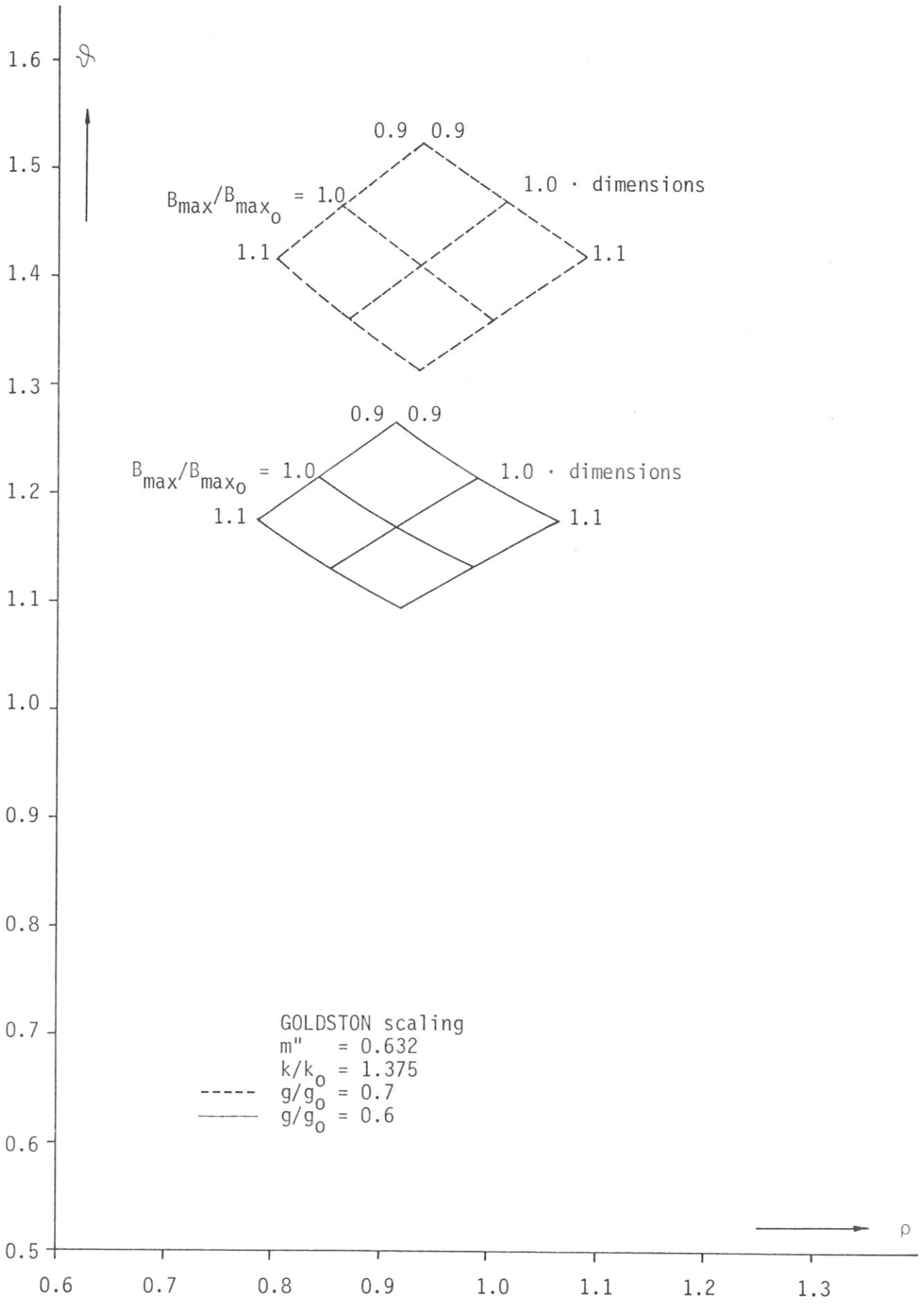

Fig. 26: Plasma temperature vs. major radius - see Figs. 12 and 12a

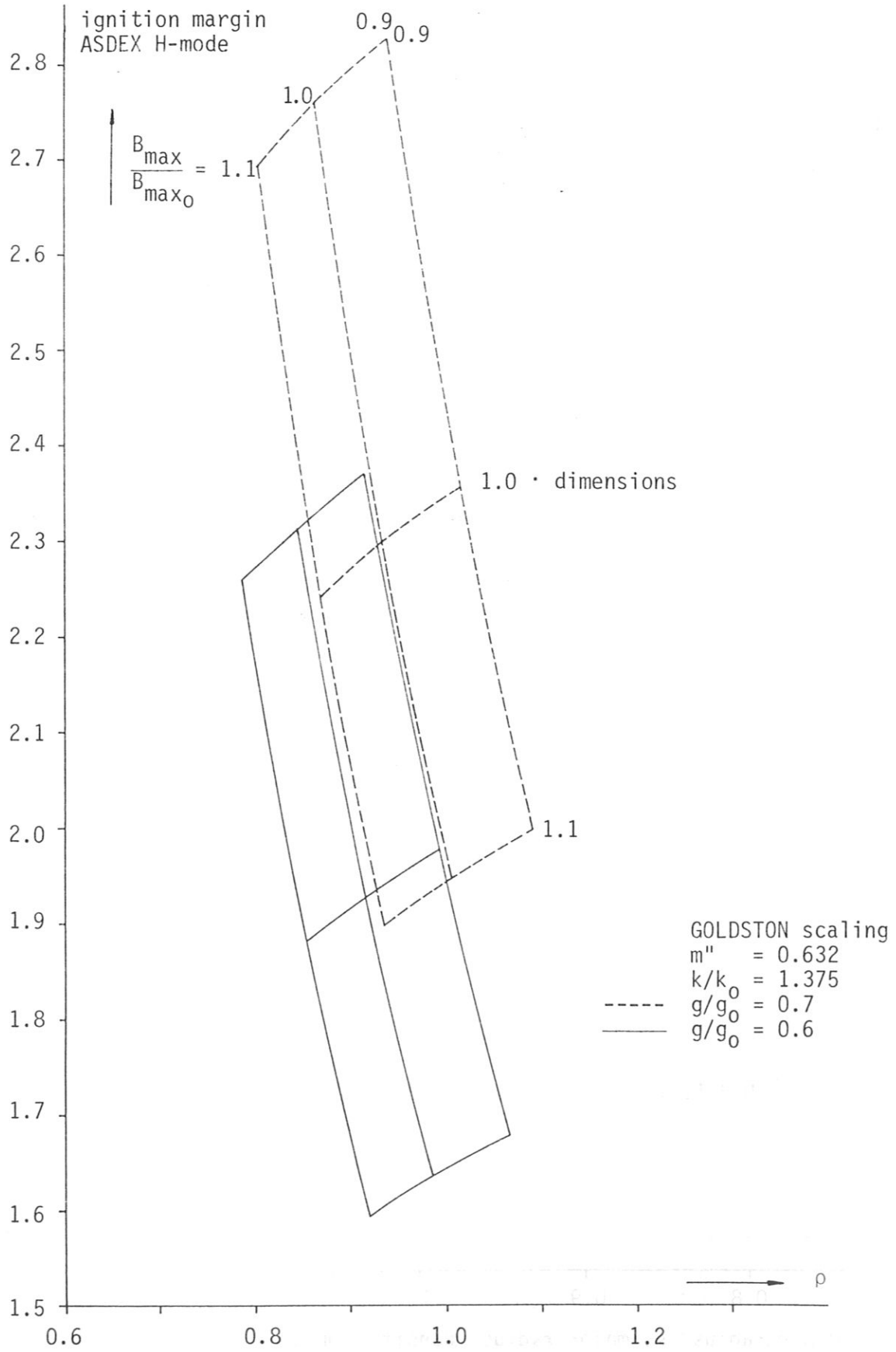

Fig. 27: ASDEX H-mode ignition margin vs. major radius - see Figs. 12/12a

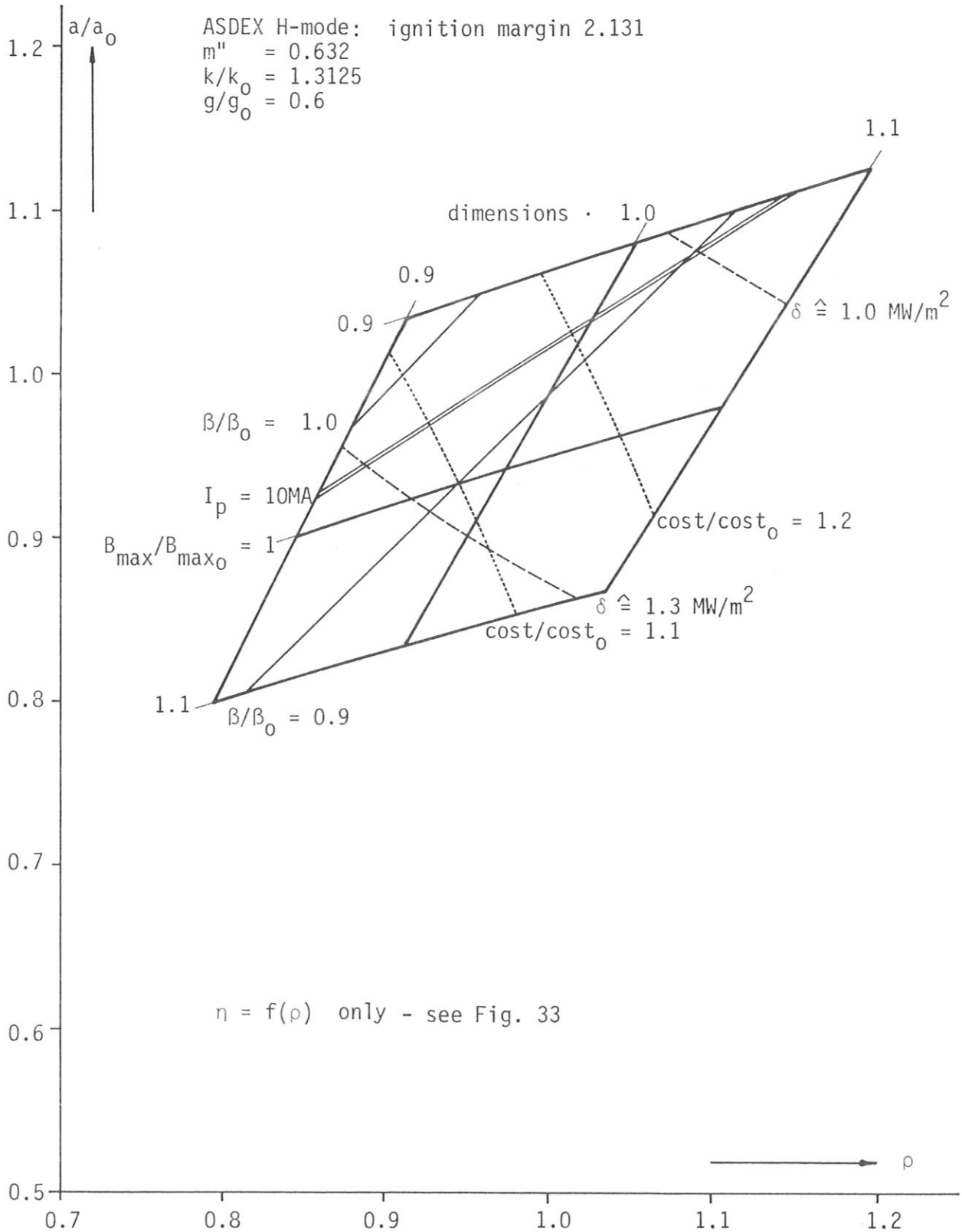

Fig. 28: Minor radius vs. major radius (density limit m"*) for an elongation of 2.1 and an ignition margin of 2.131 (ASDEX H-mode scaling) with a variation of ± 10% in maximum toroidal field and in geometry factors with parametric curves for constant neutron wall load, plasma current, total beta and relative direct capital cost.

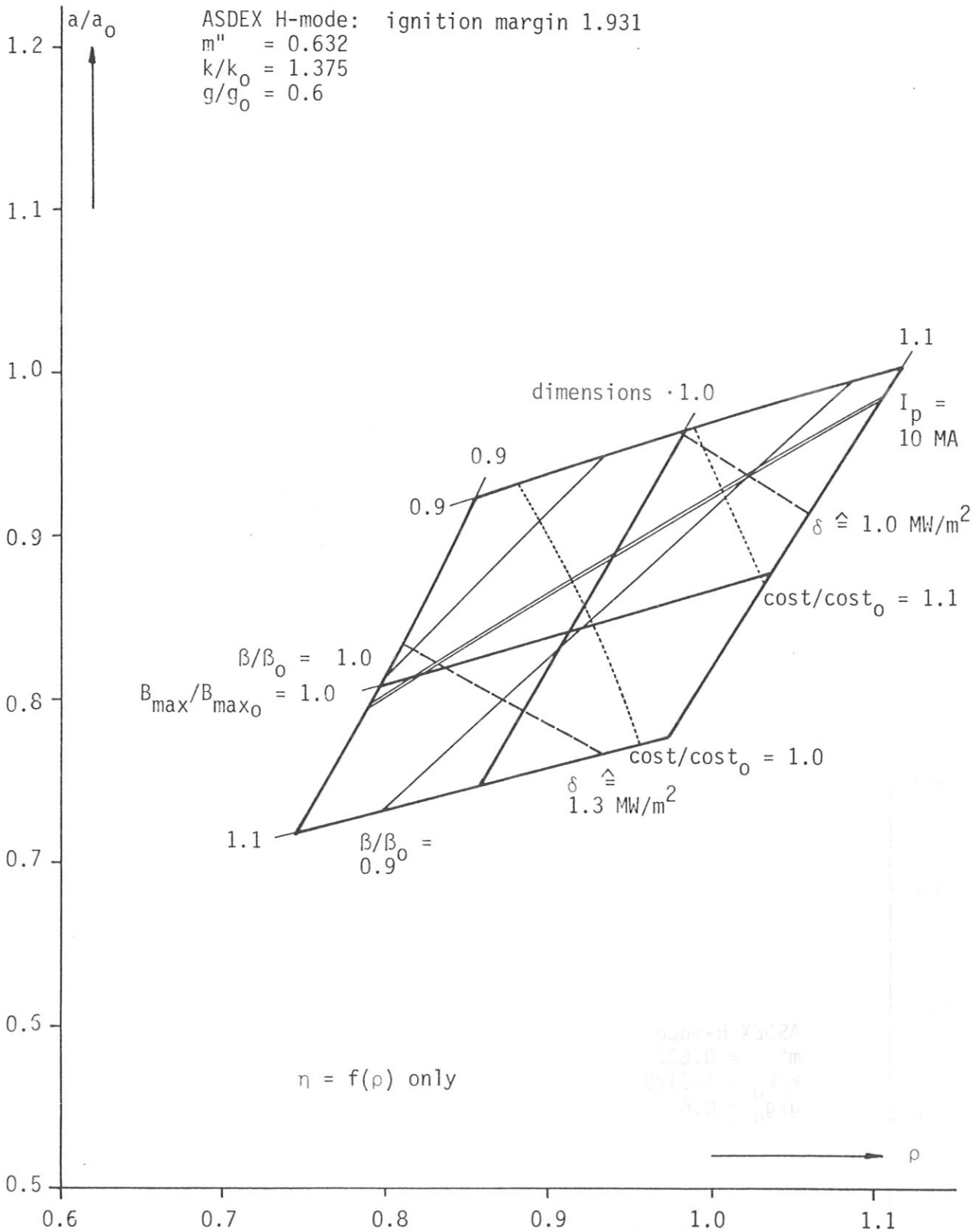

Fig. 29: Minor radius vs. major radius (density limit m"*) for an elongation of 2.2 and an ignition margin of 1.931 (ASDEX H-mode scaling) with a variation of ± 10% in maximum toroidal field and in geometry factors with parametric curves for constant neutron wall load, plasma current, total beta and relative direct capital cost.

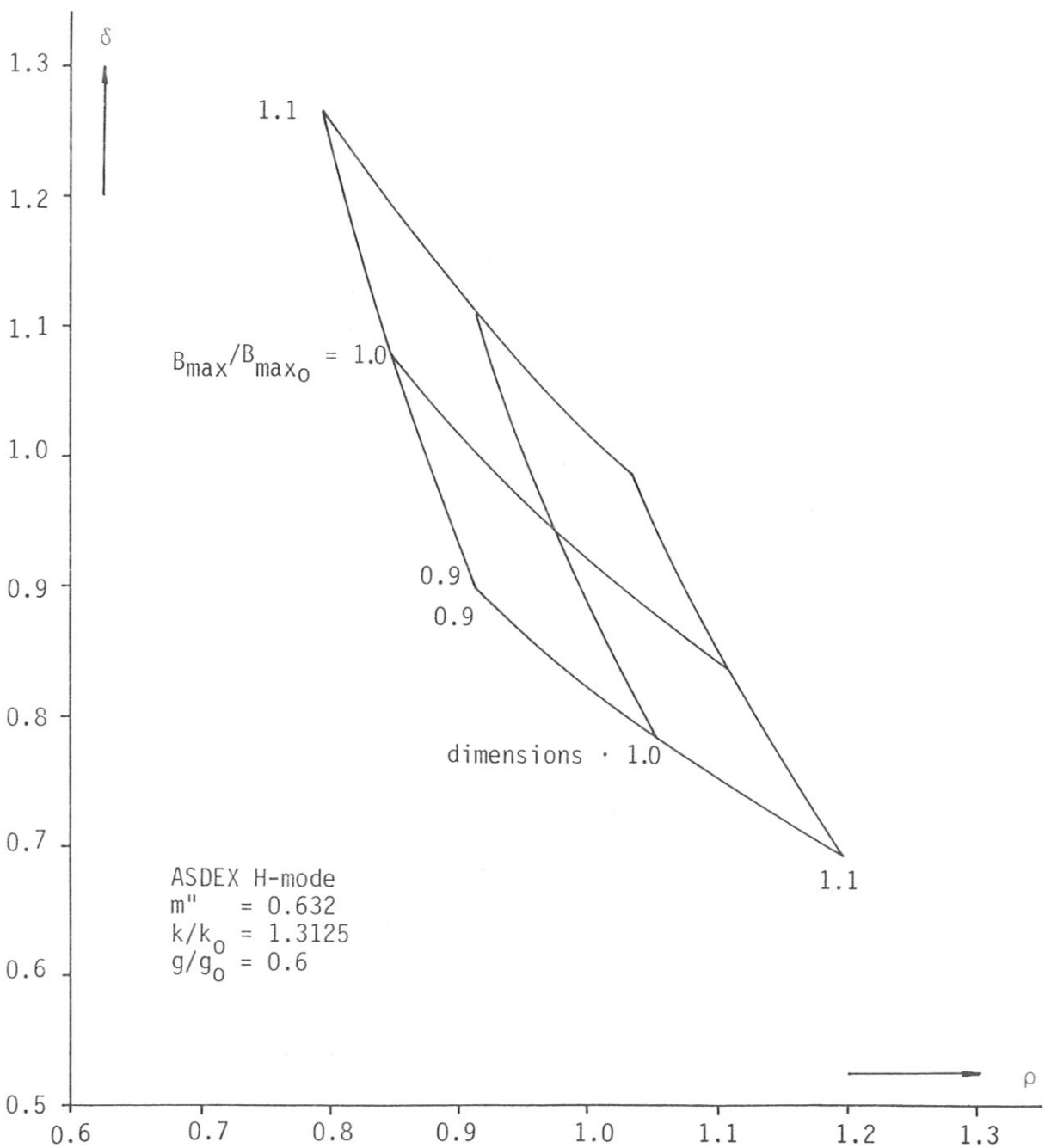

Fig. 30: Neutron wall load vs. major radius - see Fig. 28

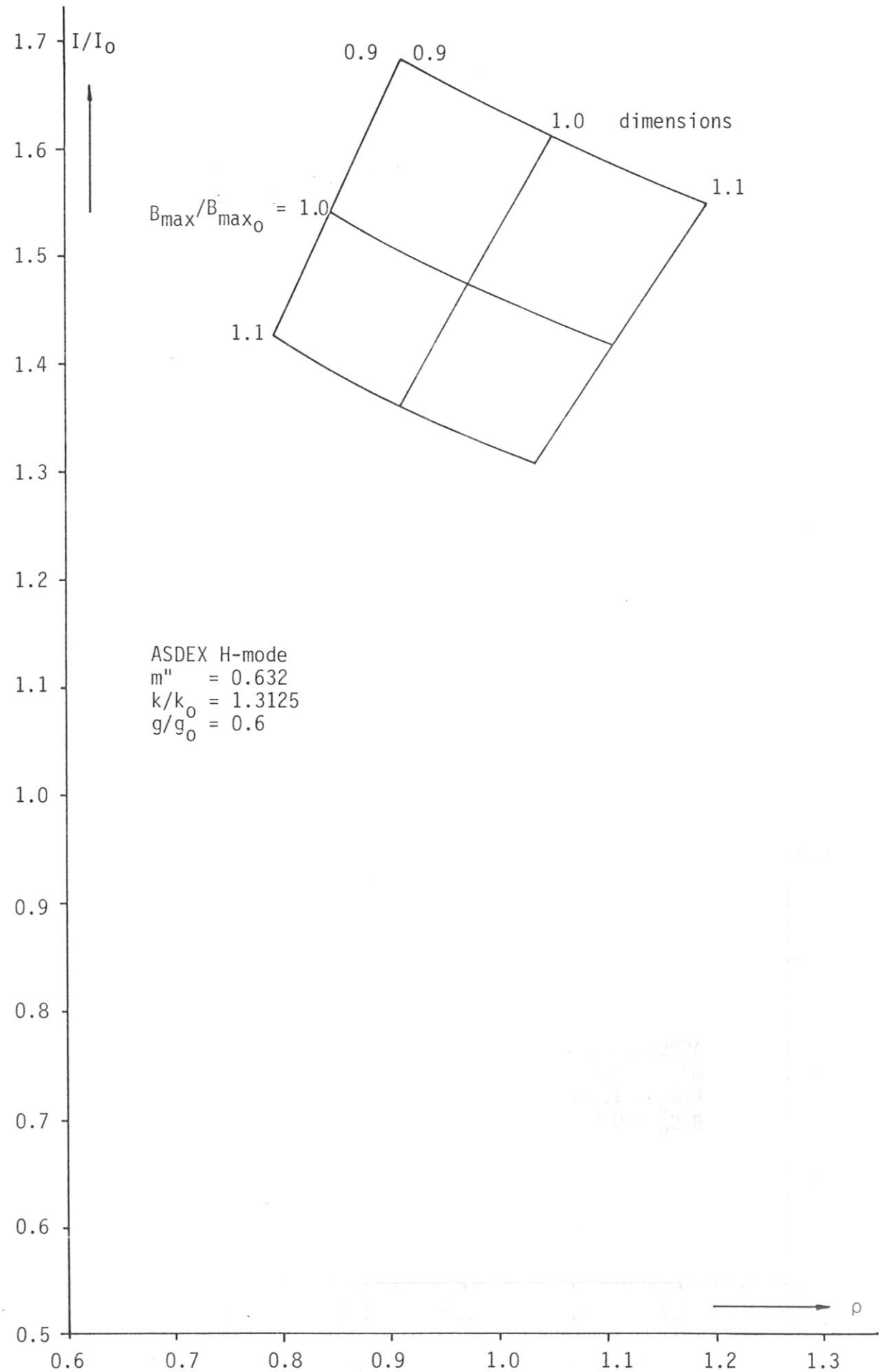

Fig. 31: Plasma current vs. major radius - see Fig. 28

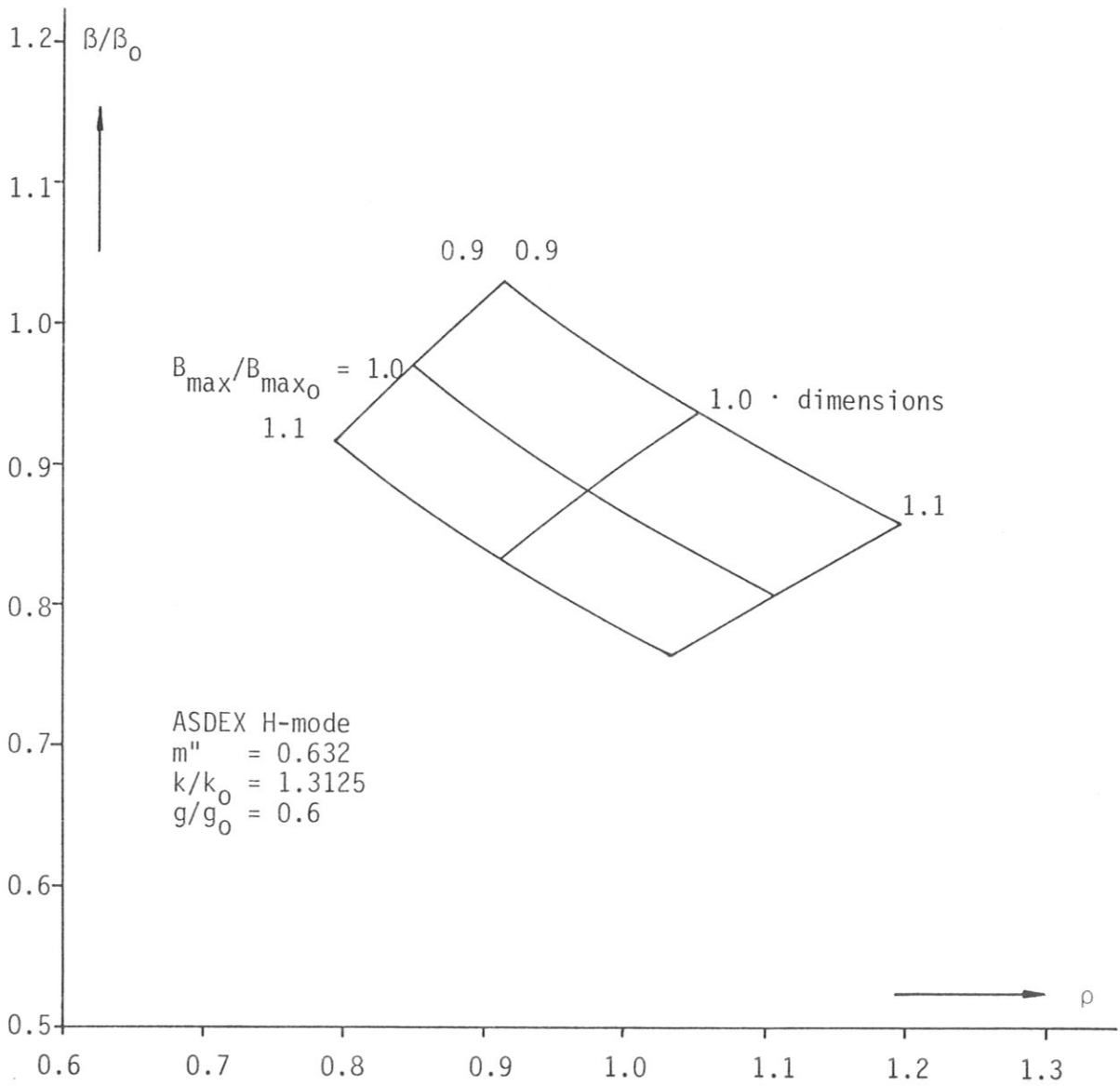

Fig. 32: Total beta vs. major radius - see Fig. 28

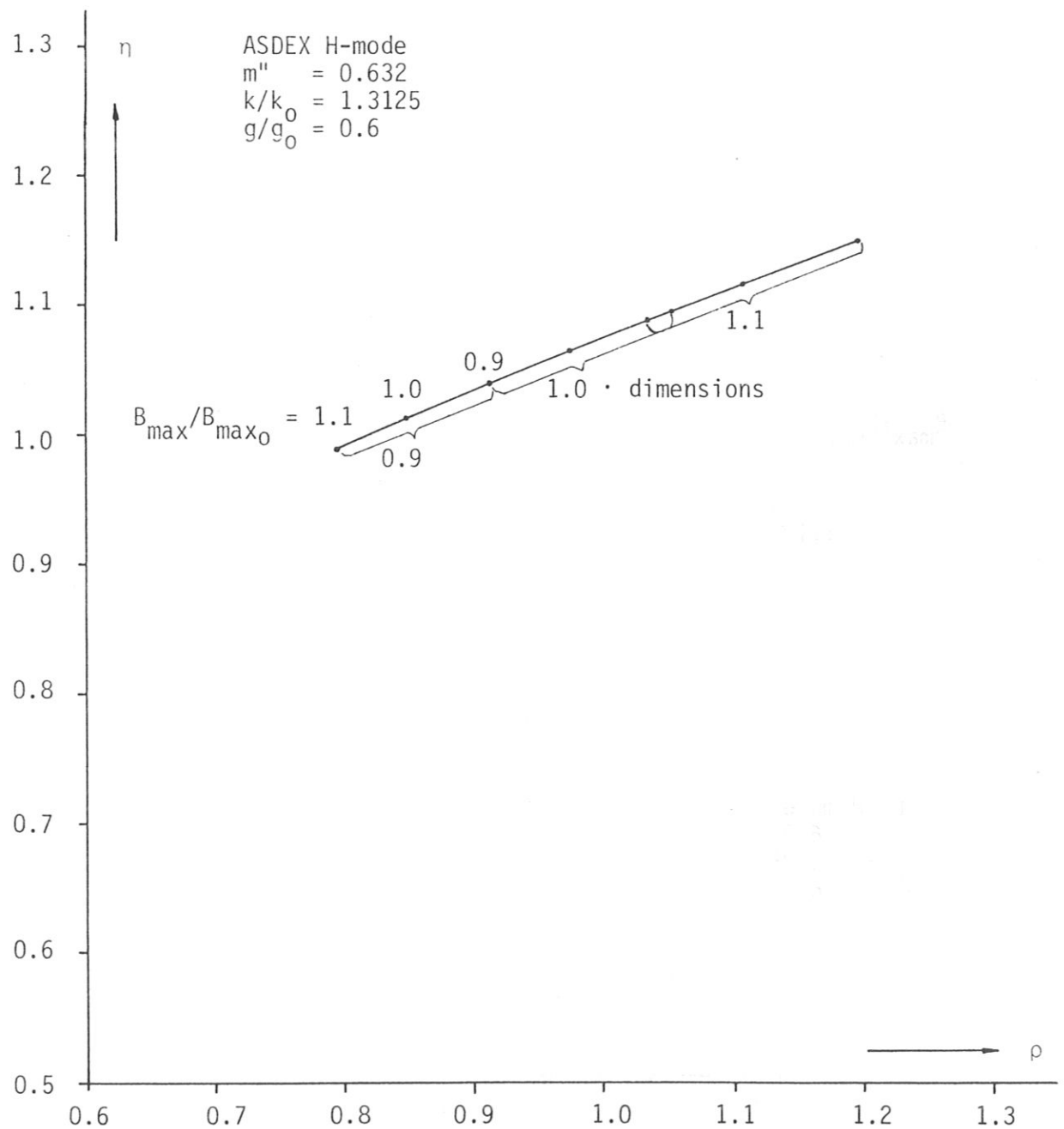

Fig. 33: Fusion power vs. major radius - see Fig. 28

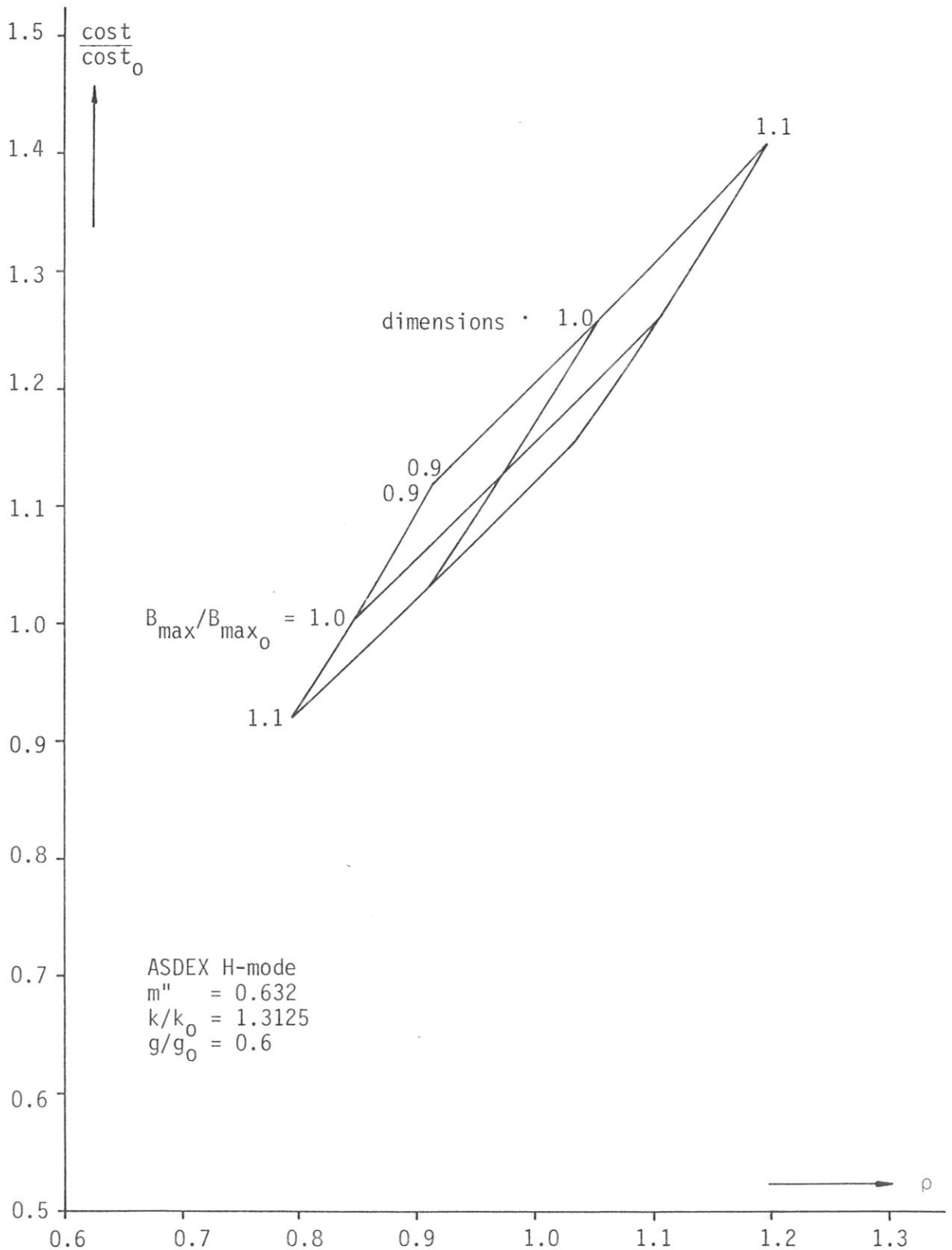

Fig. 34: Relative direct capital cost estimate vs. major radius - see Fig. 28

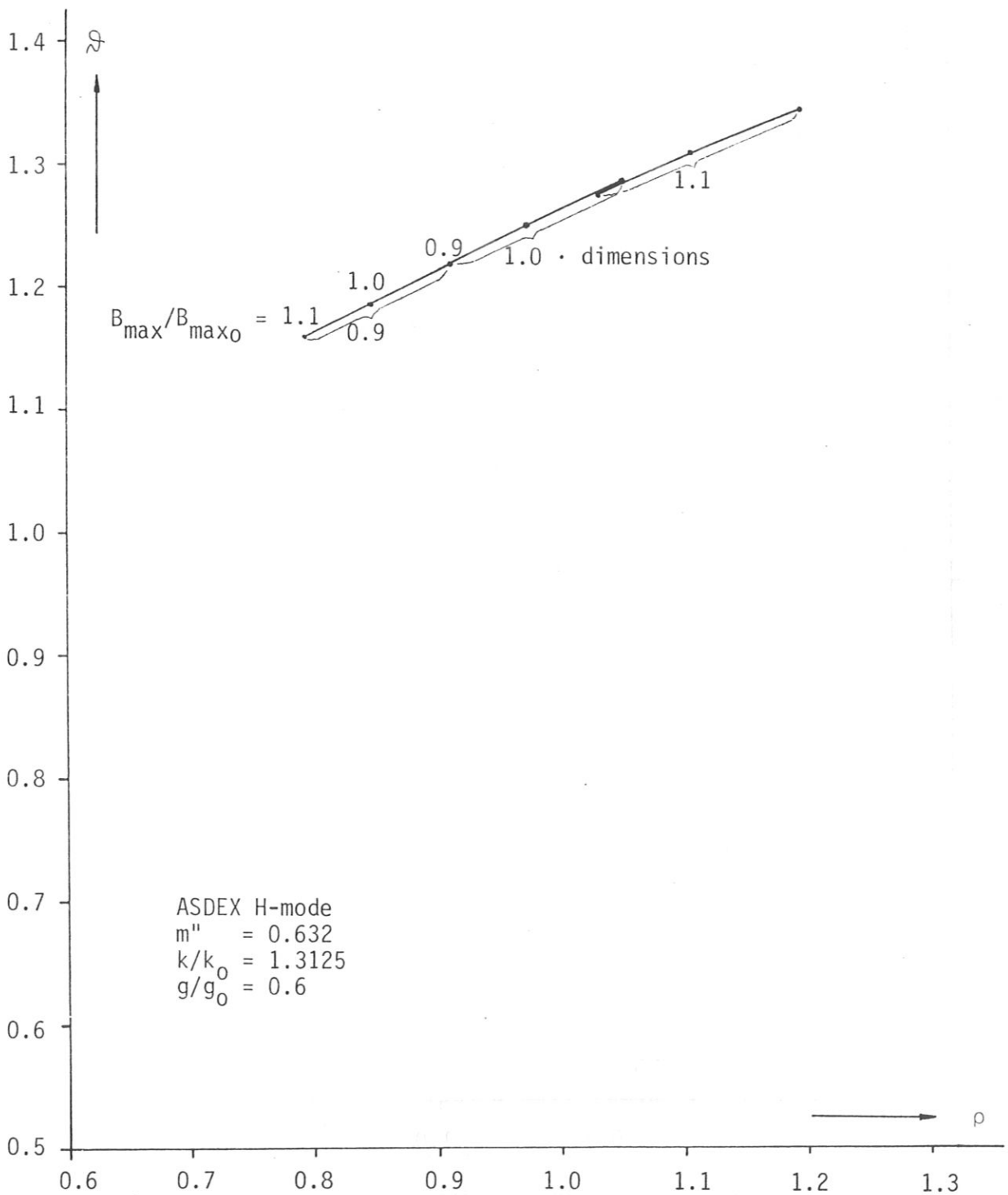

Fig. 35: Plasma temperature vs. major radius - see Fig. 28

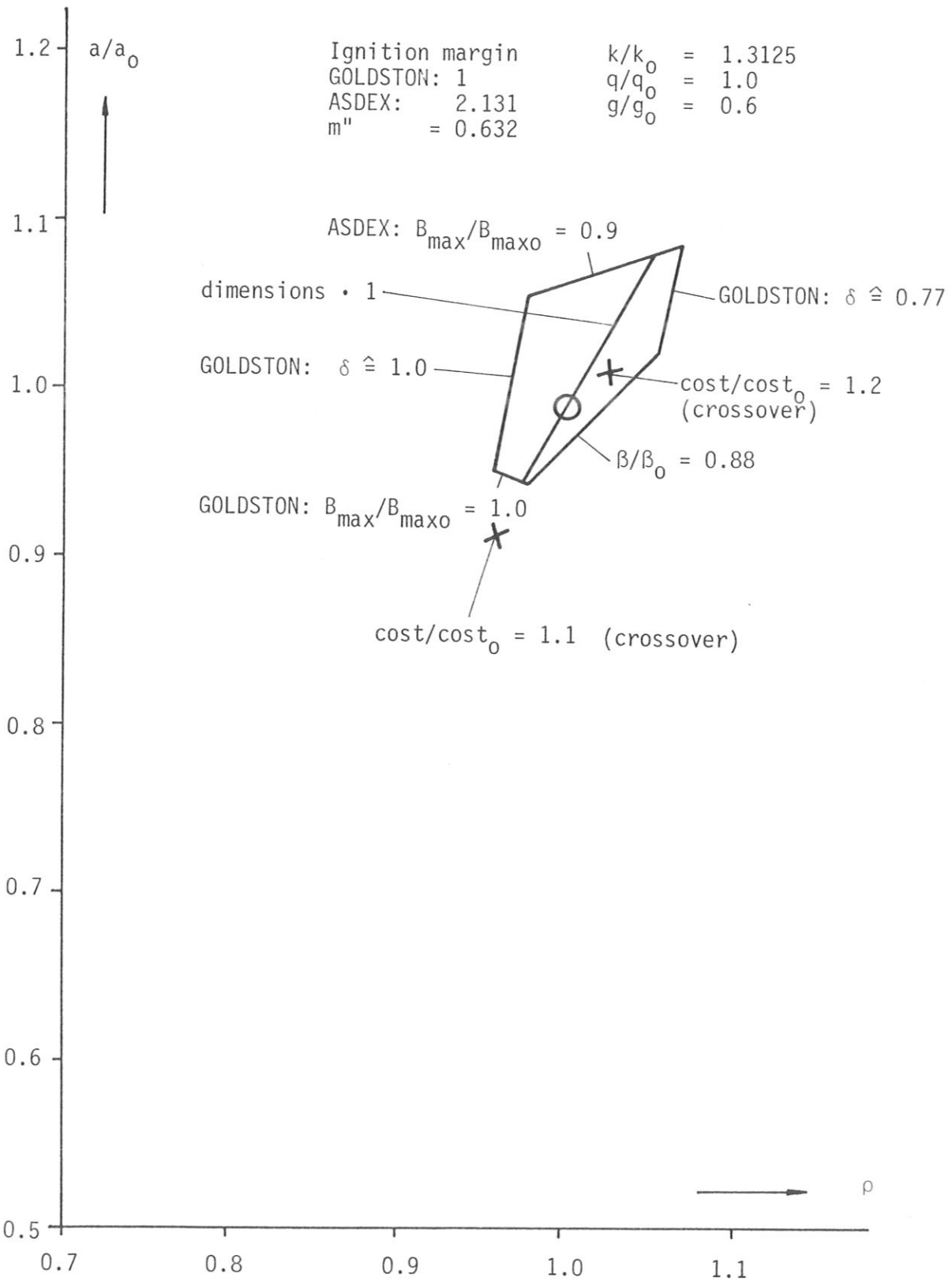

Fig. 36: Accessible domain in minor radius vs. major radius space for INTOR alternative data sets for an elongation of 2.1 when applying GOLDSTON and ASDEX H-mode scaling and the density limit m"*

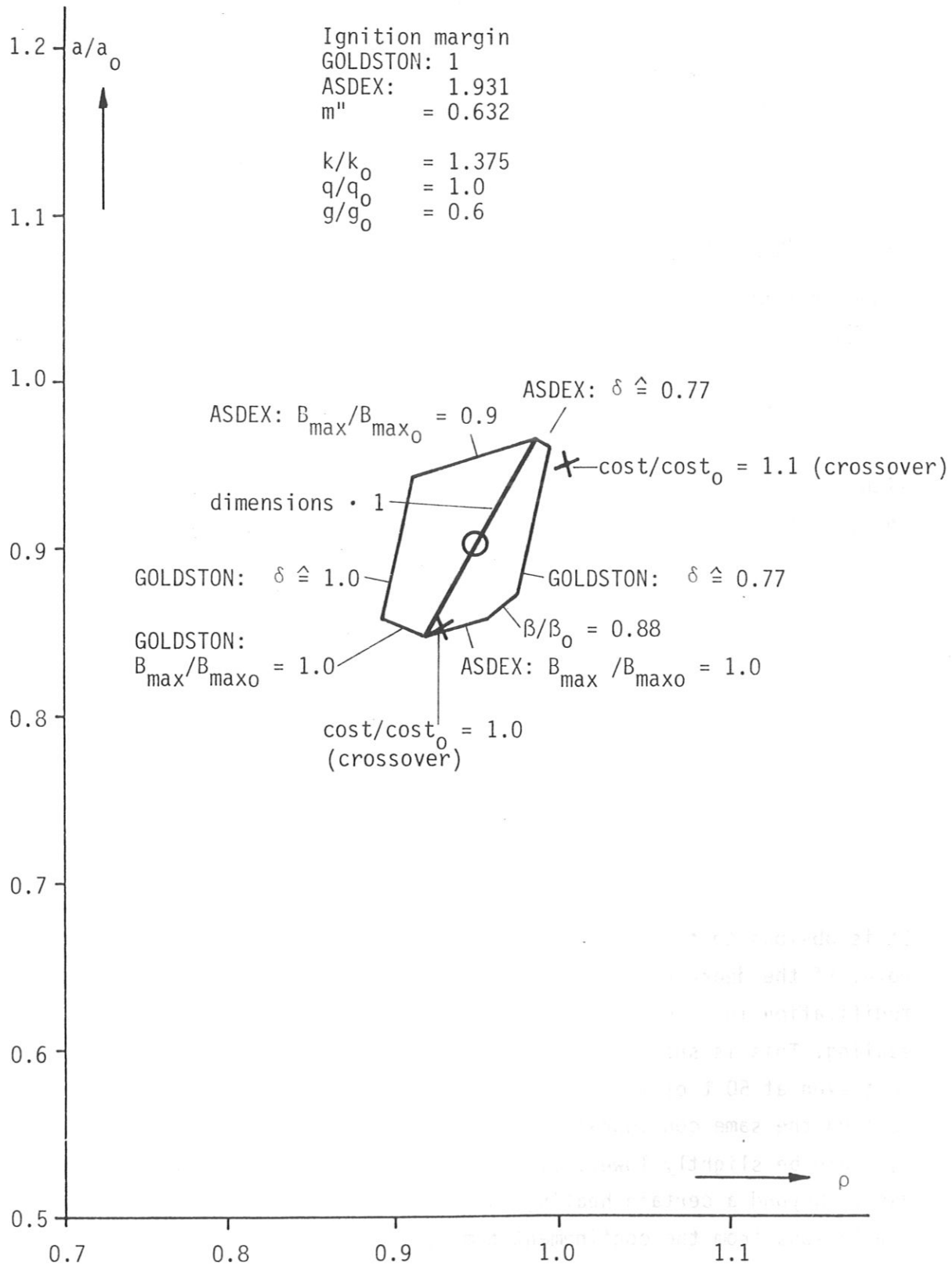

Fig. 37: Accessible domain in minor radius vs. major radius space for INTOR alternative data sets for an elongation of 2.2 when applying GOLDSTON and ASDEX H-mode sclg. and the density limit m"*

Appendix I

Reduction of the confinement scaling to the form $\frac{\tau_E}{\tau_{E_o}} = F_\tau \left(\frac{I}{I_o}\right)^{\lambda} \rho^{\mu} \left(\frac{A}{A_o}\right)^{\nu}$

In a relative form the confinement scaling usually represented as the product of the essential quantities to various respective powers can be written as /7/

$$\frac{\tau_E}{\tau_{Eo}} = \left(\frac{n_e}{n_{eo}}\right)^{\alpha_1} \left(\frac{a}{a_o}\right)^{\alpha_2} \left(\frac{k}{k_o}\right)^{\alpha_3} \rho^{\alpha_4} \left(\frac{q}{q_o}\right)^{\alpha_5} \left(\frac{B}{B_o}\right)^{\alpha_6} \left(\frac{P}{P_o}\right)^{\alpha_7} \left(\frac{I}{I_o}\right)^{\alpha_8} \vartheta^{\alpha_9} \left(\frac{A_i}{A_{io}}\right)^{\alpha_{10}} \left(\frac{Z_{eff}}{Z_{effo}}\right)^{\alpha_{11}} \qquad (I,1)$$

Assuming continuous degradation of confinement with increasing heating power one has

$$\frac{P}{P_o} = \frac{n}{n_o} \vartheta \frac{\tau_{Eo}}{\tau_E} \rho^3 \left(\frac{A_o}{A}\right)^2 \frac{k}{k_o} = \left(\frac{I}{I_o}\right)^2 \frac{A}{A_o} \rho \frac{k}{k_o} \frac{1}{M} \frac{\tau_{Eo}}{\tau_E} \qquad (I,2)$$

with eqs. (4) and (5).

One can show that the following relationships hold:

$$F_\tau = \left\{\left(\frac{q}{q_o}\right)^{\alpha_5} \left(\frac{g}{g_o}\right)^{-\alpha_6} \left(\frac{k}{k_o}\right)^{(\alpha_3+\alpha_7)} \vartheta^{(\alpha_9-\alpha_1)} M^{-(\alpha_1+\alpha_6+\alpha_7)} \left(\frac{A_i}{A_{io}}\right)^{\alpha_{10}} \left(\frac{Z_{eff}}{Z_{effo}}\right)^{\alpha_{11}}\right\}^{\left(\frac{1}{1+\alpha_7}\right)} \qquad (I,3)$$

$$\lambda = (2\alpha_1 + \alpha_6 + 2\alpha_7 + \alpha_8)/(1 + \alpha_7) \qquad (I,4)$$

$$\mu = (-2\alpha_1 + \alpha_2 + \alpha_4 - \alpha_6 + \alpha_7)/(1 + \alpha_7) \qquad (I,5)$$

$$\nu = (3\alpha_1 - \alpha_2 + 2\alpha_6 + \alpha_7)/(1 + \alpha_7) \qquad (I,6)$$

It is obvious that the exponent of power degradation plays an important role. If the degradation would be continuous - as assumed here - a slight modification in α_7 could compensate for some factor f in the absolute τ_E-scaling. This is shown in Fig. I,1 for the Goldston scaling /4/. It is seen that even at 50 % of the most optimistic numerical factor in the Goldston scaling the same configurations are possible for similar $\gamma\vartheta$ values provided α_7 would be slightly lower. If, however, the confinement degradation would vanish beyond a certain heating power or power density level, the limitations from the confinement time could be avoided altogether.

In this work the ASDEX H-mode and the Goldston scaling are used in the following form (no isotope effect: $\alpha_{10} = 0$)

$\tau_E = 0.065\ R\ I$ units: m, MA, s

$\tau_E = 0.074 \cdot a^{-0.37}\ k^{0.5}\ R^{1.75}\ P^{-0.5}\ I$ units: m, MW, MA, s

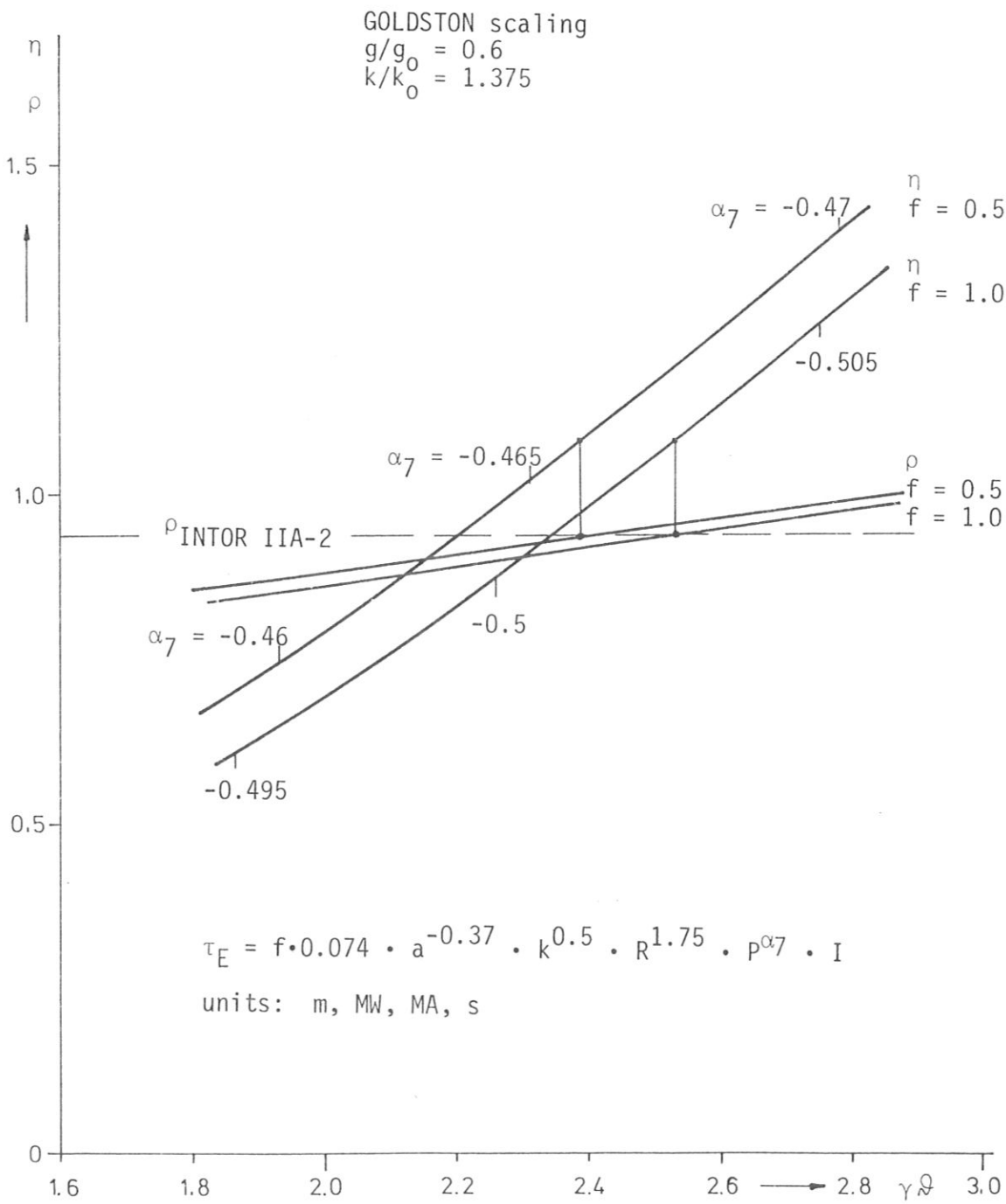

Fig. I.1: Impact of variations in f and α_7

Appendix II

Density limitation

Figures II.1 through II.6 show for Goldston and ASDEX H-mode scaling the respective curves for m, m' and m" vs. ρ pertaining to the design points as plotted in Figs. 2 and 3. The upper limits m*, m'*, m"* which indicate the corresponding density limits determine the accessible range of data sets independent of the confinement scaling. The latter, however, provides a further restriction to the accessible range.
As can be seen, m" imposes the strongest restriction for the large values of elongation.
The limits as indicated in Figs. II.1 through II.6 have been used for Figs. 2 and 3.

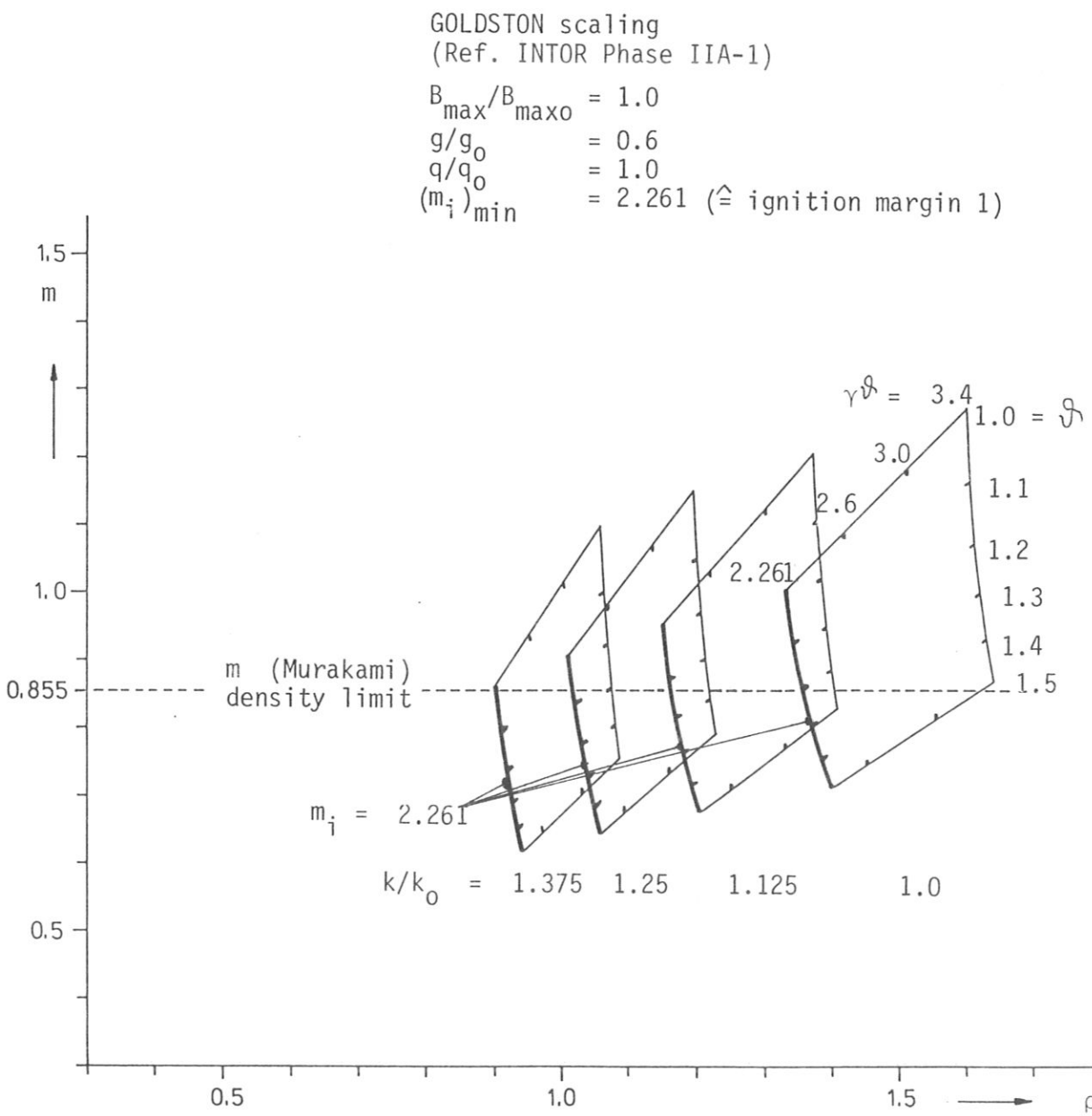

Fig. II.1: Limitation of the accessible major radius by the m (Murakami) density limit for different elongations, plasma temperatures and performance parameters (GOLDSTON scaling)

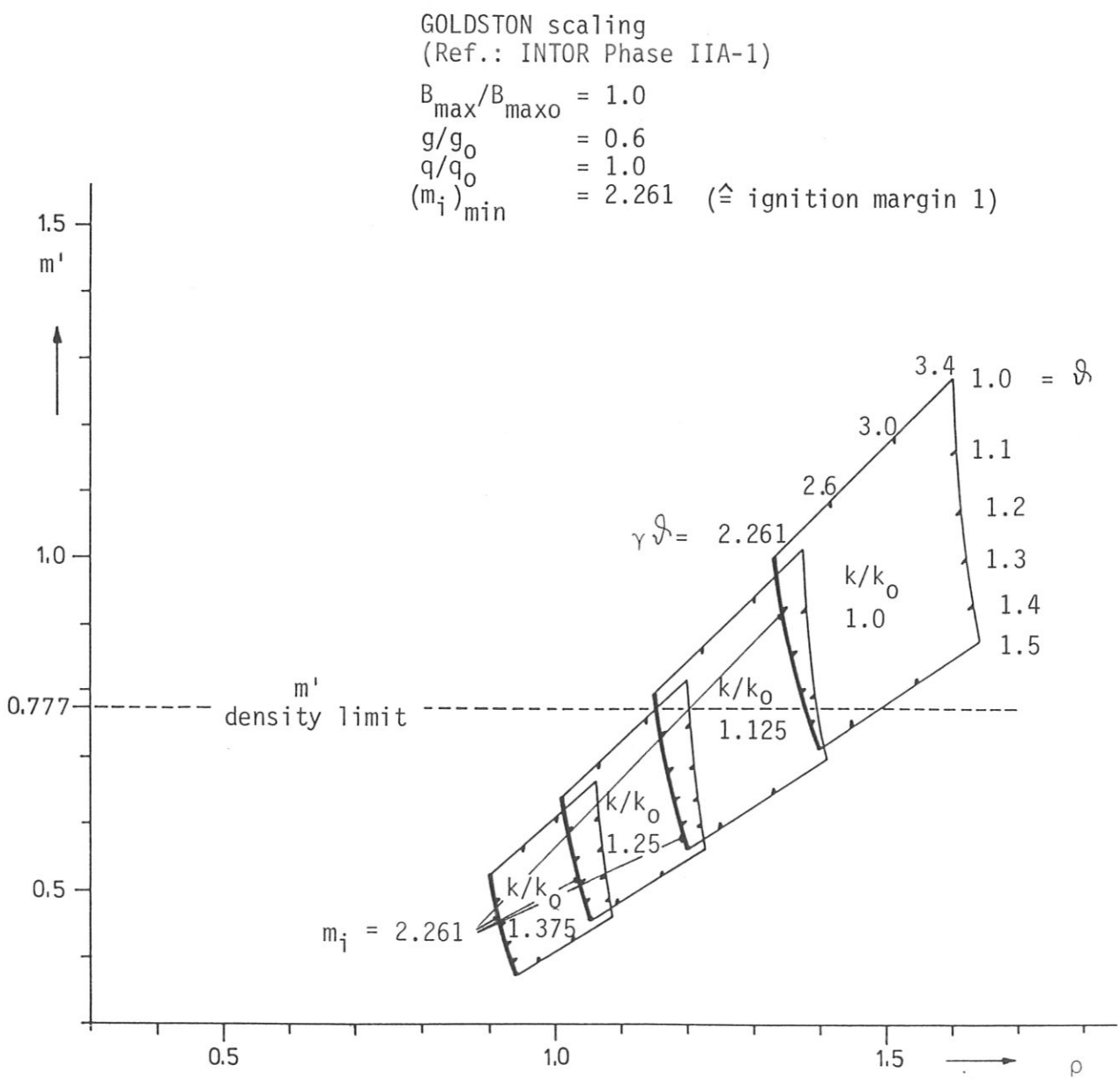

Fig. II.2: Limitation of the accessible major radius by the m' density limit for different elongations, plasma temperatures and performance parameters (GOLDSTON scaling)

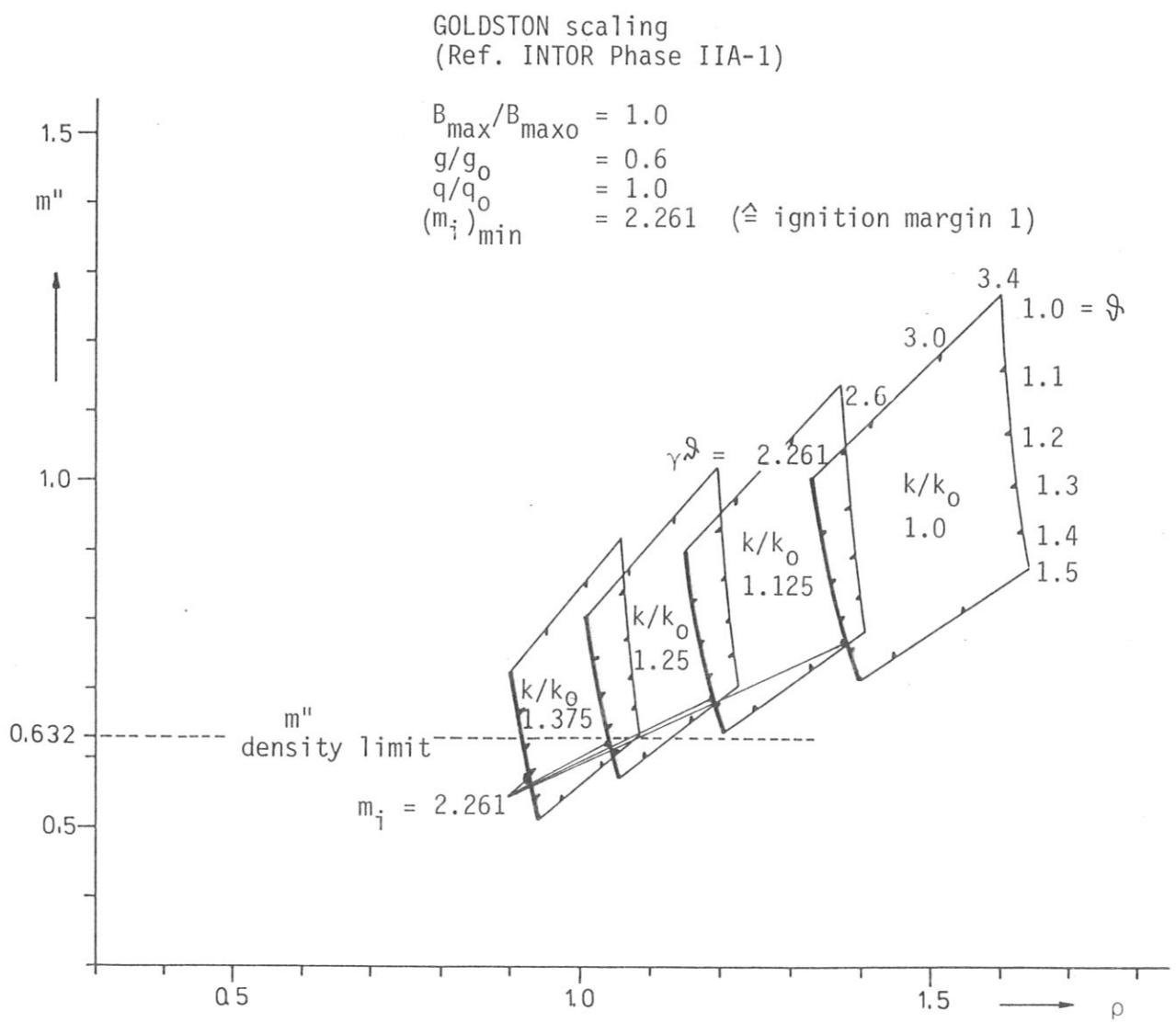

Fig. II.3: Limitation of the accessible major radius by the m" density limit for different elongations, plasma temperatures and performance parameters (GOLDSTON scaling)

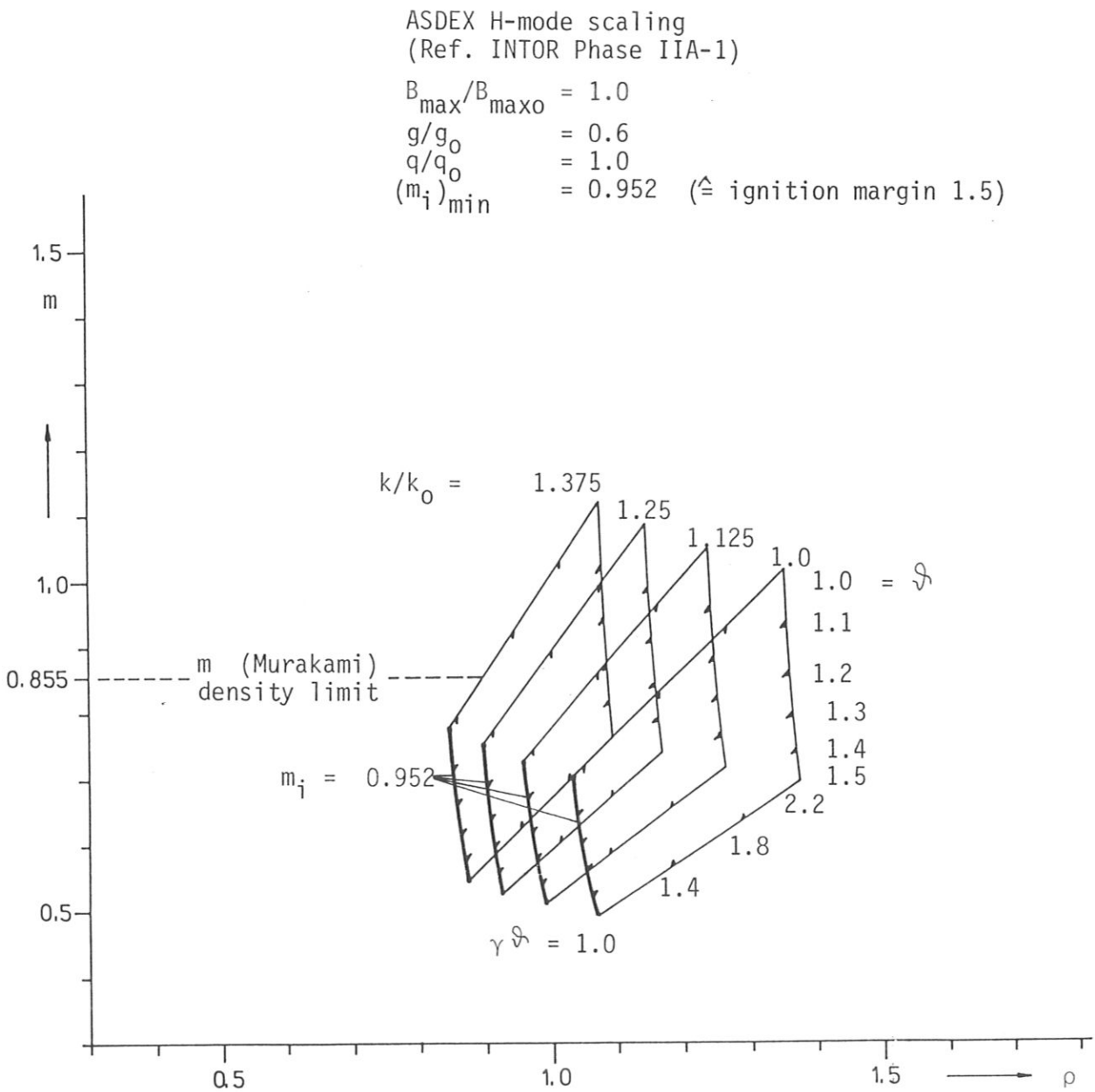

Fig. II.4: Limitation of the accessible major radius by the m (Murakami) density limit for different elongations, plasma temperatures and performance parameters (ASDEX H-mode scaling)

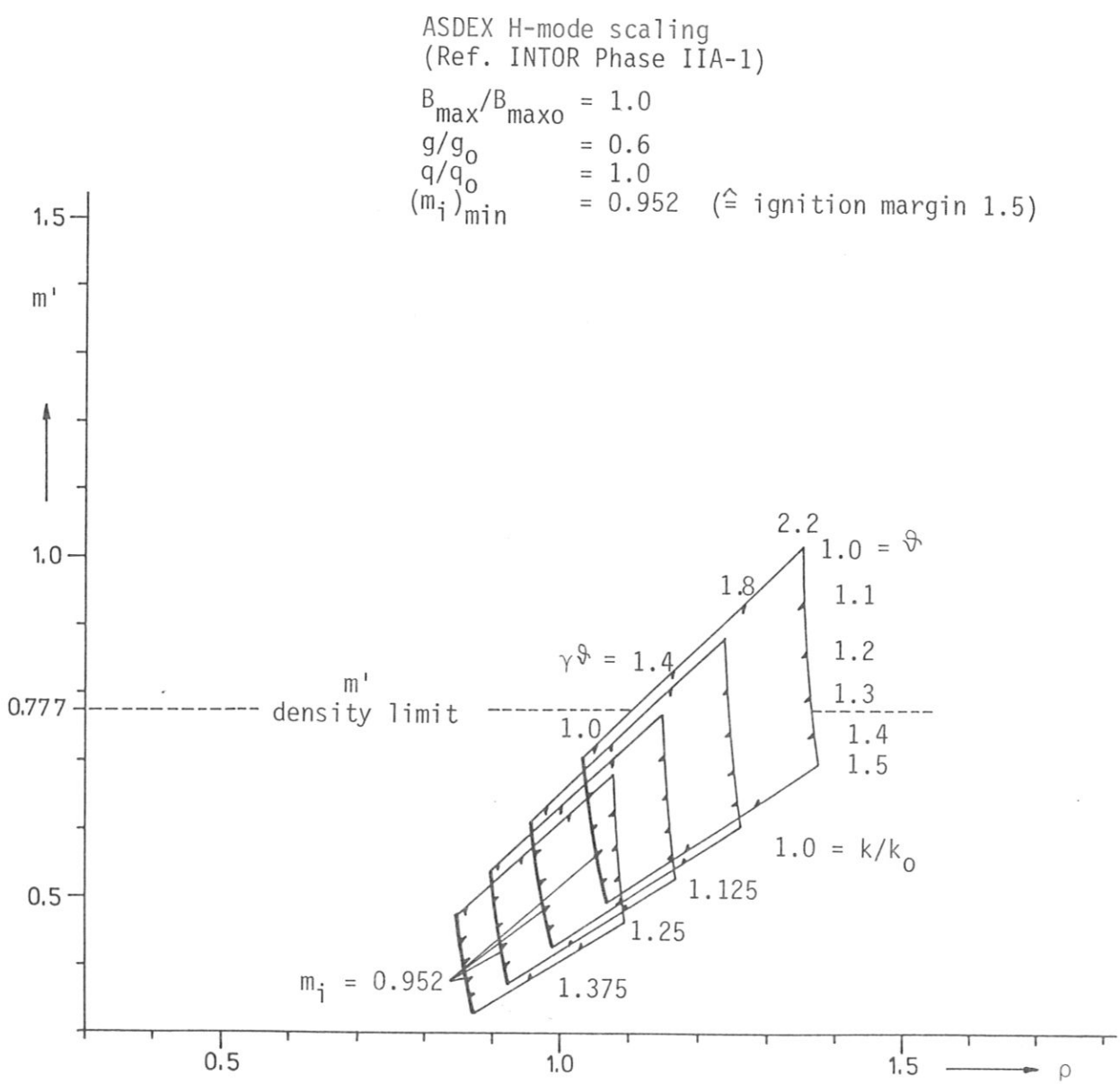

Fig. II.5: Limitation of the accessible major radius by the m' density limit for different elongations, plasma temperatures and performance parameters (ASDEX H-mode scaling)

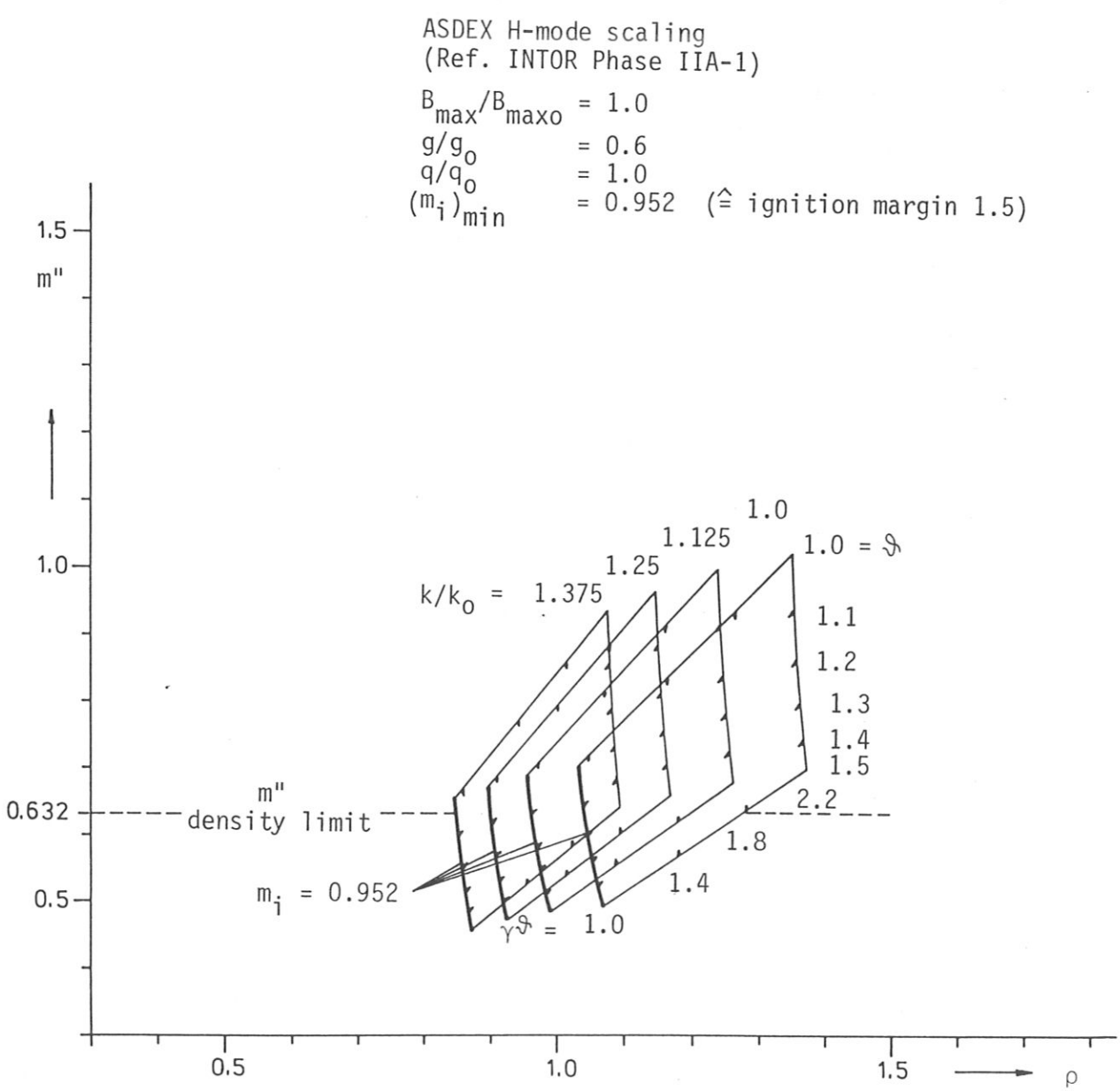

Fig. II.6: Limitation of the accessible major radius by the m" density limit for different elongations, plasma temperatures and performance parameters (ASDEX H-mode scaling)